Estuarine subtidal flow and salinity dynamics
Modelling the evolution of basin-averaged variables

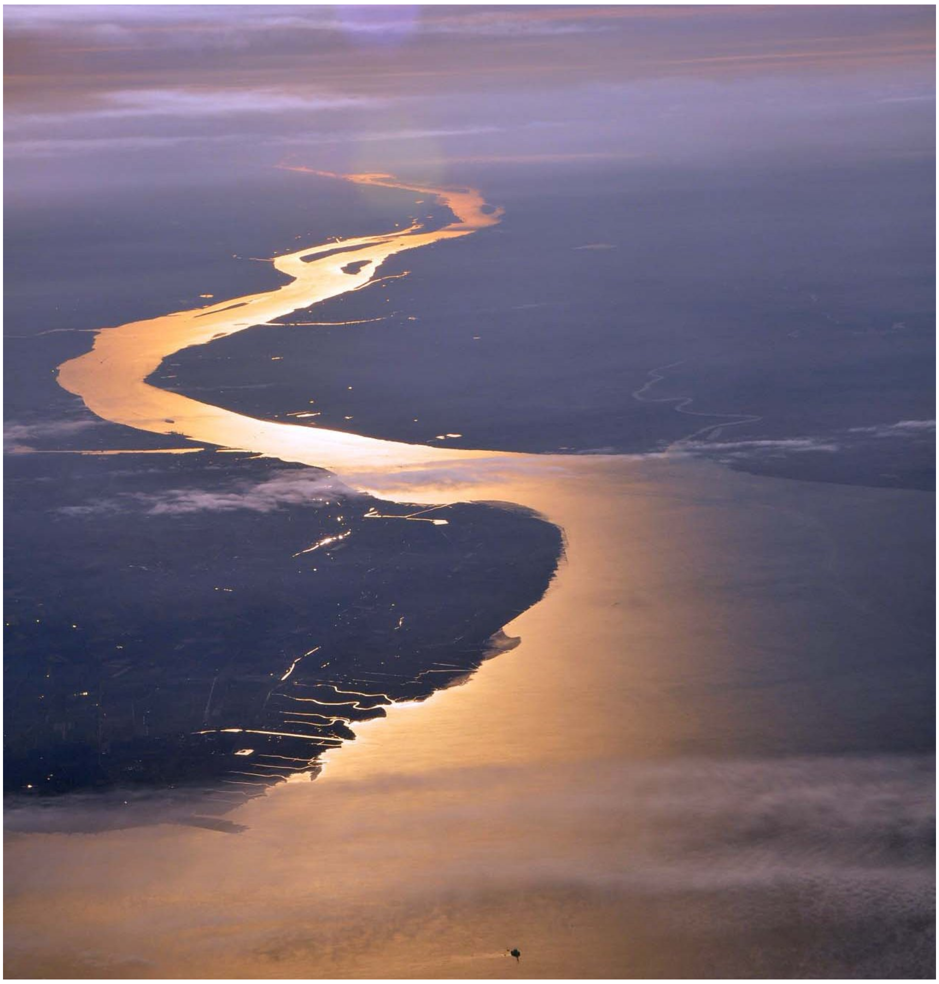

Author:
Roeland C. van de Vijsel
Student nr. 3355101

Supervisors:
prof. dr. Leo R.M. Maas
prof. dr. Huib E. de Swart

Master thesis
Meteorology, Physical Oceanography and Climate
Utrecht University

June 2015

Abstract

A model for subtidal estuarine salt and flow dynamics in a 2DV (along-channel and vertical) domain is developed, describing the evolution of variables averaged over the estuarine basin. These variables are domain-averaged horizontal and vertical salinity gradient and domain-averaged angular momentum in the 2DV-plane. The latter measures estuarine circulation strength. The model is defined under the assumptions that the lowest-order, in this case spatially linear, salt- and flow-field contributes dominantly to domain-integrals. Domain length is here dynamically related to horizontal salt gradient and defined as the furthest up-estuarine salt intrusion.

The methods applied in the current study reduce the governing equations (partial differential equations) to coupled ordinary differential equations (ODE's), i.e. evolution equations for the three basin-averaged variables. A major advantage is that (steady) solutions to ODE's are more easily found and can be readily analysed. All individual terms contributing to the evolution equations have a clear physical meaning. The influence of all terms on the model's analytical and numerical steady state solutions could be interpreted. Yet the complexity of the resulting evolution equations and solutions limits complete physical understanding and comparison to other (modelling) studies.

At least one steady state solution is associated with the typical estuarine stratification and circulation and is linearly stable. The estuary evolves into this state when perturbed from a homogeneous rest state by imposing a weak horizontal salinity gradient and angular momentum and a strong vertical stratification. The behaviour of this steady state as a function of depth and river discharge, for the parameter settings of a partially mixed estuary, is qualitatively comparable to other model studies. The vertical stratification is however unrealistically strong, most likely due to the formulated seaward boundary conditions.

Suggestions are given to improve the seaward boundary conditions and to reduce the complexity of the model, to further improve understanding of its solutions. With some adaptations, the constructed model has the potential to gain more insight into basin-averaged subtidal estuarine processes and to study its time-evolution.

Contents

Chapter 1

Introduction

1.1 Estuarine subtidal hydrodynamics

An estuary is the transition area between a river and its adjacent sea or ocean. The river discharges fresh water into the domain, while saline seawater is introduced advectively and by (mainly tidally induced) turbulent mixing. Examples of estuaries are the Elbe estuary in Germany (depicted on the front page), Ems estuary on the Dutch-German border and Western Scheldt estuary (illustrated in Figure 1.1) on the Dutch-Belgian border.

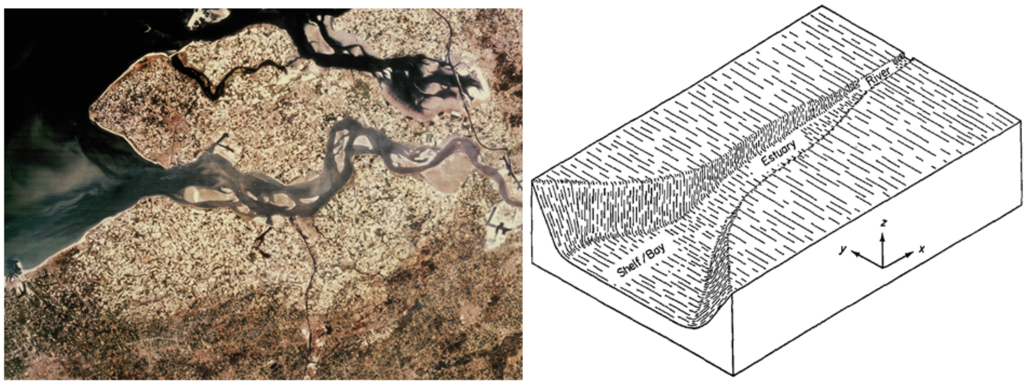

Figure 1.1: Left: areal view of the Western Scheldt estuary on the Dutch-Belgian border (from visitholland.nl). Right: idealised estuarine basin (from *Festa & Hansen* [1976].

This study aims at understanding the dynamics of the estuarine salt and flow field at typical time scales longer than the tidal period. Tidal variations are thus averaged out and the focus will be fully on subtidal dynamics. An estuary is characterised by an along-channel salinity gradient due to fresh water run-off from the river. This salinity gradient sets up a baroclinic pressure gradient force, directed landward along the channel and increasing in strength with depth [e.g., *De Swart*, 2012]. The water volume introduced by the river is forced out by a barotropic pressure gradient force that is directed seaward along the channel. This pressure gradient is constant with depth and related to gradients in free surface height. The subtidal force balance between these two pressure gradients results in the bidirectional along-channel flow pattern that is typical for many estuaries, as is shown by *Hansen & Rattray* [1965]. This so-called exchange flow draws saltier water in from the seaside at depth and advects fresher water seaward in shallower layers. The along-channel salinity gradient typically becomes weaker towards the riverward and seaward edges of the estuarine domain [*Talke et al.*, 2009-a]. Horizontal exchange flow strength consequently decreases here. Conservation of volume ensures that this is compensated by a vertical flow component and a typical estuarine, or gravitational, circulation cell is the result [e.g., *Festa & Hansen*, 1976]. The riverward part of the circulation cell is characterised by upwelling; downwelling takes place more seaward. An estuarine turbidity maximum (ETM) may occur near the bottom where landward exchange currents converge with seaward river flow and accumulates suspended sediment

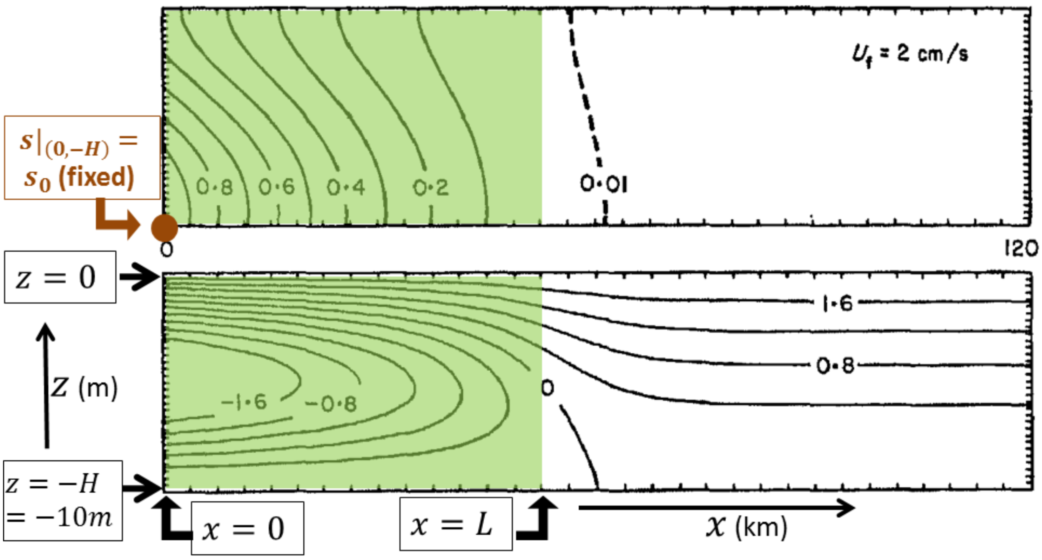

Figure 1.2: Top figure: width-averaged dimensionless salinity field for an idealised, partially mixed estuary; salinity s (psu) is scaled with constant sea salinity $s_0 = 35$ psu. Seaward boundary defined at $x = 0$, where $s|_{(x=0,z=-H)} = s_0$. Riverward boundary in *this* study is defined at intrusion length $x = L$, where $s|_{(x=L,z=-H)} \approx 0$. This length is *shorter* than the total modelled length in the original figure (120 km in the case of this figure); estuarine domain for the current study is equal to the green shaded area. Bottom figure: corresponding streamfunction field ψ (in 10^3 m^2/s). Figure adapted from *Festa & Hansen* [1976].

[e.g.. *Burchard et al.*, 2004].

Many different classes of estuaries exist, as characterized by flow pattern and salinity field, see e.g. *Dyer* [1997]. Partially mixed estuaries with their typical estuarine circulation pattern are probably most characteristic, as illustrated in Figure 1.2. Very weak turbulence allows the fresh water to flow out on top of the more saline water, as happens in typical salt wedge estuaries.

1.2 Why studying estuarine dynamics?

Studying estuarine subtidal salinity and flow dynamics is important for many reasons. Estuaries form important and unique ecosystems. For example, thanks to their intermediate salinity, estuaries provides an essential stopover for many types of fish migrating between sea and river during different stages of their lives. The salinity tolerance of these fish is very specific and thus they are dependent on the right estuarine salt field [*Marshall & Elliott*, 1998]. Apart from that, current strength influences turbidity. Increasing turbidity results in the depletion of dissolved oxygen and can lead to ecologically "dead zones" [*Talke et al.*, 2009-b].

Apart from the ecological importance, estuarine salt, current and turbidity characteristics are also economically relevant. Currents, turbidity and resulting sedimentation need to be fully understood and continuously monitored to ensure safe and sustainable shipping traffic, e.g. on the Ems and Western Scheldt estuaries in the Netherlands. Moreover, an increased riverward reach of salt water may negatively affect agricultural land that is dependent on freshwater uptake [*Winterwerp & Wang*, 2013].

Concludingly, it is essential to fully understand the response of estuarine salt and flow field to (natural or anthropogenic) changes in system parameters such as geometry, tidal forcing and river discharge. Changes in salt field, turbidity and sedimentation take place over time scales often longer than the tidal period, hence this study's focus is on tidally averaged, or subtidal, dynamics.

1.3 Previous studies

Much research has been done in the field of subtidal estuarine dynamics. Analytical expressions for cross-channel averaged salt and flow profiles were obtained by *Hansen & Rattray* [1965] and *MacCready* [2004]. Their analytical relations elucidate the role of individual physical processes and parameters. However, these solutions are restricted to simplified momentum and salt balances in steady state.

Solving similar but nonsteady cross-channel averaged balances *numerically*, see e.g. *Festa & Hansen* [1976], allows to study time evolution. However, numerical solutions cannot be explained explicitly as a function of individual processes and parameters, making them harder to interpret.

Full-scale, three-dimensional numerical models [e.g. *Burchard et al.*, 2004] yield very realistic views on estuarine dynamics, as well as the system's time evolution. Yet the increased complexity of such numerical models makes isolation and interpretation of the physical processes even more difficult.

Searching the system for the occurrence of multiple steady states is possible for both two- and three-dimensional numerical models mentioned. However, due to the system's large "parameter space" and the absence of an analytical solution it is hard or even practically impossible to systematically search for multiple equilibria within this parameter space.

1.4 Challenges

Required is a subtidal estuarine model whose equations are well analysable, such that the role of individual physical processes and parameters can be explained and all existing equilibria can be systematically detected. The model should thus be time-dependent, also to assess the stability of each equilibrium and the time evolution from one state into another.

The current study will be based primarily on a model introduced by *Maas* [1994; 2004]. This model describes the time evolution of *basin-averaged* quantities in a three-dimensional oceanic domain with closed side walls. Although this averaging causes the loss of spatial dependencies, the reward is significant. Under specific assumptions such as a linearised density field, explained further in section 2.3 and 2.4, the model depends on six coupled variables. These are the domain-averaged centre-of-mass position vector, related to the basin-averaged density gradient, and the basin-averaged angular momentum vector, a measure for the amount of overturning. Via this method, *Maas* [1994; 2004] reduces the system's original partial differential equations to a set of coupled *ordinary* differential equations for the six global variables. Although restricting assumptions have been made, the ordinary differential equations yield, under specific circumstances, analytical expressions for multiple equilibria and show rich and interesting dynamical behaviour.

Maas' model has to be altered significantly to make it applicable for estuaries. Most importantly, the longitudinal (seaward and riverward) sides should be opened to allow fluxes of mass and momentum, complicating the existing model. However a reduction from three to two dimensions can be made, provided the estuary is relatively narrow.

1.5 Research objectives

The main goal of this thesis is thus to construct a model that describes the evolution of estuarine subtidal salt and flow dynamics in terms of "global" variables and that is appropriate for analytical study. These goals are divided into separate research objectives (RO's), as presented below.

Construct a model for estuarine subtidal hydrodynamics that

1 **Is closed in terms of basin-averaged variables only.**

2 **Has simple enough model equations so that analytic steady state solutions exist.**

3 **Allows detection of multiple equilibria, if existing.**

4 **Has at least one steady state solution whose dependency on river and tidal influence is physically interpretable.**

This model should describe time-evolution of the basin-averaged variables, so that

5 **Linear stability of the steady states can be computed.**

6 **The variable's time evolution after perturbation from steady state can be computed.**

1.6 Outline of this thesis

The governing estuarine model equations are explained in chapter 2.1 and 2.2. Section 2.3 and 2.4 describe further assumptions made on the salinity and flow field and the basin-averaged variables are introduced. In sections 2.5 to 2.6, evolution equations for the global variables are derived. The individual terms in these equations are phyiscally interpreted in section 2.7.

To analyse the obtained model, steady states are computed and interpreted as a function of changing parameter settings. The methods are explained in section 3.1; corresponding results shown in section 4.1. To test if the steady states found are stable to infinitesimally small perturbations, a linear stability analysis is done, as explained in section 3.2. Results are shown in section 4.2 and compared to other model studies. Finally, it is important to know if the system actually "ends up" in some acceptable steady state once perturbed by a finite perturbation from another steady state. Hence a forward time-integration of the evolution equations is done in section 3.3 and shown in section 4.3.

Discussion of the results and attempts to further interpret these are given in §5.1 and 5.2. Suggestions for model improvement and future research is presented in §5.3. Finally, conclusions regarding the research objectives and added value of the constructed model are made in section 6.

Chapter 2

Model

2.1 Domain

The modelled estuary has length L in the along-channel or landward direction x, width W in cross-channel direction y and undisturbed water depth H in vertically upward direction z. The estuarine basin is fully rectangular, with a flat horizontal bottom, straight vertical and impermeable boundaries on the lateral (cross-channel) sides and a straight vertical separation between the estuarine domain and the adjacent sea and river on the longitudinal edges. The bottom boundary is at undisturbed water depth $z = -H$; the long-term averaged reference surface level is at $z = 0$. Following *Festa & Hansen* [1976] and *MacCready* [2004], the seaward boundary is at $x = 0$, defined where estuarine salinity s, measured in practical salinity units (psu), at the bottom first reaches the reference salinity s_0 of the adjacent sea,

$$s(x = 0, z = -H) = s_0, \tag{2.1}$$

as was illustrated in Figure 1.2. Here s_0 is assumed constantly 35 psu within the entire sea. The riverward boundary is at $x = L$, defined by the furthest up-estuarine (landward) reach of salt, as is further explained in section 2.3.

2.2 Governing equations

The balances governing subtidal estuarine salt and flow dynamics are introduced below. Prior to that, the assumptions underlying these balances are explained.

2.2.1 A priori assumptions

The focus of this study is on subtidal estuarine dynamics. Changes in free surface height due to changing river discharge are typically on a tidal time-scale, hence temporal variations in free surface level are averaged out. Gradients in the tidally-averaged free surface height $\eta(x,z)$, measured relative to reference level $z=0$, are translated into pressure variations at $z=0$. This reference level is assumed to be a rigid lid [e.g., *MacCready*, 1999].

The equations are Reynolds-averaged [e.g., *Cushman-Roisin & Beckers*, 2011] but modified for the estuarine case. In chapter 7 of *Dyer* [1997] the total along-channel and vertical velocity components (u,w) are split into tidal-averaged part, fluctuation with the tidal period and turbulent fluctuations. *Dyer* showed that the dominant estuarine subtidal x-momentum balance contains stress terms due to turbulent flow correlations as well as tidal flow correlations. It is here assumed that these two stress terms are of similar nature and can thus be combined into one (modified) Reynolds-stress divergence term.

Channel width W is assumed small compared to the Rossby radius of deformation, hence Coriolis effects can be neglected. Uniformity in cross-channel direction is assumed. Cross-channel wind stress is neglected. The horizontal scales of a typical estuary are much larger than the vertical scale, so hydrostatic pressure is assumed. Furthermore, the Boussinesq approximation is applied [e.g., *Cushman-Roisin & Beckers*, 2011]. A linearised equation of state is assumed where salinity variations contribute dominantly to density variations.

2.2.2 Resulting equations

All quantities and equations considered in this study are tidally-averaged. Under the previous assumptions the governing equations are as follows.

For an average sea salinity $s_0 = 35$ psu and reference temperature of 10 degrees Celcius , the linear equation of state reads [*Cushman-Roisin & Beckers*, 2010]

$$\rho = \rho_0(1+\beta s), \tag{2.2}$$

with total density ρ, constant reference density $\rho_0 \approx 1000$ kg m^{-3} and salinity contraction coefficient $\beta \approx 7.8 \cdot 10^{-4}$ psu^{-1}. From here on, s will be considered rather than ρ. The salt balance reads

$$\frac{\partial s}{\partial t} + \frac{\partial}{\partial x}\left(us - K_h\frac{\partial s}{\partial x}\right) + \frac{\partial}{\partial z}\left(ws - K_v\frac{\partial s}{\partial z}\right) = 0, \tag{2.3}$$

where the total horizontal and vertical salt fluxes are hereafter abbreviated

$$f_S = us - K_h \frac{\partial s}{\partial x} \text{ and } g_S = ws - K_v \frac{\partial s}{\partial z}, \tag{2.4}$$

with horizontal and vertical eddy diffusion coefficients K_h and K_v.

The dominant alongchannel momentum balance becomes [*Dyer*, 1997]

$$\frac{\partial u}{\partial t} + u\frac{\partial u}{\partial x} + w\frac{\partial u}{\partial z} = -\frac{1}{\rho_0}\frac{\partial p'}{\partial x} + \frac{\partial}{\partial x}(A_h \frac{\partial u}{\partial x}) + \frac{\partial}{\partial z}(A_v \frac{\partial u}{\partial z}), \tag{2.5}$$

where p' is the dynamic pressure; A_h and A_v are the horizontal and vertical eddy viscosity coefficients. Under the mentioned assumptions the cross-channel momentum balance reduces to

$$v = 0, \tag{2.6}$$

where v is the cross-channel velocity component. Given the absence of cross-channel variations and flow, estuarine dynamics will only be described in the (x, z)-plane from here on. The vertical momentum balance reduces to hydrostatic balance

$$0 = -\frac{1}{\rho_0}\frac{\partial p'}{\partial z} - \beta g s, \tag{2.7}$$

with gravitational acceleration $g = 9.81$ m s^{-2}. Finally, the continuity equation reads

$$\frac{\partial u}{\partial x} + \frac{\partial w}{\partial z} = 0. \tag{2.8}$$

2.2.3 Boundary conditions

The governing equations are closed with the following boundary conditions.

Surface boundary

At $z = 0$ a vanishing vertical salt flux and vertical velocity (rigid lid) is assumed, as well as no alongchannel wind stress. Hence

$$\frac{\partial s}{\partial z}|_{z=0} = 0, \tag{2.9}$$

$$w|_{z=0} = 0, \tag{2.10}$$

$$\frac{\partial u}{\partial z}|_{z=0} = 0. \tag{2.11}$$

Bottom boundary

At $z = -H$ a vanishing vertical salt flux and vertical velocity is assumed, as well as a no-slip condition. Hence

$$\frac{\partial s}{\partial z}|_{z=-H} = 0, \tag{2.12}$$

$$w|_{z=-H} = 0, \tag{2.13}$$

$$u|_{z=-H} = 0. \tag{2.14}$$

Riverward boundary

The riverward boundary, $x = L$, is defined as the furthest up-estuarine reach of salt. Completely fresh water is thus found everywhere at and riverward of this position, expressed in boundary conditions as

$$s|_{x=L} = 0, \text{ and} \tag{2.15}$$

$$\frac{\partial s}{\partial x}|_{x=L} = 0, \tag{2.16}$$

so that there is no salt flux through the riverward boundary. From (2.16) and e.g. *MacCready* [2004] follows that the baroclinic velocity u_c vanishes here, since there is no baroclinic driving force. Assuming that the vertical velocity component is purely baroclinic, this yields

$$u|_{x=L} = u_Q \tag{2.17}$$

$$w|_{x=L} = 0, \tag{2.18}$$

with $u_Q(z)$ the river discharge velocity field, and $u = u_Q + u_c$. Finally, the river discharge condition reads

$$u_R = \frac{1}{H}\int_{-H}^{0} u \; dz, \tag{2.19}$$

with depth-averaged river discharge velocity u_R. Note that, by definition of u_c, its depth-average vanishes. For the current model, $u_R \leq 0$. The discharge condition is satisfied irrespective of the along-channel position.

Seaward boundary

At the seaward boundary, $x = 0$, conditions for the salinity and flow fields are required as well. Contrary to formulations used by e.g. *Festa & Hansen* [1976], it is shown in §2.3 and 2.4 that such a closure cannot be adopted for the current model. After discussing essential additional assumptions on the estuarine flow and salt field in these sections, alternative boundary conditions are introduced in section §2.6.

Horizontal pressure gradient

Finally, an expression for horizontal pressure gradient $\frac{\partial p'}{\partial x}$ is required. The pressure condition at the rigid lid reads [*Cushman-Roisin & Beckers*, 2011]

$$p'|_{z=0} = p_{atm} + \rho_0 g \eta, \tag{2.20}$$

with atmospheric pressure p_{atm} at sea level. With this condition, integration of hydrostatic balance (2.7) and taking the x-derivative yields

$$\frac{\partial p'}{\partial x} = \frac{dp_{atm}}{dx} + \rho_0 g \frac{d\eta}{dx} + \rho_0 \beta g \int_z^0 \frac{\partial s(x, \tilde{z}, t)}{\partial x} d\tilde{z}.$$

Since vertical variations in the horizontal salinity gradient are typically very small for estuaries, the pressure gradient is written as

$$\frac{\partial p'}{\partial x} = \frac{dp_{atm}}{dx} + \rho_0 g \frac{d\eta}{dx} - \rho_0 \beta g \frac{\partial s}{\partial x} z. \tag{2.21}$$

An expression for the free-surface gradient can be found by assuming, only for this purpose, that the along-channel momentum balance is dominated by pressure gradient and vertical mixing, with constant eddy viscosity, i.e.

$$0 \approx -\frac{1}{\rho_0} \frac{\partial p'}{\partial x} + A_v \frac{\partial^2 u}{\partial z^2}. \tag{2.22}$$

Substituting (2.21) into (2.22), depth-integrating three times, again assuming for the moment that $\frac{\partial s}{\partial x}$ is approximately independent of z and applying boundary conditions (2.11), (2.14) and discharge condition (2.19), an expression for $\frac{d\eta}{dx}$ is obtained [*MacCready*, 2004]. The pressure gradient becomes

$$\frac{\partial p'}{\partial x} = -\frac{3 A_v \rho_0}{H^2} u_R - \rho_0 g \beta \left(z + \frac{3}{8} H \right) \frac{\partial s}{\partial x}. \tag{2.23}$$

2.3 Linear approximation of salinity field

The first step towards deriving a subtidal estuarine model in terms of its global variables is identification of these global variables. First, a measure for the estuarine global salinity stratification, both horizontally and vertically, is essential, as will be discussed hereafter. Second, quantification of the basin-averaged estuarine circulation is required, as is considered in §2.4.

The basin-averaged oceanic model introduced by *Maas* [1994, 2004] also identified the global density stratification as one of the involved variables.

Following *Maas*, a "global Taylor expansion" of the dynamic density, i.e. salinity, field is made. This is a multidimensional Legendre series expansion [e.g., *Stienstra*, 2009] with expansion coefficients equal to the moments of the salinity field. Thanks to the physical interpretation of these moments, *Maas* and the current study aim at describing density dynamics through the evolution of these moments.

Maas showed that, owing to the orthogonality of the global expansion, the evolution of each moment is independent of its higher-order moments. Therefore, the expansion can be approximated by a version truncated after any desired order; the higher-order moments need no consideration. *Maas* employed this to linearise a three-dimensional oceanic density field and to reduce its governing partial differential equations to a set of coupled ordinary differential equations.

In the current study, a similar approach is taken to linearise the estuarine salt field. The global Taylor expansion of s around the geometrical centre $(x, z) = \left(\frac{L}{2}, -\frac{H}{2}\right)$ of the estuarine domain reads

$$s(x, z, t) = M(t) + X(t)\left(x - \frac{L}{2}\right) + Z(t)\left(z + \frac{H}{2}\right) + \text{HOTs}, \tag{2.24}$$

where "HOTs" denote higher-order terms. The lowest-order moments (LOMs) are given by

$$M(t) = \frac{1}{LH}\iint s\ dxdz, \tag{2.25}$$

$$X(t) = \frac{\iint \left(x - \frac{L}{2}\right) s\ dxdz}{\iint \left(x - \frac{L}{2}\right)^2\ dxdz}, \tag{2.26}$$

$$Z(t) = \frac{\iint \left(z + \frac{H}{2}\right) s\ dxdz}{\iint \left(z + \frac{H}{2}\right)^2\ dxdz}. \tag{2.27}$$

Throughout this study and unless specified otherwise, integrals imply integration over full basin length or depth, i.e. $\int dx = \int_0^L dx$ and $\int dz = \int_{-H}^0 dz$. Then M is the domain-averaged salinity; X and Z are proportional to the salt field's horizontal and vertical centre-of-mass position relative to $\left(\frac{L}{2}, -\frac{H}{2}\right)$.

In the model presented by *Maas* [1994, 2004], a zero net buoyancy flux is assumed, so that M is constant. It is therefore possible and convenient to redefine the density field as a linear perturbation field which is zero at the geometrical centre and whose basin-averaged density perturbation vanishes. For an estuary, the net buoyancy flux does not vanish in general, so it is either impossible or unpractical to redefine the salinity field in a similar way. Numerical model results of [*Festa & Hansen*, 1976] indicate that linearising the salinity profile is only acceptable when estuarine domain length is varied with the up-estuarine reach of salt, as further motivated in Appendix A.1. Hence, basin length L is here defined as the salt intrusion length, $x = L_i$ (see Figure 1.2), which changes dynamically with forcing conditions, parameter settings and internal dynamics.

Substitution of the seaward boundary definition (2.1) into (2.24) yields an expression for M,

$$M(t) \approx s_0 + \frac{L}{2}X + \frac{H}{2}Z, \tag{2.28}$$

where HOTs were assumed very small. With this expression, the salt field (2.24) can be linearly approximated as (see Figure 2.1)

$$\boxed{s \approx s_0 + xX(t) + (z+H)Z(t),} \tag{2.29}$$

where HOTs in (2.24) were assumed negligibly small as well.

This linear approximation is only acceptable within the so-called "inner domain" of the estuarine basin. As illustrated in Figure 2.1, this inner domain is surrounded by thin "outer layers" in which the HOTs cannot be neglected and s is assumed to deviate from (2.29). This deviation is such that boundary conditions, as given in §2.2.3 are satisfied. The outer layers have thickness δ_s downwards from the surface, thickness δ_b upward from the bottom, thickness

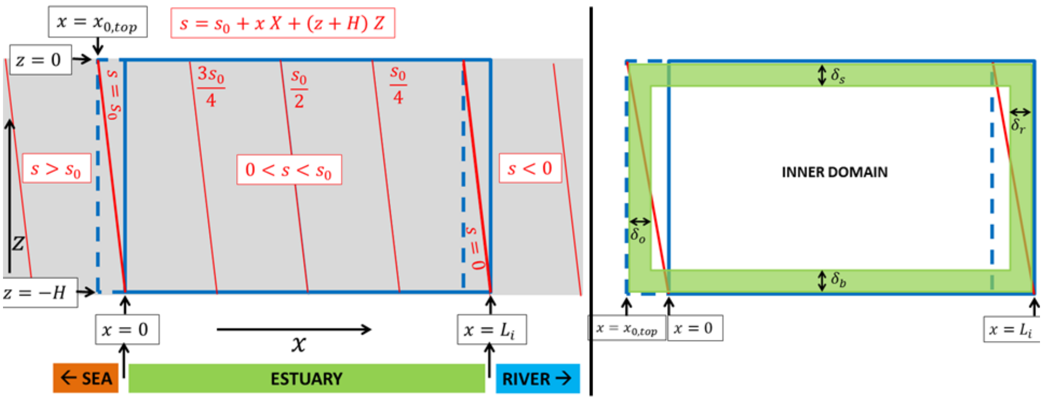

Figure 2.1: Left figure: estuarine integration domain, between $x = 0$, $x = L_i$, $z = -H$ and $z = 0$. Blue dashed line at $x = x_{0,top}$ is the most seaward x-position of estuarine water. Red lines are isohalines of linearised salt field (2.29). Right figure: distinction between "inner domain" (white), in which salt field is linearised (and the flow field too, as will be explained in §2.4), and "outer layers" (green) with thickness δ_s at the surface, δ_b at the bottom, δ_r seaward from the riverward boundary and δ_o up-estuary from the position $x = x_{0,top}$. In the outer layers, linearisation of salt and flow field is not applicable. At the edges of the outer layers, boundary conditions, as in §2.2.3 are satisfied.

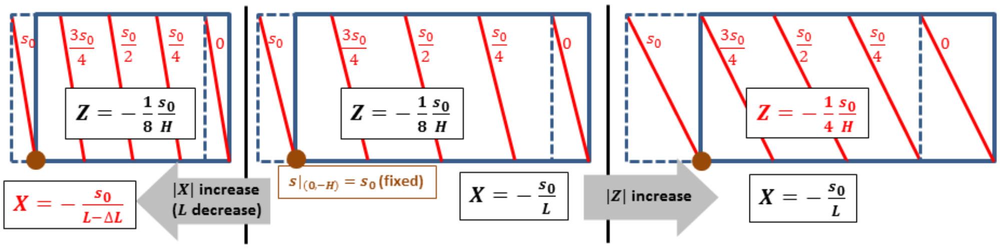

Figure 2.2: Middle figure: default case, with basin-averaged horizontal and vertical salt gradient X and Z and domain length $L = -s_0/X$. Left figure: decreased domain length, hence steeper horizontal salt gradient, while Z is constant. Right figure: increased vertical stratification, while X is constant.

δ_r into the estuary away from the riverward boundary at $x = L$ and thickness δ_o into the estuary away from some point $x = x_{0,top}$, which is outside the estuarine integration domain, i.e. seaward of $x = 0$. The seaward position $x = x_{0,top}$ is defined as the most seaward reach of the ($s = s_0$)-isopycnal, hence from (2.29) this follows as

$$x_{0,top} = -\frac{HZ}{X}. \tag{2.30}$$

From a physical viewpoint, $x_{0,top}$ can be seen as the furthest seaward outflow of estuarine (less saline) water.

In order to satisfy the boundary conditions at the outward bounds, which are not compatible with the linear salt and flow field, the HOTs must be important in the outer layers. However, they are assumed to have only a small influence on *domain*-integrals since the outer layers are assumed very thin. Under this assumption,

$$X(t) \approx \frac{1}{LH}\iint \frac{\partial s}{\partial x}\, dx\, dz \tag{2.31}$$

$$Z(t) \approx \frac{1}{LH}\iint \frac{\partial s}{\partial z}\, dx\, dz, \tag{2.32}$$

i.e. the first order moments of the salt field are approximately equal to the domain-averaged horizontal and vertical salinity gradient, idem to *Maas* [1994; 2004]. For estuaries, it is hence expected that $X \leq 0$ and $Z \leq 0$, i.e. the linear salt field decreases towards the river and the salt field is stably stratified in the vertical. The domain-averaged salinity equals s_0 in the absence of horizontal and vertical stratification and decreases as X or Z become more negative. From here on, X and Z will be always interpreted as (approximately) the domain-averaged horizontal and vertical salinity gradient.

Increased tidal energy will enhance vertical mixing both within the estuary and in its adjacent coastal sea. It is expected that such increased mixing will reduce vertical stratification, so that $|x_{0,top}|$ is reduced. Physically, this can be seen as a reduction of the extent of seaward outflow of estuarine water, as this water is mixed with seawater more rapidly. Note that in the current model, as long as vertical stratification Z is strong enough, $x_{0,top}$ is shifted sufficiently with respect to $x = 0$, so that $x = 0$ lies inside the "inner domain", but if Z is so weak that $|x_{0,top}| < \delta_o$, position $x = 0$ is inside the seaward outer domain.

With $(X, Z) \leq 0$, indeed the up-estuary salinity intrusion is furthest at the bottom. Hence the salt intrusion length L_i is here defined as the point where

$$s(x = L_i, z = -H) = 0. \qquad (2.33)$$

Neglecting HOTs, (2.29) thus yields

$$L(t) = L_i(t) \approx -\frac{s_0}{X(t)}. \qquad (2.34)$$

The salinity intrusion increases if the horizontal salinity gradient weakens, as shown in Figure 2.2.

Note that the model prescribes negative salinity in part of the estuary if $Z < 0$ and that also M becomes negative if vertical stratification becomes very strong. This is inherent to the employed definition of the domain and the linear salt field. It is assumed here that Z is typically weak, corresponding to partially or well mixed estuaries. In this case, M will be positive and it is expected that locally negative salinity values have little influence on the evolution of X and Z and thus these consequences are accepted here.

2.4 Linear approximation of flow field

Maas [1994, 2004] showed that the evolution equations for global density stratification are closed by introduction of an additional moment, the domain-averaged angular momentum vector around the geometrical centre of the three-dimensional oceanic domain. A similar closure will be pursued here, introducing J, the basin-averaged angular momentum, as a measure of estuarine circulation. Since the estuarine basin is in the (x, z)-plane, J is actually the cross-channel (y-) component of a three-dimensional angular-momentum vector. Contrary to the model by *Maas*, J is not defined relative to the *centre* of the domain but with respect to some different rotation axis position $(x, z) = (x_j, z_j)$, defined later in this section. At this position, the horizontal and vertical baroclinic velocity components switch sign.

For estuaries, one can write (see also Figure 2.3)

$$u(x, z, t) = u_Q(z, t) + u_c(x, z, t), \tag{2.35}$$

with u_Q the depth-dependent velocity profile associated with river discharge and u_c the purely baroclinic (density-driven) velocity field. Since J is assumed *only* to measure the gravitational circulation, its definition should exclude u_Q. Furthermore assuming the vertical velocity component w is purely baroclinic,

$$J(t) = \frac{1}{LH} \iint \left[(z - z_j)(u - u_Q) - (x - x_j)\, w \right] \, dx \, dz. \tag{2.36}$$

Contrary to the Lagrangian perspective that was employed by *Maas*, a fully Eulerian perspective is adopted here. Furthermore, multiple "implicit" closures were employed in Appendix A.2 of *Maas* [2004] to relate specific integrals to the angular momentum moment and to close the equations. These closures are based on assumptions of which several are not acceptable for the estuarine case. For both reasons, an alternative method is required to incorporate J into the estuarine equations for X and Z. This method is to derive for (u, w) an expression *explicitly* dependent on the moments (X, Z, J), as is explained below.

2.4.1 Derivation of expression for u and w

Motivated by the typically cubic and quadratic z-profiles for u_c and u_Q respectively [*MacCready*, 2004] (see Figure 2.3), the division of depth into an "inner" or middle layer and a relatively thin surface and bottom layer, as explained in §2.3 and illustrated in Figure 2.1, is also applied to the horizontal velocity profile. Baroclinic component u_c is approximated as a linear profile, $\widehat{u_c}$, in the middle depth-layer. This linearisation is relaxed in the surface and bottom layers, such that the boundary conditions posed in §2.2.3 are satisfied. Further details are given in Appendix A.2.1. Bottom friction affects the river outflow, u_Q, throughout the depth of the column. It is here assumed, however, that the influence of friction is dominant within the thin bottom layer but relatively small upward from this layer. It is therefore assumed that, to lowest order, u_Q is a constant, $\widehat{u_Q}$, at all depths except in the bottom layer, where it decreases to zero at the bottom. Furhermore, the bottom and surface layers are assumed so thin that the deviations in u_c, u_Q from $\widehat{u_c}, \widehat{u_Q}$ in these layers have negligible influence when integrating over the entire domain. Thus in any domain-integral, one might as well replace u_Q and u_c by a profile that is constant respectively linear in z, throughout the *entire* basin-depth, i.e. also in surface and bottom layers. These approximations imply,

$$u_Q \to u_R \quad \text{and} \quad u_c \to u_D \propto -\left(z + \frac{H}{2}\right), \tag{2.37}$$

hence the vertical rotation axis position is at

$$z_j = -\frac{H}{2}. \tag{2.38}$$

Now u is approximated as $u_R + u_D$ throughout the column. Depth-dependent flow component u_D satisfies the condition of zero net baroclinic transport; its magnitude is determined next. Notice that this linearisation inevitably implies that the effect of bottom friction on u_Q is "transferred" to u_c to yield u_R and u_D. Angular momentum J thus becomes

$$\boxed{J(t) = \frac{1}{LH} \iint \left[(z - z_j)\, u_D - (x - x_j)\, w\right]\, dx\, dz}, \tag{2.39}$$

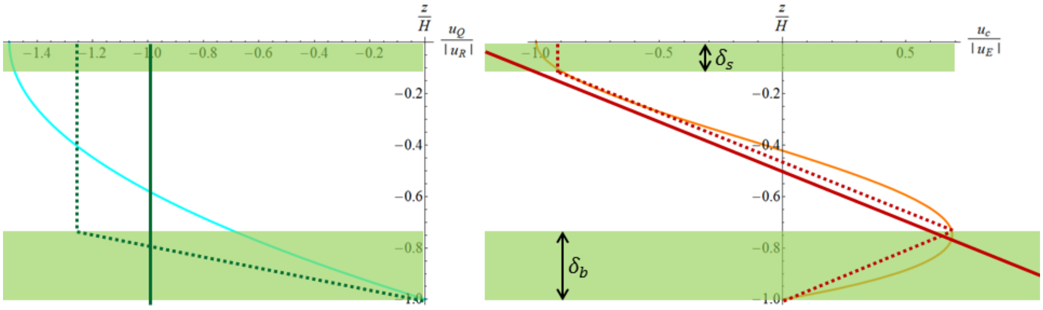

Figure 2.3: Left figure: cyan solid line: scaled river velocity profile $u_Q/|u_R|$ versus dimensionless depth z/H, as in equation (A.1), with depth-averaged (river discharge) velocity $u_R(\leq 0)$. Green shaded area: "outer layers" at surface and bottom. Green dotted line: "initial" low-order approximation of $u_Q/|u_R|$, with $u_Q/|u_R| \to \widehat{u_Q}/|u_R|$ in middle and surface layers ($\widehat{u_Q}$ constant in z) and $u_Q/|u_R|$ decreasing to zero in bottom layer. Green solid line: "final" low-order approximation of $u_Q/|u_R|$, approximating u_Q as a constant, u_R, for all depths. Right figure: orange solid line: scaled baroclinic profile $u_c/|u_E|$ versus dimensionless depth z/H, as in equation (A.1), with exchange flow magnitude u_E (constant in z). Green shaded area: "outer layers" at surface and bottom. Red dotted line: "initial" low-order approximation of $u_c/|u_E|$, with $u_c/|u_E| \to \widehat{u_c}/|u_E|$ in the middle layers ($\widehat{u_c}$ linear in z), $u_c/|u_E|$ satisfying $(\partial u_c/\partial z)|_{z=-H} = 0$ in the surface layer and $u_c/|u_E|$ decreasing to zero in the bottom layer. Red solid line: "final" low-order approximation of $u_c/|u_E|$, approximating u_c as a linear profile u_D for all depths.

and hence also includes the effect of bottom-friction on the river flow. Thus for a typical estuarine ciculation cell, with baroclinic flow seaward (riverward) in the upper (deeper) layers and upwelling (downwelling) on the riverward (seaward) part of the estuary, domain-averaged angular momentum $J \leq 0$.

Assume that w can also be approximated as a linear or constant profile in the middle depth-layer and deviates from this profile in the bottom and surface layer, to satisy $w = 0$ at top and bottom boundary. The velocity components (u_D, w) are assumed to constitute a gravitational circulation cell that is perfectly elliptic to first approximation. This is motivated by the streamfunction profiles presented by *Festa & Hansen* [1976]. Further details are given in Appendix A.2.1.

The circulation cell is confined between the bottom and surface boundaries and by the along-channel positions where the baroclinic pressure gradient force vanishes, i.e. where the horizontal salinity gradient $\frac{\partial s}{\partial x}$ vanishes. It is here assumed that these longitudinal boundaries of the circulation cell are formed by the thin vertical "outer layers" in which $\frac{\partial s}{\partial x}$ and thus (u_D, w) rapidly decrease to zero. It is assumed that $\frac{\partial s}{\partial x}$ vanished at the most seaward respectively landward reach of the ($s = s_0$)-isopycnal respectively ($s = 0$)-isopycnal, i.e. $x = x_{0,top}$ and $x = L_i$, respectively. Further details are given in Appendix A.2.2. Hence

$$\frac{\partial s}{\partial x} = 0 \text{ at } x = x_{0,top} \text{ and } x = L_i, \text{ for all } z. \tag{2.40}$$

From e.g. *MacCready* [2004], the magnitude of the exchange flow is largest where the depth-averaged salinity gradient is largest. It is then natural to choose horizontal cell centre x_j half-way between $x_{0,top}$ and L_i, i.e.

$$x_j = \frac{1}{2}(x_{0,top} + L_i) = -\frac{s_0 + HZ}{2X}, \tag{2.41}$$

as shown in Figure 2.4. The streamfunction profile ψ_D that yields linear expressions for $u_D = -\frac{\partial \psi_D}{\partial z}$ and $w = \frac{\partial \psi_D}{\partial x}$ and describes this elliptic circulation cell reads

$$\psi_D = \psi_0 \left[\left(\frac{x - x_j}{L_i - x_j} \right)^2 + \left(\frac{z - z_j}{0 - z_j} \right)^2 \right]. \tag{2.42}$$

Then $u_D = -\frac{8}{H^2}\psi_0 \left(z + \frac{H}{2}\right)$ and $w = 4\psi_0 \frac{X(s_0 + 2xX + HZ)}{(s_0 - HZ)^2}$. Substitution of these expressions in definition (2.39) for J yields an expression for streamfunction

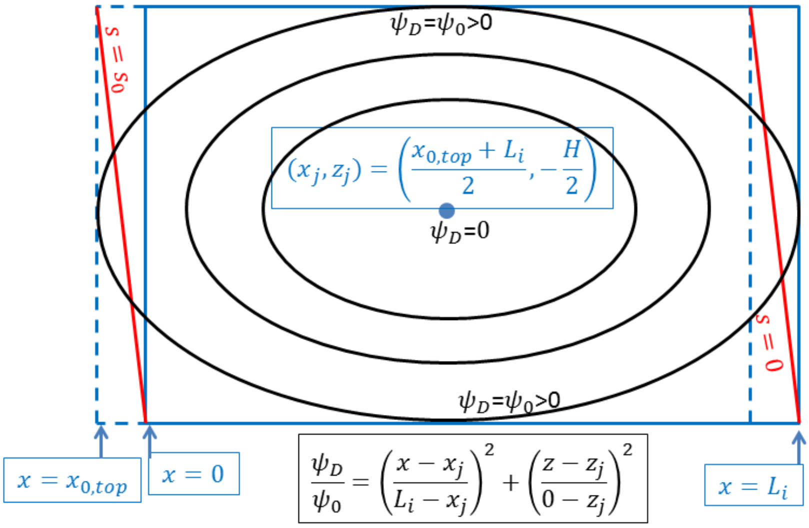

Figure 2.4: Illustration of baroclinic streamfuncion field ψ_D, as in (2.42), elliptical and centred around the rotation-axis position $\{x_j, z_j\}$; horizontally bounded by $x = x_{0,top}$ and $x = L_i$ and vertically by $z = 0$ and $z = -H$.

magnitude ψ_0, so that

$$\boxed{u \approx u_R + \frac{6\ A(Z)\ J}{H^2\ B(Z)} \left(z + \frac{H}{2}\right)}\ , \tag{2.43}$$

$$\boxed{w \approx -\frac{3H\ X\ Z\ J}{B(Z)} - \frac{6X^2\ J}{B(Z)} \left(x - \frac{L}{2}\right)}\ , \text{ with} \tag{2.44}$$

$$\boxed{A(Z) = (s_0 - HZ)^2} \text{ and } \boxed{B(Z) = (s_0^2 + HZ(-s_0 + 2HZ))}. \tag{2.45}$$

These linear expressions for u and w are *only* acceptable in the "inner domain"; HOTs become important in the outer layers in order to satisy boundary conditions. Note that, with the employed expression (2.42) for ψ_D, the horizontal velocity is (to lowest order) only dependent on z and the vertical velocity is only dependent on x.

2.4.2 Interpretation of linearised (u, w)

From here on, assume $(X, Z, J) \leq 0$, as expected for estuaries. The expressions for u_D and w indeed give a baroclinic flow field that is seaward (riverward) above (below) $z = z_j$ and upward (downward) riverward (seaward) of $x = x_j$. Dependencies of (u_D, w) on (X, Z, J) are interpreted below.

Net vertical transport $\mathcal{W}$

Domain-averaged vertical transport, $\mathcal{W} = -\frac{3H\ X\ Z\ J}{B(Z)}$, is always upward since the circulation cell is never enclosed completely within the integration domain for $Z < 0$ (see Figure 2.4). As Z becomes more negative, an increasingly large part of the downwelling flow is seaward of $x = 0$. These currents and hence $\mathcal{W}$ are stronger if J is stronger. For $Z < -\frac{s_0}{H}$, rotation axis x_j is seaward of $x = 0$ and thus part of the *upwelling* region is too. Hence, one might expect that $\mathcal{W}$ decreases again once Z becomes steeper than $-\frac{s_0}{H}$. In fact, however, this decrease starts when $Z < -\frac{\sqrt{2}}{2}\frac{s_0}{H}$. The fact that this decrease starts already for weaker stratification can possibly be explained by other effects, such as longitudinal stretching of the circulation cell and hence weaker $w = \frac{\partial \psi_D}{\partial x}$, if Z becomes more negative. Such stretching also happens when L increases, i.e. when X weakens to zero. Alternatively, $\mathcal{W}$ is weaker when averaged over a longer domain, hence $\mathcal{W} \propto -X$. The proportionality to H is probably because the baroclinic pressure gradient force, and thus net upwelling, is stronger for larger depth.

Horizontal gradient of w

Velocity gradient $\frac{\partial w}{\partial x}$ gives the upwelling/downwelling strength and thus proportional to J. If $|X|$ weakens to zero, so does $\frac{\partial w}{\partial x}$. This is either due to the vanishing of the baroclinic pressure gradient force in this case, or because the domain becomes increasingly long, so that $\frac{\partial \psi_D}{\partial x} = w$ is reduced. For more stable stratification, $\frac{\partial w}{\partial x}$ weakens. Also, $\frac{\partial u}{\partial z}$ weakens when Z becomes more negative than $-\frac{s_0}{3H}$. Both effects might be interpreted as the surpressing effect of vertical stratification on the exchange flow. This is illustrated by the domain-averaged steady salt balance for long (> 30 km) and partially to well mixed estuaries [equation (2.17) of *Valle-Levinson*, 2010]. This balance is between net gain of salt due to the exchange flow acting on a vertically stratified estuary and net loss of salt due to river flow. A stronger vertically stratified estuary hence requires a smaller exchange flow to balance the river-induced outflow of salt.

Vertical gradient of u_D

As mentioned above, $\frac{\partial u_D}{\partial z}$ weakens with strengthening Z, but only for $Z < -\frac{s_0}{3H}$. The strengthening of $\frac{\partial u_D}{\partial z}$ with strengthening vertical stratification as long as $Z > -\frac{s_0}{3H}$ is due to other mechanisms. These might include the coupling between u_D and w via ψ_D, so that u_D changes when w changes. Furthermore, $\frac{\partial u_D}{\partial z} \propto \frac{1}{H^2}$, contrary to the expectation that the baroclinic pressure gradient and thus exchange flow increases with increasing depth. This behaviour is a direct consequence of the assumption of an elliptic streamfunction profile whose semi-major axis is proportional to water depth. The smaller the depth, the stronger the vertical gradient in ψ_D, so that u_D becomes stronger. It is expected, however, that u_D is not as strongly weakened with increasing depth, because $|J|$ is expected to increase with depth. Finally note that u_D is not related to density gradient X. It depends on baroclinicity indirectly via J however.

2.5 Evolution equations in general form

Now that all dynamic variables s, u and w have been described in terms of X, Z and J, evolution equations for these low-order moments are pursued. This is done by taking the time derivatives of their respective definitions (2.26), (2.27) and (2.39), as is further explained in Appendix B.1. For the Eulerian perspective employed herein, $\frac{dx}{dt} = 0$ and $\frac{dw}{dt} = 0$. Some domain-integrals contain one of the terms $\frac{\partial s}{\partial t}$, $\frac{\partial u}{\partial t}$ or $\frac{\partial w}{\partial t}$. There, substitute respectively salt balance (2.3), $x-$momentum balance (2.5) and "0". The latter is based on the assumption that $\frac{\partial w}{\partial t}$ is negligible, since the vertical momentum balance (2.7) is assumed to reduce to hydrostatic balance.

Most terms on the right-hand sides of the resulting equations are spatial integrals containing (products of) s, u or w and their spatial derivatives. If *domain*-integrals contain any of the terms

$$\frac{\partial^2 s}{\partial x^2},\ \frac{\partial^2 s}{\partial z^2},\ \frac{\partial u}{\partial x},\ \frac{\partial w}{\partial z},\ \text{or higher-order derivatives of } s, u, w, \tag{2.46}$$

the linearised expressions (2.29), (2.43) and (2.44) can *not* be substituted, because the constant and linear terms in these expressions would vanish, so that the unspecified higher-order terms cannot be neglected anymore. In other words, as long as the lowest-order (constant or linear) approximation yields nonzero terms, it is acceptable to ignore nonlinearities in the thin outer layers, when integrating over the entire domain. However, for terms in (2.46), these nonlinearities may be dominant. Domain-integrals containing such terms must hence be rewritten with partial integration into boundary integrals and other domain integrals whose integrand *can* be computed with the linearised (s, u, w). Whenever domain integrals contain none of the previous terms, but *only* any or several of the terms

$$s,\ \frac{\partial s}{\partial x},\ \frac{\partial s}{\partial z},\ u,\ \frac{\partial u}{\partial z},\ w,\ \frac{\partial w}{\partial x}, \tag{2.47}$$

multiplied by any polynomial in x or z, the linearised (s, u, w) are substituted.

Viscous and diffusive coefficients $A_{h,v}, K_{h,v}$ are assumed constant within the "inner" domain. In the outer layers, these coefficients may differ from their "inner" values and be spatially dependent. However, as argued above, the outer layers are assumed so thin that both their local nonlinearities in (s, u, w) and deviations in $A_{h,v}, K_{h,v}$ from the constant "inner" values have negligible influence on the domain-integrals. Hence, in any domain-integral, the "inner" values for $A_{h,v}, K_{h,v}$ can be used. Only in cases where terms from (2.46) are involved, the viscous and diffusive "outer layer"-coefficients are used. Diffusivity and viscosity coefficients in domain-integrals are denoted by subscript "int", e.g. $K_{v,int}$; in boundary integrals, the boundary is specified in these coefficients by a corresponding subscript, e.g. $A_{v,bot}$ at $z = -H$.

Finally, the boundary conditions from §2.2.3 are applied, as is shown in Appendix B.2. Assuming that u_D vanishes in total when the baroclinic driving force vanishes at $x = L$ and after reducing river profile u_Q to a constant, u_R, the boundary condition (2.17) becomes

$$u|_{x=L} = u_R. \tag{2.48}$$

The evolution equation for X, Z and J are then given by (2.56), (2.64) and (2.69). For convenience, these equations are presented in §2.7 rather than here, to present them together with the interpretation of each individually contributing term. Note that the terms (4), (8), (9), (18) and (19) vanish when using the boundary conditions.

The linear expressions (2.29), (2.43) and (2.44) for s, u and w must be substituted to close these equations. In addition, boundary conditions for s, $\frac{\partial s}{\partial x}$, u_D and w at the seaward boundary and an expression for $\frac{\partial u}{\partial z}$ at the bottom are required. These conditions are presented hereafter.

2.6 Additional boundary conditions

Bottom boundary

In addition to the no-slip relation, an expression for $\left(A_v \frac{\partial u}{\partial z}\right)|_{z=-H}$ is required. Assume that the bottom layer has thickness δ_b and that u is approximately linear within this layer. Then

$$\left(A_v \frac{\partial u}{\partial z}\right)|_{z=-H} = A_{v,bot} \frac{\widehat{u}|_{z=-H+\delta_b}}{\delta_b}, \tag{2.49}$$

where $\widehat{u}$ is the linear profile (2.43) in the inner domain. Hereafter, both δ_b is used, as well as its dimensionless counterpart

$$\epsilon_b = \frac{\delta_b}{H}. \tag{2.50}$$

Seaward boundary

Festa & Hansen [1976] employ the fact that the circulation cell is well developed at the seaward boundary, $x = 0$, to formulate the corresponding boundary conditions for salt and flow field. As illustrated in Figure 2.1, this also applies to the current estuarine model, as long as Z is sufficiently strong that seaward boundary $x = 0$ is *not* within the seaward "outer layer" between $x = x_{0,top}$ and $x = x_{0,top} + \delta_o$. If Z would always be strong enough, then the seaward boundary conditions would just be

$$\begin{aligned}
s|_{x=0} &= \widehat{s}|_{x=0}, \\
\frac{\partial s}{\partial x}|_{x=0} &= X, \\
u_D|_{x=0} &= \widehat{u_D}|_{x=0}, \\
w|_{x=0} &= \widehat{w}|_{x=0},
\end{aligned}$$

where $\widehat{s}$ is from the linear salt field (2.29) and $\widehat{u_D} = \widehat{u} - u_R$, where $\widehat{u}$ is u from (2.43) and $\widehat{w}$ is from (2.44).

However, these closure relations do not hold for very weak stratification, since $\frac{\partial s}{\partial x}|_{x=0}$, $u_D|_{x=0}$ and $w|_{x=0}$ all rapidly weaken as soon as $x = 0$ shifts into the seaward "outer layer" and vanish completely for vanishing vertical stratification. The linear expression $\widehat{s}$ *does* remain valid also for such very weak values of Z, so its boundary condition reads

$$s|_{x=0} = \widehat{s}|_{x=0} = s_0 + (z + H)Z. \tag{2.51}$$

To ensure that the seaward boundary conditions for salinity gradient and baroclinic flow field are applicable for *any possible* vertical stratification strength, including vanishing Z, some formulation

$$\begin{aligned}
\frac{\partial s}{\partial x}|_{x=0} &= P_s(Z)\ X, \\
u_D|_{x=0} &= P_u(Z)\ \widehat{u_D}|_{x=0}, \\
w|_{x=0} &= P_w(Z)\ \widehat{w}|_{x=0},
\end{aligned}$$

is pursued, where $P_{s,u,w}(Z) = 1$ for all Z, except when Z becomes very weak, and $P_{s,u,w}(Z = 0) = 0$. The function

$$P(Z) \propto \left(-\frac{ZH}{s_0}\right)^{1/n}$$

approximates this behaviour increasingly well for increasing constant $n >> 1$. However, choosing a large value for n severely complicates the boundary conditions and thus the model, which will hinder (analytical) study of the model results. Instead, the simplest possible formulation, where $n = 1$, is chosen,

$$\frac{\partial s}{\partial x}|_{x=0} = -\frac{c\ H\ Z}{s_0}X, \tag{2.52}$$

$$u|_{x=0} = u_R - \frac{a\ H\ Z}{s_0}\widehat{u_D}|_{x=0}, \tag{2.53}$$

$$w|_{x=0} = -\frac{b\ H\ Z}{s_0}\widehat{w}|_{x=0}. \tag{2.54}$$

Positive constants a, b and c are chosen such that the magnitude of $\frac{\partial s}{\partial x}|_{x=0}$, $u_D|_{x=0}$ and $w|_{x=0}$ never exceeds the magnitude of X, $\widehat{u_D}|_{x=0}$ and $\widehat{w}|_{x=0}$, respectively, i.e.

$$0 \leq\ -\{a, b, c\}\frac{HZ}{s_0}\ \leq 1. \tag{2.55}$$

2.7 Evolution equations in final form

Application of the boundary conditions from §2.2.3 yielded (see §2.5) equations (2.56), (2.64) and (2.69), which are presented below. The evolution equations below are divided into separate terms, such that each term has a distinct physical meaning. Subsequently, the remaining boundary conditions from §2.6 and the linear salt and flow fields (2.29), (2.43) and (2.44) are substituted in each of these terms. These terms are presented here and interpreted individually, always assuming that $(X, Z, J) \leq 0$.

Several terms on the right-hand side of the evolution equations contain a time derivative. It is easier to interpret these time-dependent terms all at the same time, which is done in §2.7.4

Hereafter and throughout this study, descriptions like "stronger", "weaker" or "enhanced" always refer to the *absolute magnitude* of X, Z, J and u_R, even though their values are always ≤ 0. Hence "strengthening J" implies that the circulation gets stronger, i.e. J becomes more *negative*. Symbols $\uparrow$ and $\downarrow$ will be used throughout this report to indicate that some value (mostly zero) is approached from smaller or from larger values, respectively.

2.7.1 Evolution of X

After application of the boundary conditions from §2.2.3 (further details in Appendix B.2), the evolution equation (B.3) for X reduces to (recall that term (4) vanished in previous steps)

$$\frac{dX}{dt} = \underbrace{-\frac{6}{L^3 H}\frac{dL}{dt}\iint s\ dxdz}_{(1)} \tag{2.56}$$

$$+\underbrace{\frac{12}{L^3H}\iint u_R\ s\ dxdz}_{(2a)}+\underbrace{\frac{12}{L^3H}\iint u_D\ s\ dxdz}_{(2b)}\underbrace{-\frac{12}{L^3H}\iint K_{h,int}\frac{\partial s}{\partial x}\ dxdz}_{(2c)}$$

$$\underbrace{-\frac{6}{L^2H}\int (u_R\ s)\,|_{x=0}\ dz}_{(3a)}\underbrace{-\frac{6}{L^2H}\int (u_D\ s)\,|_{x=0}\ dz}_{(3b)}+\underbrace{\frac{6}{L^2H}\int \left(K_{h,sea}\ \frac{\partial s}{\partial x}\right)|_{x=0}\ dz}_{(3c)}$$

$$\underbrace{-\frac{3}{L}\frac{dL}{dt}X}_{(5)},$$

Boundary conditions and linear (s, u, w) are substituted. Then

$$(2a) = \frac{12u_R}{L^2}M = \frac{12u_R}{s_0^2}X^2\left(\frac{s_0+HZ}{2}\right). \tag{2.57}$$

Term $(2a)$ is the domain-averaged seaward salt flux due to advection of domain-averaged salinity M by river flow velocity u_R. As long as $M > 0$, i.e. for $Z > -\frac{s_0}{H}$, this flux is negative. The river then causes a seaward retreat of the intrusion length, or steepening of salt gradient X, i.e. $\frac{dX}{dt} = \frac{s_0}{L^2}\frac{dL}{dt} < 0$.

$$(2b) = \frac{6A(Z)JX^2Z}{s_0^2B(Z)} \tag{2.58}$$

Term $(2b)$ is the domain-averaged horizontal salt flux due to exchange flow u_D acting on a vertically stratified salt field, importing saltier water and exporting fresher water. In the absence of vertical stratification, the exchange salt flux vanishes, even though u_D may be nonzero. Flux $(2b)$ weakens horizontal salt gradient X due to the net up-estuarine advection of salt by u_D, thus increasing the intrusion length, as illustrated in Figure 2.5.

$$(2c) = -\frac{12K_{h,int}X^3}{s_0^2} \tag{2.59}$$

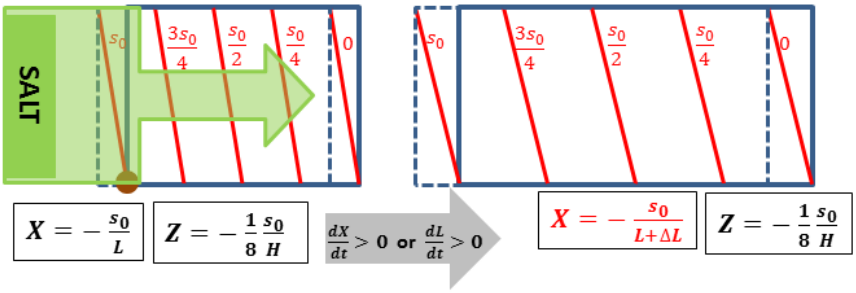

Figure 2.5: Positive (inward) basin-averaged horizontal salt flux increases the up-estuarine reach of salt and hence increases L_i, or weakens horizontal salinity gradient X. This is the case for terms (2b) and (2c). Term (2a) does the opposite (decreasing L), as long as vertical stratification $|Z| < -s_0/H$.

Term (2c) represents the domain-averaged diffusive horizontal salt flux, spreading salt up-estuary, hence stretching the domain or weakening X.

$$(3a) = -\frac{6u_R X^2}{s_0^2}\left(s_0 + \frac{HZ}{2}\right) \tag{2.60}$$

Since river discharge velocity u_R is a constant, it can be taken outside the integral in term (3a). This term therefore represents the river-induced outward advection of the salinity, depth-averaged over the seaward boundary, $\bar{s}|_0$, where

$$\bar{s}|_0 = \frac{1}{H}\int_{-H}^{0} s\ dz = s_0 + \frac{HZ}{2}. \tag{2.61}$$

As long as $\bar{s}|_0 > 0$, i.e. for $Z > -\frac{2s_0}{H}$, flux (3a) decreases the seaside-averaged salinity, which reduces the domain-averaged horizontal salinity gradient, i.e. $\frac{dX}{dt} > 0$. Note that the two river-induced salt fluxes, i.e. (2a) acting throughout the domain and (3a) acting at the seaside only, can have opposite effects on $\frac{dX}{dt}$, for particular values of Z.

$$(3b) = \frac{3aHA(Z)JX^2Z^2}{s_0^3 B(Z)} \tag{2.62}$$

Term (3b) represents the depth-averaged exchange flow-induced salt flux at the seaward boundary. If $Z \uparrow 0$, the circulation cell is closed at the seaward bound so that u_D vanishes at $x = 0$.

As long as $Z < 0$, horizontal exchange flow u_D at $x = 0$ increases the depth-averaged salinity at the seaward bound. The domain-averaged along-channel salt gradient X thus becomes larger, i.e. $\frac{dX}{dt} < 0$ (see Figure 2.6). Hence exchange flow u_D that transports salt at the seaward boundary only (3b) has an opposite effect on $\frac{dX}{dt}$ than u_D transporting salt throughout the estuary (2b).

$$(3c) = -\frac{6cHK_{h,sea}X^3Z}{s_0^3} \tag{2.63}$$

Term (3c) is the diffusive horizontal salt flux, depth-averaged over the seaward boundary. Seaside salinity gradient $\frac{\partial s}{\partial x}|_{x=0}$ scales with Z, hence so does (3c). Idem to (3b), $\bar{s}|_0$ is increased, steepening X.

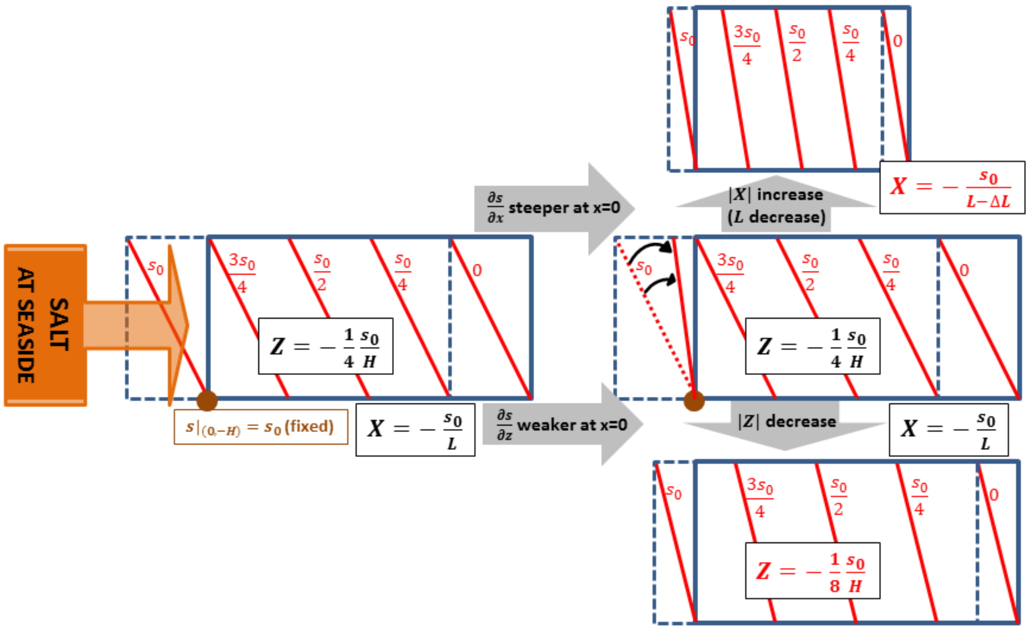

Figure 2.6: Effect of positive depth-averaged salt transport at the seaward boundary, $x = 0$ (middle left and right figures). This flux increases the total salinity at $x = 0$. Since salinity at the seaward bottom has fixed value, this results in i) local weakening of vertical salt gradient $\partial s/\partial z$ and ii) local strengthening of horizontal salt gradient $\partial s/\partial x$. Averaged over the domain, this results in i) a decrease of $|Z|$ (bottom figure) and ii) an increase of $|X$ (top figure).

2.7.2 Evolution of Z

After application of the boundary conditions from §2.2.3 (further details in Appendix B.2), the evolution equation (B.8) for Z reduces to (recall that terms (8) and (9) vanished in previous steps)

$$\frac{dZ}{dt} =$$
$$\underbrace{\frac{12}{LH^3}\int (z\ u_R\ s)\,|_{x=0}\ dz}_{(6a)} + \underbrace{\frac{12}{LH^3}\int (z\ u_D\ s)\,|_{x=0}\ dz}_{(6b)} \underbrace{-\frac{12}{LH^3}\int \left(z\ K_{h,sea}\frac{\partial s}{\partial x}\right)|_{x=0}\ dz}_{(6c)}$$
$$+\underbrace{\frac{12}{LH^3}\iint w\ s\ dxdz}_{(6d)} \underbrace{-\frac{12}{LH^3}\iint K_{v,int}\ \frac{\partial s}{\partial z}\ dxdz}_{(6e)} \tag{2.64}$$
$$+\underbrace{\frac{6}{LH^2}\int (u_R\ s)\,|_{x=0}\ dz}_{(7a)} + \underbrace{\frac{6}{LH^2}\int (u_D\ s)\,|_{x=0}\ dz}_{(7b)} \underbrace{-\frac{6}{LH^2}\int \left(K_{h,sea}\ \frac{\partial s}{\partial x}\right)|_{x=0}\ dz}_{(7c)}$$
$$\underbrace{-\frac{1}{L}\frac{dL}{dt}Z}_{(10)}$$

Boundary conditions and linear (s, u, w) are substituted. Term $(6a, b, c)$ together is the "depth-weighted" horizontal salt flux, depth-averaged over the seaward boundary. This flux is due to river flow $(6a)$, exchange flow $(6b)$ and diffusion $(6c)$, all evaluated at the seaside. They read

$$(6a) = \frac{6u_R X}{Hs_0}\left(s_0 + \frac{HZ}{3}\right); (6b) = \frac{6aA(Z)JXZ}{Hs_0B(Z)}; (6c) = \frac{6cK_{h,sea}X^2Z}{s_0^2} \tag{2.65}$$

Term $(6b)$ and $(6c)$ vanish if $Z \uparrow 0$ due to seaward boundary conditions (2.53) and (2.52).

Note that term $(6a)$ can be both negative and positive, dependent on the vertical stratification strength. The term is interpreted as follows. River-

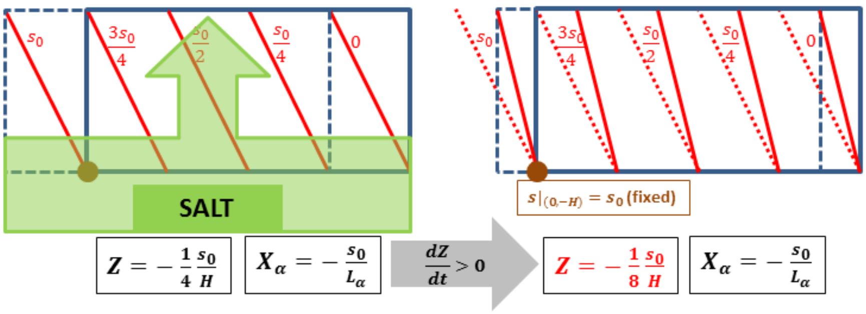

Figure 2.7: Domain-averaged vertical transport of salt increases salinity in shallower layers and decreases salinity in deeper layers. This weakens the vertical stratification.

induced salt flux at the seaward bound, $u_R s|_{x=0}$, is weighted with depth z, so the contribution of this flux in the deepest layers is most important. For stable stratification $Z < 0$, $u_R s|_{x=0}$ is always < 0 at the bottom and becomes less negative (or even positive, dependent on Z) towards the surface. If Z is weak, $u_R s|_{x=0}$ stays negative over a relatively long range upward from the bottom. Hence, $u_R s|_{x=0}$ strongly decreases salinity in the deeper layers at $x = 0$, which makes stratification less stable, i.e. $\frac{dZ}{dt} > 0$. However, as Z becomes stronger (Z more negative), $u_R s|_{x=0}$ becomes much more rapidly less negative, upward from the bottom. $u_R s|_{x=0}$ may even become positive in relatively deep layers, if Z is strong enough. Hence, as Z becomes stronger, $u_R s|_{x=0}$ causes less decrease of deep-layer salinity, i.e. $\frac{dZ}{dt}$ becomes less positive. If Z becomes strong enough, namely $Z < -\frac{3s_0}{H}$, term (6a) even *stabilises* the stratification, i.e. $\frac{dZ}{dt} < 0$.

In term (6b), exchange flux $(u_D s)|_{x=0}$ always increases salinity in deeper layers at $x = 0$ and increases salinity less (or even decreases salinity) in shallower layers. $(u_D s)|_{x=0}$ is also weighted with depth, so the flux in the deeper layers contributes most. This stabilises vertical stratification.

Diffusive salt flux $-K_{h,sea}\frac{\partial s}{\partial x}|_{x=0}$ in (6c) increases salinity at $x = 0$ but is constant with depth. However, this flux is weighted with depth, so the salinity-increase in deeper layers contributes more, i.e. $\frac{dZ}{dt} < 0$.

$$(6d) = -\frac{6JX}{H^2 B(Z)}\left(s_0^2 + 3HZ[s_0 + HZ]\right) \tag{2.66}$$

Term (6d) is the domain-averaged, vertical advective salt flux due to baroclinic flow component w. If the domain-averaged vertical advective salt flux is upward, this increases (decreases) salinity in the upper (deeper) layers, weakening the vertical stratification, as illustrated in Figure 2.7. However, it is found that the Z-dependent part, $\left(s_0^2 + 3HZ[s_0 + HZ]\right)/B(Z)$, is always positive, so that (6d) is always negative. Hence (6d) *strengthens* vertical stratification, contrary to the reasoning above. The reason for this is probably that, towards the river, salinity decreases and finally becomes negative, whereas w becomes more positive if you move riverward past $x = x_j$. Hence, more negative salinity is advected more strongly upward, such that the domain-averaged vertical salt flux is downward.

$$(6e) = -\frac{12K_{v,int}Z}{H^2} \tag{2.67}$$

Term (6e) is the domain-averaged vertical diffusive salt flux. Internal diffusive mixing weakens the existing stratification.

The combined terms (7a, b, c) represent the horizontal salt flux, depth-averaged over the seaward boundary, with

$$(7a) = -\frac{6u_R X}{H s_0}\left(s_0 + \frac{HZ}{2}\right); (7b) = \frac{3aA(Z)JXZ^2}{s_0^2 B(Z)}; (7c) = -\frac{6cK_{h,sea}X^2 Z}{s_0^2} \tag{2.68}$$

Remember that via equation (2.1), salinity at the seaside bottom is fixed. Hence, for any positive (inward) depth-averaged horizontal salt flux, the resulting increase of $\bar{s}|_0$ (salinity depth-averaged over seaward boundary, see (2.61)) can *only* be obtained by a weakening of the local vertical salt gradient $\frac{\partial s}{\partial z}|_{x=0}$. So $\frac{dZ}{dt} > 0$. Such a positive depth-averaged salt flux can be either due to exchange flux $(u_D s)|_{x=0}$ in $(7b)$, similar to $(3b)$, or due to diffusive flux $(7c)$, as illustrated in Figure 2.6. As long as $\bar{s}|_0 > 0$, i.e. for $Z > -\frac{s_0}{H}$, the river flux $(7a)$ *decreases* $\bar{s}|_0$, enhancing Z. For $Z < -\frac{s_0}{H}$, also $(7a)$ weakens Z.

2.7.3 Evolution of J

After application of the boundary conditions from §2.2.3 (further details in Appendix B.2), the evolution equation (B.12) for J reduces to (recall that terms (18) and (19) vanished in previous steps)

$$\begin{aligned}\frac{dJ}{dt} = &\underbrace{-\frac{1}{L}\frac{dL}{dt}J}_{(11)} + \underbrace{\frac{1}{LH}\int \left[(z-z_j)u^2\right]|_{x=0}\, dz}_{(12)} \\ &+ \underbrace{\frac{1}{LH}\iint u\ w\ dxdz}_{(13)} \underbrace{-\frac{1}{LH}\iint (z-z_j)\frac{1}{\rho_0}\frac{\partial p'}{\partial x}\, dxdz}_{(14)} \underbrace{-\frac{1}{LH}\int (A_{h,sea}\ w)|_{x=0}\, dz}_{(15)} \\ &\underbrace{-\frac{1}{LH}\int \left((z-z_j)A_{v,bot}\frac{\partial u}{\partial z}\right)|_{z=-H}\, dx}_{(16a)} \underbrace{-\frac{1}{LH}\iint A_{v,int}\frac{\partial u}{\partial z}\, dxdz}_{16b} \\ &+ \underbrace{\frac{dx_j}{dt}\frac{1}{LH}\iint w\ dxdz}_{(17)}.\end{aligned} \tag{2.69}$$

Boundary conditions and linear (s, u, w) are substituted. Getting rid of all odd terms in the integrand of (12), see Appendix B.2, it reduces to

$$(12) = \frac{1}{LH}\int (z-z_j)\,(2u_R\ u_D)\,|_{x=0}\, dz = \frac{aHu_R A(Z)JXZ}{s_0^2 B(Z)} \tag{2.70}$$

In term (12), angular momentum at the seaward boundary, $(z-z_j)u_D|_{x=0}$, is advectively transported by river flow u_R. Since u_R is out of the estuary, there is loss of angular momentum, hence the estuarine circulation slows down, i.e. $\frac{dJ}{dt} > 0$.

$$(13) = \frac{1}{LH} \iint u_R w \; dxdz = -\frac{3Hu_R JXZ}{B(Z)}. \tag{2.71}$$

The first equality is because w only depends on x, such that the odd function u_D cancels in (13). This term is the river-induced advection of w-momentum. For $Z < 0$, domain-averaged flow is upward, $\mathcal{W} > 0$, and rotation axis x_j is seaward of the geometrical centre of the integration domain, $x_j < L/2$. Hence the net uplift $\mathcal{W}$ of seaward directed riverflow u_R results in a domain-averaged "counterclockwise" turning of the flow, hence $\frac{dJ}{dt} < 0$.

$$(14) = \frac{1}{12} g H^2 \beta X. \tag{2.72}$$

Term (14) is the depth-weighted shear, induced by the baroclinic pressure gradient force $\propto -\frac{1}{\rho_0}\frac{\partial p'}{\partial x}$. As shown in equation (2.23), this force consists of spatially constant parts, which do not affect J, and a depth-dependent part, $+g\beta z X$. Since the alongchannel, landward acceleration increases with depth due to X, term (14) generates a shear $\frac{\partial u}{\partial z} < 0$ that enhances J. The deeper the estuary, the further this shear can develop.

$$(15) = \frac{3A_{h,sea} bHJX^2 Z(s_0 + HZ)}{s_0^2 B(Z)} \tag{2.73}$$

Term (15) can be interpreted as follows. The boundary value $w|_{x=0}$ is given by (2.54), whereas condition (2.40) demands that $w = 0$ at $x = x_{0,top}$. Hence w-momentum is horizontally transferred between $x = 0$ and $x = x_{0,top}$, weakening w at $x = 0$. Hence this is a "Rayleigh-damping"-like term of the vertical velocity at the seaward boundary [*Maas*, 2004]. As long as $x_j > 0$, i.e. for $Z > -\frac{s_0}{H}$, the baroclinic flow is *downward* at $x = 0$, so that a slowdown of $w|_{x=0}$ reduces angular momentum, i.e. weakens J. However, $x_j < 0$ for $Z < -\frac{s_0}{H}$, so that the flow is *upward* at $x = 0$. In that case, a slowdown of $w|_{x=0}$ increases $\frac{\partial w}{\partial x}$ and thus *enhances* J.

$$(16a) = \underbrace{\frac{A_{v,bot} u_R}{2H\epsilon_b}}_{(16a1)} + \underbrace{\frac{3A_{v,bot}(-1 + 2\epsilon_b)A(Z)J}{2H^2 \epsilon_b B(Z)}}_{(16a2)} \tag{2.74}$$

Term $(16a1)$ represents a negative domain-averaged vorticity input due to bottom-layer shear on river flow u_Q, whose magnitude scales with u_R. Note that this enhances J, although it is *not* related to the gravitational circulation. Term $(16a2)$ weakens J due to bottom-layer friction acting on u_D.

$$(16b) = -\frac{6A_{v,int}A(Z)J}{H^2B(Z)} \tag{2.75}$$

Term $(16b)$ represents the effect of friction on u_D in the "inner domain". The stronger the vertical shear $\frac{\partial u_D}{\partial z}$ is, the stronger is the reduction of this gradient by vertical mixing of momentum. This shear-reduction weakens J.

2.7.4 Interpretation of non-steady terms

The "final form" evolution equations (2.56), (2.64) and (2.69) contain several time-dependent terms on the right-hand sides of the equations, namely

$$(1) = -\frac{6}{L^3H}\frac{dL}{dt}\iint s\ dxdz = -\frac{6}{L^2}\frac{dL}{dt}M = -\frac{6}{s_0}\left(\frac{s_0+HZ}{2}\right)\frac{dX}{dt}, \tag{2.76}$$

$$(5) = -\frac{3}{L}\frac{dL}{dt}X = 3\frac{dX}{dt}, \tag{2.77}$$

$$(10) = -\frac{1}{L}\frac{dL}{dt}Z = \frac{Z}{X}\frac{dX}{dt}, \tag{2.78}$$

$$(11) = -\frac{1}{L}\frac{dL}{dt}J = \frac{J}{X}\frac{dX}{dt}, \tag{2.79}$$

$$(17) = \frac{dx_j}{dt}\frac{1}{LH}\iint w\ dxdz = -\frac{3HJZ}{2B(Z)X}\left((s_0+HZ)\frac{dX}{dt} - HX\frac{dZ}{dt}\right), \tag{2.80}$$

where all boundary conditions and the linear expressions for s, u and w have been substituted after each last equality-sign.

The interpretation of these terms is best started with a look at term (11). Rename the term $\frac{1}{L}\frac{dL}{dt}$ as $\alpha(t)$. Then

$$\frac{dJ}{dt} \propto -\alpha(t)J. \tag{2.81}$$

Now suppose that the domain-length increases, i.e. $\frac{dL}{dt} > 0$, hence $\alpha(t) > 0$. Then $\frac{dJ}{dt} > 0$, according to the relation above, i.e. circulation J is slowed down. This is, most likely, due to the "instantaneous" increase in L. Suppose that the "total circulation", LHJ, with L the "original" domain length, is conserved during this instantaneous domain-stretching. Because the same amount of circulation is now averaged over a longer domain, $|J|$ is weakened, i.e. $\frac{dJ}{dt} > 0$. In the opposite case, i.e. an instantaneous reduction of domain length, the total circulation is suddenly averaged over a smaller area, such that $\frac{dJ}{dt} = -\alpha(t)J < 0$, since $\alpha(t) < 0$. Hence the domain-averaged circulation is enhanced. However, in the latter interpretation it is not entirely clear why LHJ should be fixed while part of the domain in which this circulation takes place is "truncated". The longer the domain initially is, i.e. the smaller $|\alpha(t)|$, the less pronounced are these effects.

A similar reasoning can be employed for term (10), since this gives

$$\frac{dZ}{dt} \propto -\alpha(t)Z. \tag{2.82}$$

It can also be imagined that the "total" vertical stratification LHZ is conserved while domain-length instantaneously increases (decreases), so that domain-averaged stratification, Z, is suddenly weakened (enhanced).

For horizontal salinity gradient X, the interpretation of term (5) is ambiguous. On the one hand, an identical reasoning as for J and Z can be adopted. However, since X is directly coupled to L, it is not sure whether e.g. an instantaneously decreased domain length L still instantaneously satisfies the condition $s|_{x=L,z=-H} = 0$, or that salinity at the "new" position $(x = L, z = -H)$ has not yet adapted and is hence larger than zero.

Since part of term (1) exactly cancels term (5), it could be that, due to the coupling of X and L, there is indeed no effect on $\frac{dX}{dt}$ due to *solely* an instantaneous change in X. The combination of (1) + (5) involves Z, but this combined term could not be explained so far.

Finally, term (17) has probably an effect on $\frac{dJ}{dt}$ that is comparable to term (11), but as (instantaneous) changes in $x_j(t)$ can be due to changes in X as well as Z, interpretation of term (17) is too complex at this stage.

2.7.5 Final evolution equations in compact notation

With the previously found expressions for all individual terms as functions of X, Z and J, equations (2.56), (2.64) and (2.69) can be written more compactly. After taking all time-dependent terms to the left-hand side,

$$\begin{aligned}\frac{dX}{dt}\left(1 + \frac{3HZ}{s_0}\right) &= \frac{3X^2(Hs_0u_RZ - 2X(cHK_{h,sea}Z + 2K_{h,int}s_0))}{s_0^3} \\ &+ \frac{3A(Z)JX^2Z(aHZ + 2s_0)}{s_0^3 B(Z)},\end{aligned} \tag{2.83}$$

$$\begin{aligned}&\frac{dZ}{dt} - \frac{Z}{X}\frac{dX}{dt} = \\ &\frac{3JX\left(HZ\left(aA(Z)(HZ + 2s_0) - 6s_0^2(HZ + s_0)\right) - 2s_0^4\right)}{H^2 s_0^2 B(Z)} - \frac{12K_{v,int}Z}{H^2} - \frac{u_RXZ}{s_0},\end{aligned} \tag{2.84}$$

$$
\begin{aligned}
\frac{dJ}{dt} &- \frac{J\left[2B(Z)\frac{dX}{dt} + 3HZ\left(HX\frac{dZ}{dt} - \frac{dX}{dt}[HZ+s_0]\right)\right]}{2B(Z)X} = \\
&- \frac{3A(Z)J(-2A_{v,bot}\epsilon_b + A_{v,bot} + 4A_{v,int}\epsilon_b)}{2H^2\epsilon_b B(Z)} + \frac{A_{v,bot}u_R}{2H\epsilon_b} + \frac{1}{12}\beta g H^2 X \\
&+ \frac{HJXZ\left(a\ u_R A(Z) + 3\left(A_{h,sea} b\ X(HZ+s_0) - s_0^2 u_R\right)\right)}{s_0^2 B(Z)}.
\end{aligned}
\tag{2.85}
$$

The dynamic variables are $X(t)$, which is coupled to domain length $L(t) = -s_0/X$, $Z(t)$ and $J(t)$. Physical constants are s_0, g and β. Physical parameters, for which typical values have to be chosen, are H, $\epsilon_b = \delta_b/H$, u_R, $K_{h,int}$, $K_{h,sea}$, $K_{v,int}$, $A_{h,sea}$, $A_{v,int}$ and $A_{v,bot}$. Constants a, b and c have to be tuned emperically to obtain appropriate seaward boundary conditions. Omnipresent Z-dependent functions are $A(Z) = (s_0 - HZ)^2$ and $B(Z) = s_0^2 + HZ(-s_0 + 2HZ)$.

Default values for the physical constants are defined in §3.1. Typical scales for dynamic variables X (or L), Z and J are determined in §2.7.6.

A system of closed evolution equations for X, Z, J only has been successfully constituted, so **research objective 1 has been fulfilled.**

2.7.6 Scales for dynamic variables

Typical scales for X, Z and J are derived from model studies by *Festa & Hansen* [1976], hereafter abbreviated as FH76. For default depth and river discharge, $H = 10$ m and $u_R = -0.02$ m/s, the top-to-bottom salinity difference along the estuary ranges from approximately 1 to 14 psu. Hence the scale of Z is roughly

$$
[Z] = \frac{\Delta s}{H} \sim 0.1 \ - \ 1.4 \text{ psu/m}, \tag{2.86}
$$

with an average of 0.75 psu/m. A useful alternative variable is the dimensionless vertical stratification,

$$
\zeta = \frac{ZH}{s_0}, \tag{2.87}
$$

where $\zeta = (s|_{z=0} - s|_{z=-H})/s_0$, i.e. the along-channel averaged salinity difference between surface and bottom, expressed in numbers of sea salinity s_0. Then typical values for ζ will be

$$
[\zeta] \sim 0.03 \ - \ 0.4, \tag{2.88}
$$

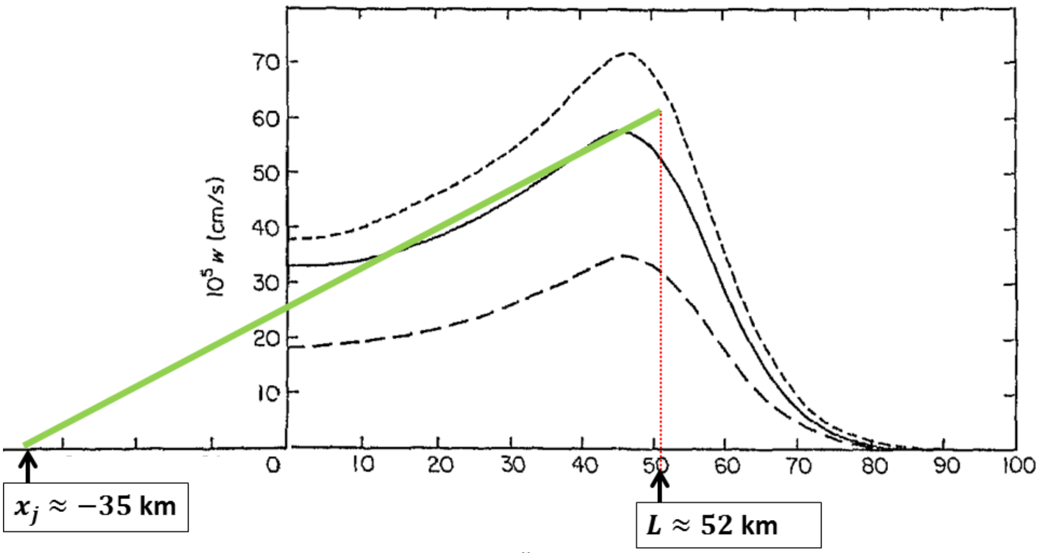

Figure 2.8: Vertical velocity w (in 10^{-5} cm/s) versus along-channel distance, for $u_R = 2$cm/s and $H = 10$ m. Curves represent w at depth $z = -0.75H$ (wide dashed line), $z = -0.5H$ (solid line) and $z = -0.25H$ (small dashed line). An estimate of horizontal rotation axis position x_j and linear function $w(x)$ is derived from this. Figure adapted from *Festa & Hansen* [1976].

with an average of $\zeta = -0.21$.

Next, typical values for intrusion length L are derived from numerical model simulations by FH76. As shown in Figure 1.2, this length is estimated as the reach of the $s = 0.05s_0$ isopycnal. For the various numerical experiments shown by FH76, this gives a typical scale

$$[L] \sim 50 \ - \ 100 \text{ km} \ \leftrightarrow \ |X| \sim 3.5 \cdot 10^{-4} \ - \ 7 \cdot 10^{-4} \text{ psu/m}. \qquad (2.89)$$

A typical magnitude for angular momentum J is derived from FH76 as well. From Figure 2.5, the depth-averaged vertical velocity profile as a function of x is estimated. Extrapolation of this (linear) estimate yields an estimate for rotation axis position, $x_j \approx -35$ km. Next to this, the magnitude of the horizontal exchange flow u_D is estimated from model results in FH76 to be in the range of 10 to 30 cm/s. Using definition (2.39) for basin-averaged angular momentum, J, its typical scale is found to be

$$[J] \sim 0.35 \ - \ 0.70 \text{ m}^2/\text{s}, \qquad (2.90)$$

with an average of about 0.5 m^2/s.

Chapter 3

Methods

3.1 Computing steady states

Now that a closed set of evolution equations has been found, the first analysing step is the computation of its steady states (X, Z, J). All time-derivatives in equations (2.83), (2.84) and (2.85) are set to zero, both on the left-hand side (LHS) *and* on the right-hand side (RHS) of the equality signs. It was attempted to find analytical solutions of (X, Z, J) from these full steady balances. In specific cases, analytic solutions to the steady balances exist, as shown in §4.1. Remaining cases must be solved numerically.

The following default parameter values are chosen, following *Festa & Hansen* [1976]. No distinction has been made between diffusive and viscous coefficient values in the inner domain and at the boundaries.

$$\begin{aligned} H &= 10 \text{ m} \\ K_{v,int} &= 1 \cdot 10^{-4} \text{ m}^2 \text{ s}^{-1} \\ K_{h,int} = K_{h,sea} &= 100 \text{ m}^2 \text{ s}^{-1} \\ A_{v,bot} = A_{v,int} &= 1 \cdot 10^{-3} \text{ m}^2 \text{ s}^{-1} \\ u_R &= -2 \cdot 10^{-2} \text{ m s}^{-1}, \end{aligned}$$

Festa & Hansen found that changing A_h between 1 and 10^6 times A_v does not change the results significantly, hence a default value of $A_h = 10^3 A_v$ is adopted here, so $A_{h,sea} = 1$ m^2 s^{-1}.

It is here assumed that bottom layer depth δ_b scales with total water depth H, so that dimensionless bottom layer depth ϵ_b is constant. *Schramkowski et al.* [2010] modelled subtidal estuarine dynamics with a bottom boundary layer thickness δ_{BBL} of 1 meter and width-averaged depth of 15.8 m.

Although the bottom layer in the current model is not a bottom *boundary* layer, it is here assumed that the fractions δ_b/H and δ_{BBL}/H are similar, so $\delta_{BBL}/H = 1/15.8 \approx 0.06$, so $\epsilon_b = \frac{\delta_b}{H} = 6 * 10^{-2}$.

As shown in §2.6, seaward boundary conditions scale with $-\{a, b, c\}\frac{HZ}{s_0}$. It is physically expected that the strongest vertical stratification possible is $Z = -\frac{s_0}{H}$, i.e. the maximal alongchannel-averaged salinity difference between bottom and surface is s_0. Since it is also expected that the seaward boundary values for $\frac{\partial s}{\partial x}$, u_D and w never exceed in magnitude the "inner domain" values X, $\widehat{u_D}|_{x=0}$ and $\widehat{w}|_{x=0}$, the constants are chosen at $a = b = c = 1$.

To see if multiple equilibria exist and to fulfill RO3, the steady balances are solved numerically for (X, Z, J) using the *Mathematica* command *NSolve*. This finds *all* existing solutions, both real and complex.

To fulfill RO4, steady states are computed as a function of river and tidal influence. *Hansen & Rattray* [1966] classify estuaries based on densimetric Froude number $F_m = \frac{|u_R|}{\sqrt{gH\Delta\rho/\rho}}$ and flow ratio $P = \frac{|u_R|}{u_T}$. Density-difference between river- and seawater, $\Delta\rho$, and estuarine water density ρ are assumed approximately constant in the current case. Then the only variables in F_m and P are u_R, H and root-mean squared tidal velocity u_T. Both *MacCready & Geyer* [2010], eq.(13) and *Valle-Levinson* [2010], eq.(2.6) indicate that A_v is proportional to H and depth-averaged tidal flow amplitude. To conlude, in the estuarine classification proposed by *Hansen & Rattray* [1966], the variables u_R, H and A_v are involved. Although it would suffice to vary only two of them, the influence of all three variables on the estuarine dynamics will be considered in this study. Here, assume $A_v = A_{v,int} = A_{v,bot}$.

Steady states (X, Z, J) as a function of u_R are numerically computed with *Mathematica* command *FindRoot*. Starting from one of the solutions for $(X, Z, J)|_{u_{R,0}}$ found with *NSolve*, the default $u_{R,0}$ is perturbed by small Δu_R. With *FindRoot*, a new steady solution $(X, Z, J)|_{u_{R,0}+\Delta u_R}$ is found, using solution $(X, Z, J)|_{u_{R,0}}$ as starting values for the numerical solving procedure. Then, choose $u_{R,0} + 2\Delta u_R$ and solve $(X, Z, J)|_{u_{R,0}+2\Delta u_R}$ using starting value $(X, Z, J)|_{u_{R,0}+\Delta u_R}$, etc. This numerical continuation procedure is similarly applied while varying H or A_v, fixing all other parameters at their default. The results are shown in §4.1.

3.2 Linear stability analysis

It will be shown in §4.1 that both physically acceptable as well as physically unrealistic steady state solutions exist. **To answer RQ5** and to test if the physically acceptable states are stable to infinitesimally small perturbations, a linear stability analysis is performed. The left-hand sides of evolution equations (2.83), (2.84) and (2.85) contain functions of *various* time-derivatives. When considering steady solutions, it suffices to set *all* these time-derivatives individually to zero. For the dynamical analysis that will be done in this and the next section however, this is not possible. Thus, the evolution equations are rewritten so that on their left-hand sides, they read *only* dX/dt, dZ/dt and dJ/dt, respectively, and the right hand sides contain only steady terms.

To this end, devide (2.83) by the factor $C(Z) = 1 + \frac{3HZ}{s_0}$ to obtain an evolution equation for dX/dt only. Then, substitute the latter equation into the right-hand side of equation (2.84) and rewrite this as a new evolution equation for Z only. Finally, both the new evolution equations for X and for Z are substituted into the right-hand side of (2.85), to yield a new evolution equation $\frac{dJ}{dt}$. Notice that all equations contain the factor $C(Z)$ in the denominators. This function has a root at $Z = -\frac{s_0}{3H}$. If Z reaches this value, time-derivatives $\frac{dX}{dt}$, $\frac{dZ}{dt}$ and $\frac{dJ}{dt}$ go to $\pm\infty$. The reason for this should be sought in the combination of terms (1) and (5) in the original X-evolution equation. For some reason, which could not be explained thus far, these two terms exactly balance the term $\frac{dX}{dt}$ on the left-hand side of equation (2.56).

Then, using these new evolution equations, the steady states (X, Z, J) are perturbed by infinitesimal perturbations (X', Z', J') and a Taylor-expansion is made of the pertubed system of equations, i.e.

$$\frac{d}{dt}\begin{pmatrix} X' \\ Z' \\ J' \end{pmatrix} = \mathcal{J} \cdot \begin{pmatrix} X' \\ Z' \\ J' \end{pmatrix} + \text{HOTs}. \tag{3.1}$$

To determine linear stability, the eigenvalue-equation of Jacobian $\mathcal{J}$ is computed and the steady solutions (X, Z, J) are substituted in the eigenvalues $\lambda_{1,2,3}$. The steady solution is linearly stable, unstable or neutral if the *maximal real part* of the eigenvalues is resp. negative, positive or zero [e.g. *Dijkstra*, 2013].

3.3 Forward integration of evolution equations

Provided that a physically acceptable steady state is linearly stable, it is important to know if the system actually ends up in this steady state when it is perturbed by some *finite amplitude* perturbation (dX, dZ, dJ) from another steady state. Therefore, the new evolution equations (ordinary differential equations) derived in §3.2 (with only dX/dt, dZ/dt or dJ/dt on the left-hand sides) are solved numerically as a function of time, using *Mathematica* command *NDSolve*. Choose some value u_R and amplitudes for dX, dZ and dJ. Then, all 8 combinations $(X \pm dX, Z \pm dZ, J \pm dJ)$ are used as initial conditions for *NDSolve*.

Chapter 4

Results

4.1 Steady state solutions

To fulfill RO3, multiple equilibrium steady states solutions were found at default parameters. These solutions can be divided into three categories, namely

A. Solutions for which either one (or more) of X, Z or J is *positive*. This is physically not expected for the current estuarine model and river discharge velocity $u_R \leq 0$;

B. $(X, Z, J)_{hom} = (0, 0, J_{hom})$, i.e. non-zero J in homogeneous salt field;

C. $(X, Z, J)_{est} < 0$, i.e. the expected "estuarine" situation.

To achieve RO4, solutions in all three categories are interpreted below.

4.1.1 Category A: physically unrealistic steady states

Mathematically the model does not forbid steady states that do not meet these "estuarine" characteristics of $(X, Z, J) \leq 0$ for $u_R \leq 0$. Many of the expressions defined in this model, e.g. intrusion length L_i and boundary conditions at $x = 0$, were based on the assumption that $(X, Z, J) \leq 0$. These expressions likely loose their physical meaning for solutions from category A; yet they are *mathematically* allowed.

4.1.2 Category B: $(X, Z, J)_{hom} = (0, 0, J_{hom})$

The category B solution has negative J, while the domain is completely homogeneous in s, i.e. $(X, Z) = 0$. One expects that density gradients arise when $u_R < 0$, but this is not the case for this solution. The reason for this is that, at $X = 0$, $L = -\frac{s_0}{X}$ is infinitely long. Almost all terms in the evolution equations of X, Z and J are averaged over domain size LH, so their influence on the evolution $\frac{d}{dt}(X, Z, J)$ is "infinitely dilluted" if $L \to \infty$. Hence, if $X = 0$,

$$\frac{dX}{dt}|_{X=0} = 0, \tag{4.1}$$

$$\frac{dZ}{dt}|_{X=0} = -\frac{12K_{v,int}}{H^2}Z, \tag{4.2}$$

i.e. when starting from $X = 0$, any vertical stratification is mixed away, so that $X = 0$ also "demands" $Z = 0$. In this homogeneous estuary, $(X, Z) = 0$,

$$\frac{dJ}{dt}|_{(X,Z)=0} = \underbrace{\frac{A_{v,bot}u_R}{2\delta_b}}_{(16a1)} \underbrace{-\frac{6}{H^2}\frac{A_{v,bot}}{2\delta_b}\left(\frac{H}{2} - \delta_b\right)J}_{(16a2)} \underbrace{-\frac{6A_{v,int}}{H^2}J}_{(16b)}. \tag{4.3}$$

Hence angular momentum J is forced by river-induced shear $(16a1)$ in the bottom layer. Once J becomes nonzero due to this shear generation, exchange flow u_D arises, which is damped by bottom friction $(16a2)$ and internal mixing $(16b)$. The resulting steady state value for J is hence not associated with a closed, gravitational circulation cell, but only with the river-induced bottom-layer shear, and reads

$$J_{hom} = \frac{\frac{A_{v,bot}u_R}{2\delta_b}}{\frac{6}{H^2}\left[\frac{A_{v,bot}}{2\delta_b}\left(\frac{H}{2} - \delta_b\right) + A_{v,int}\right]} = \frac{Hu_R}{3\left[(1 - 2\epsilon_b) + 4\epsilon_b\frac{A_{v,int}}{A_{v,bot}}\right]}. \tag{4.4}$$

4.1.3 Category C: estuarine situation, $(X, Z, J)_{est} < 0$

$(X, Z, J)_{est}$ as a function of u_R - description of results

"Estuarine" steady state solutions as a function of river discharge velocity are plotted in Figure 4.1. It shows that, even in the absence of river discharge, the basin contains angular momentum and is horizontally and vertically stratified, contrary to the expectations. Horizontal salinity gradient $|X|$ increases, or intrusion length L_i retreats, with strengthening river discharge. This agrees with model studies, e.g. *Festa & Hansen* [1976]. ζ is always ≤ -2, so the top-to-bottom salinity difference is always two or more times the sea salinity. This is illustrated in Figure 4.2. As expected from the model formulation, salinity becomes negative landward of the $(s = 0)$-isopycnal. However, for $\zeta < -2$, this region of negative salinity is very large

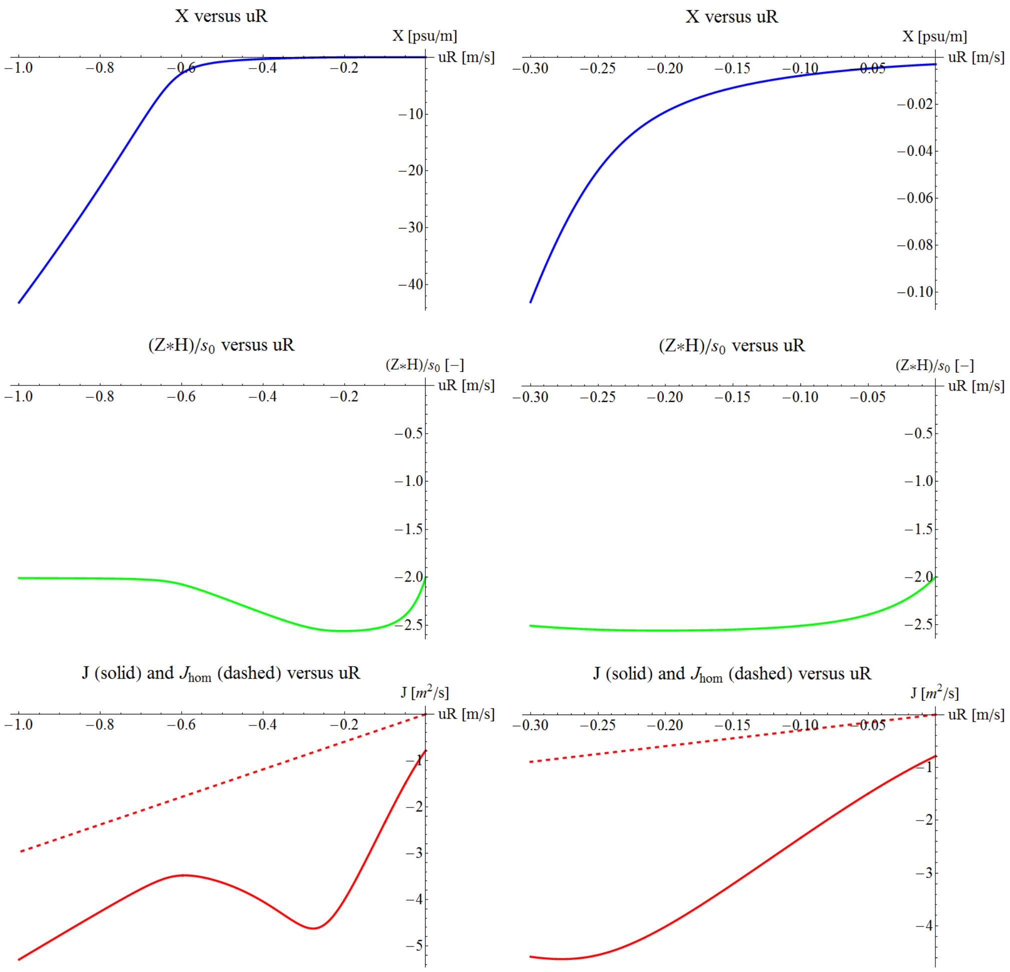

Figure 4.1: "Estuarine " steady solutions $(X,\ ZH/s_0,\ J)_{est}$ versus river discharge u_R. Note that u_R varies along the horizontal axis.

and the vertical top-to-bottom salinity difference is more than $2s_0$, which is not physically realistic. The choice for $(a, b, c) = 1$ made in §3.1 is thus not realistic either, since this implies that the magnitude of $\frac{\partial s}{\partial x}$, u_D and w at $x = 0$ is larger than the magnitude that the linearised salt and flow field would obtain at $x = 0$. $\zeta \uparrow -2$ both in the limit $u_R \uparrow 0$ and $u_R \to -\infty$. J never approaches "homogeneous" value J_{hom}, because X and Z never vanish.

The inspected range of river discharge values can be divided into three different parts, all three with qualitatively different behaviour of X, Z and J. For $u_R \in [-0.2, 0]$ m/s, the strengthening of X with river discharge intensifies while u_R gets more negative. Vertical stratification gets more stable with strengthening river discharge, but reaches a maximum around $u_R = -0.22$

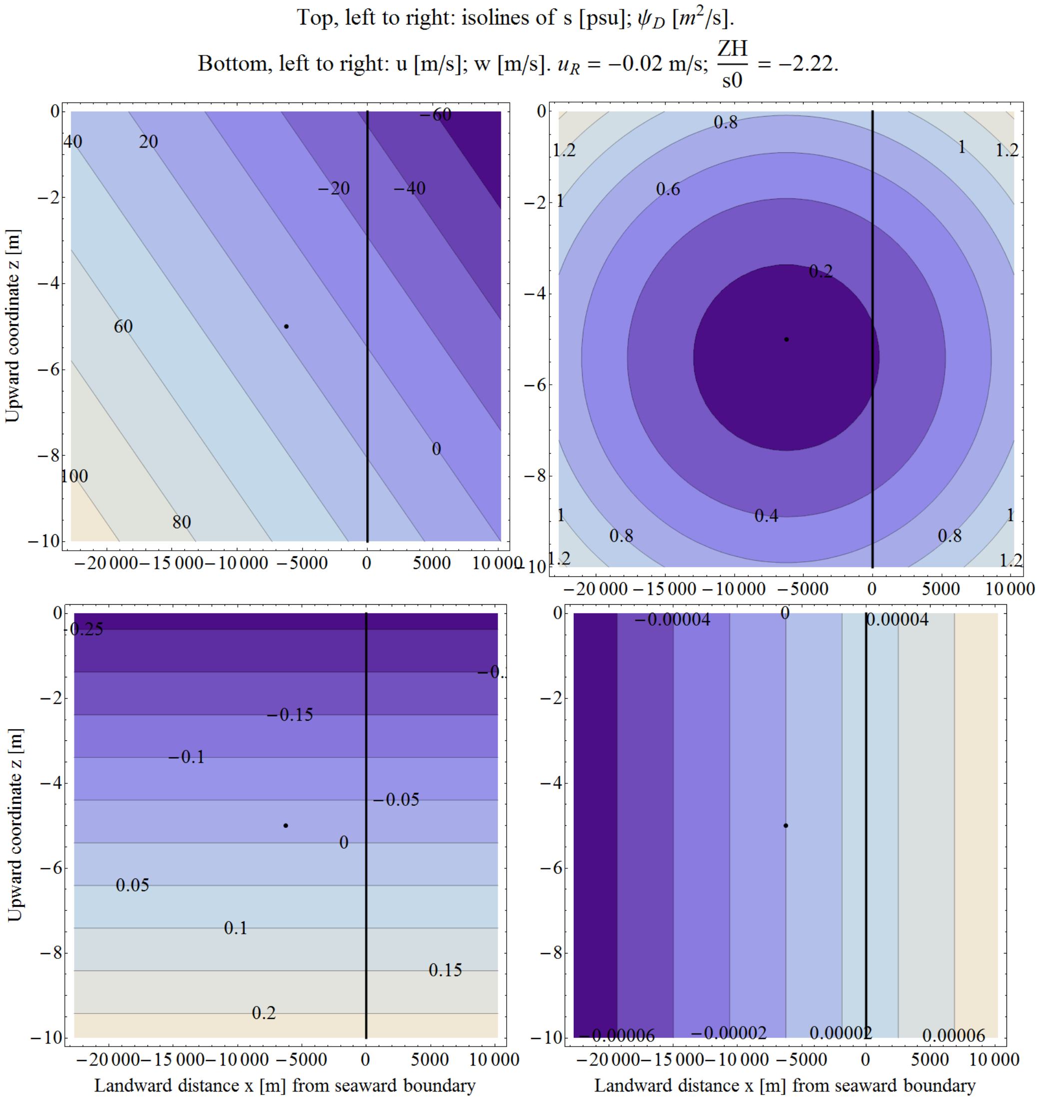

Figure 4.2: Spatial representation of the linearised salt and flow field, corresponding to $(X, Z, J)_{est}$. Domain presented runs horizontally from $x = x_{0,top}$ to $x = L$, where the vertical line is at $x = 0$. The integration domain is hence on the right of this line. The black dot represents (x_j, z_j)

m/s. For small u_R, the strengthening of J with river discharge intensifies while u_R gets more negative. At $u_R \approx -0.13$ m/s, there is an inflection point; from here on the enhancement of J due to u_R weakens; J reaches a local intensity-maximum around $u_R = -0.28$ m/s.

For $u_R \in [-0.6, -0.2]$ m/s, the strengthening of X with u_R is more intense than in the first region, as is shown in Figure 4.3. u_R weakens vertical stratification, but this weakening effect is reduced as u_R approaches -0.7

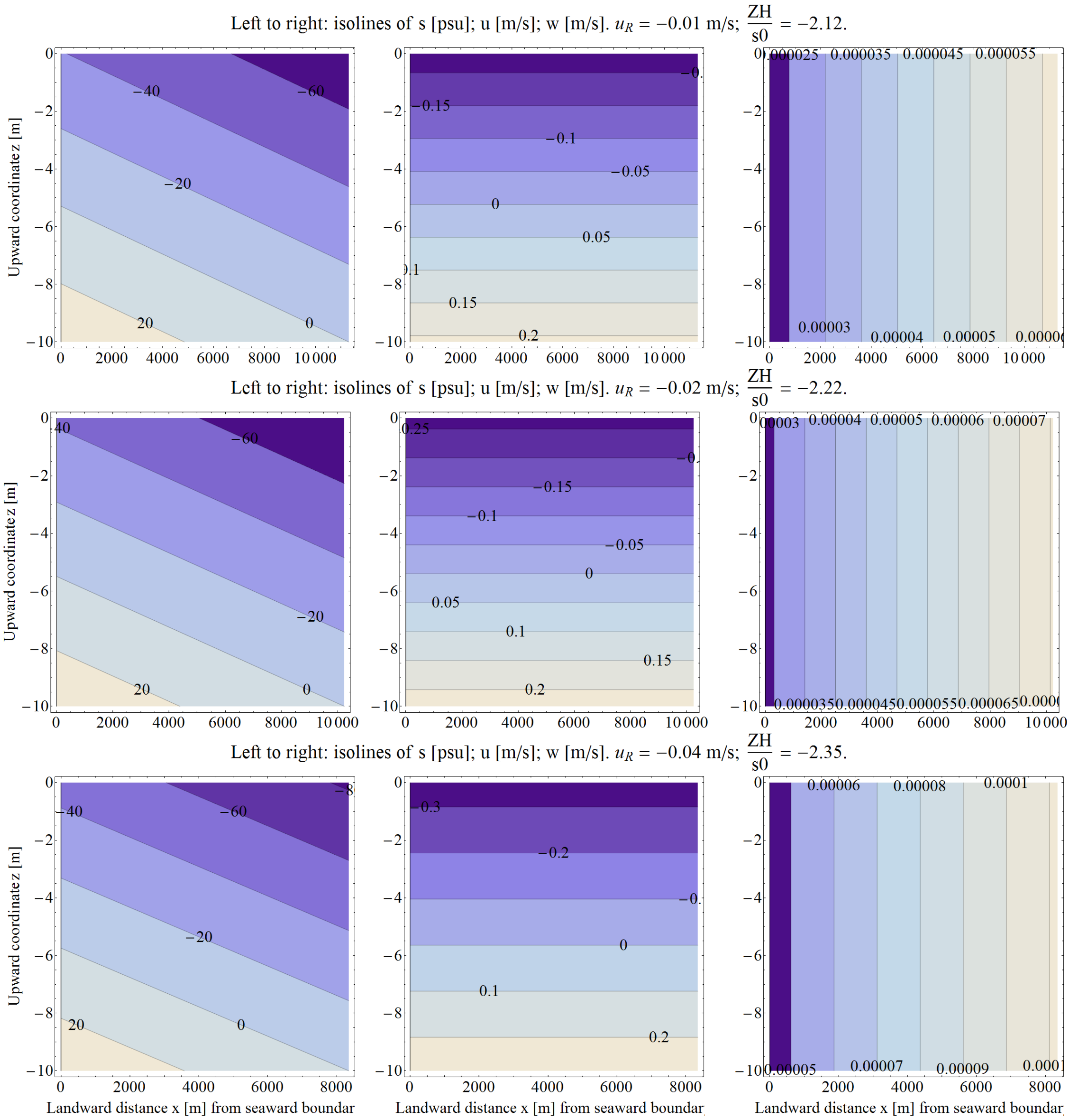

Figure 4.3: As in Figure 4.2, but for variable river discharge velocity u_R. Contrary to Figure 4.2, the estuarine domain is here plotted from $x = 0$ to $x = L$.

m/s. The effect of u_R on the magnitude of J is similar, the weakening effect on J being reduced towards $u_R = -0.6$ m/s.

For $u_R < -0.6$ m/s, the strengthening of X with u_R is even more intense than in the second region. As u_R further strengthens, X approaches a linear profile. ζ asymptotically approaches the constant -2 and J asymptotically approaches a linear profile. The model results for river discharges ranging from 1 to 4 cm/s are compared to numerical model simulations done by *Festa & Hansen* [1976], hereafter abbreviated as FH76. The results are shown in Figure 4.3. The salinity field and baroclinic velocity field are computed based on their linear expressions (2.29), (2.43) and (2.44). As river discharge increases, intrusion length decreases from 11 to 8 km, which is about an order magnitude shorter than the intrusion length varying from 70 to 35 km found by FH76. As river discharge increases, vertical stratification and the magnitude of u_D and w increase, which agrees with FH76. The horizontal exchange flow is, however, throughout the domain length typically a factor two stronger than the value maximally reached (at the seaside en-

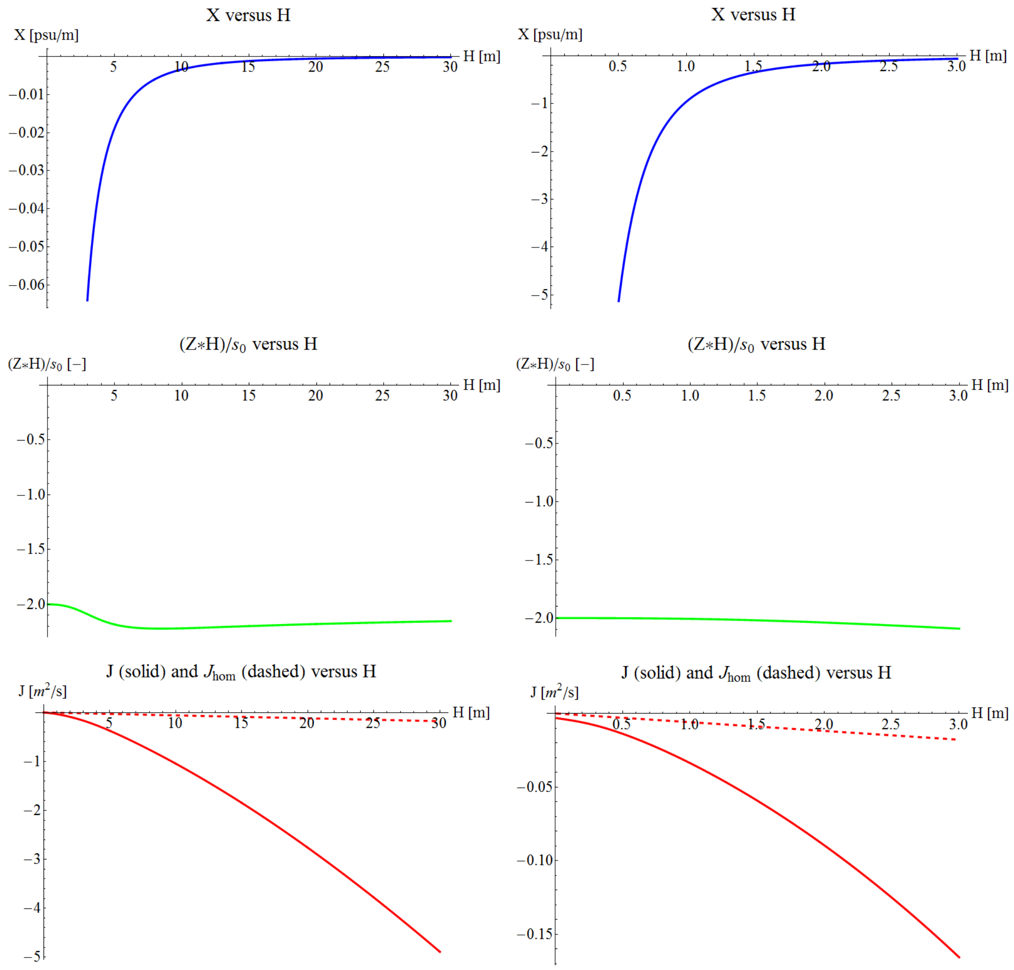

Figure 4.4: "Estuarine " steady solutions $(X,\ ZH/s_0,\ J)_{est}$ versus depth H. Note that H varies along the horizontal axis

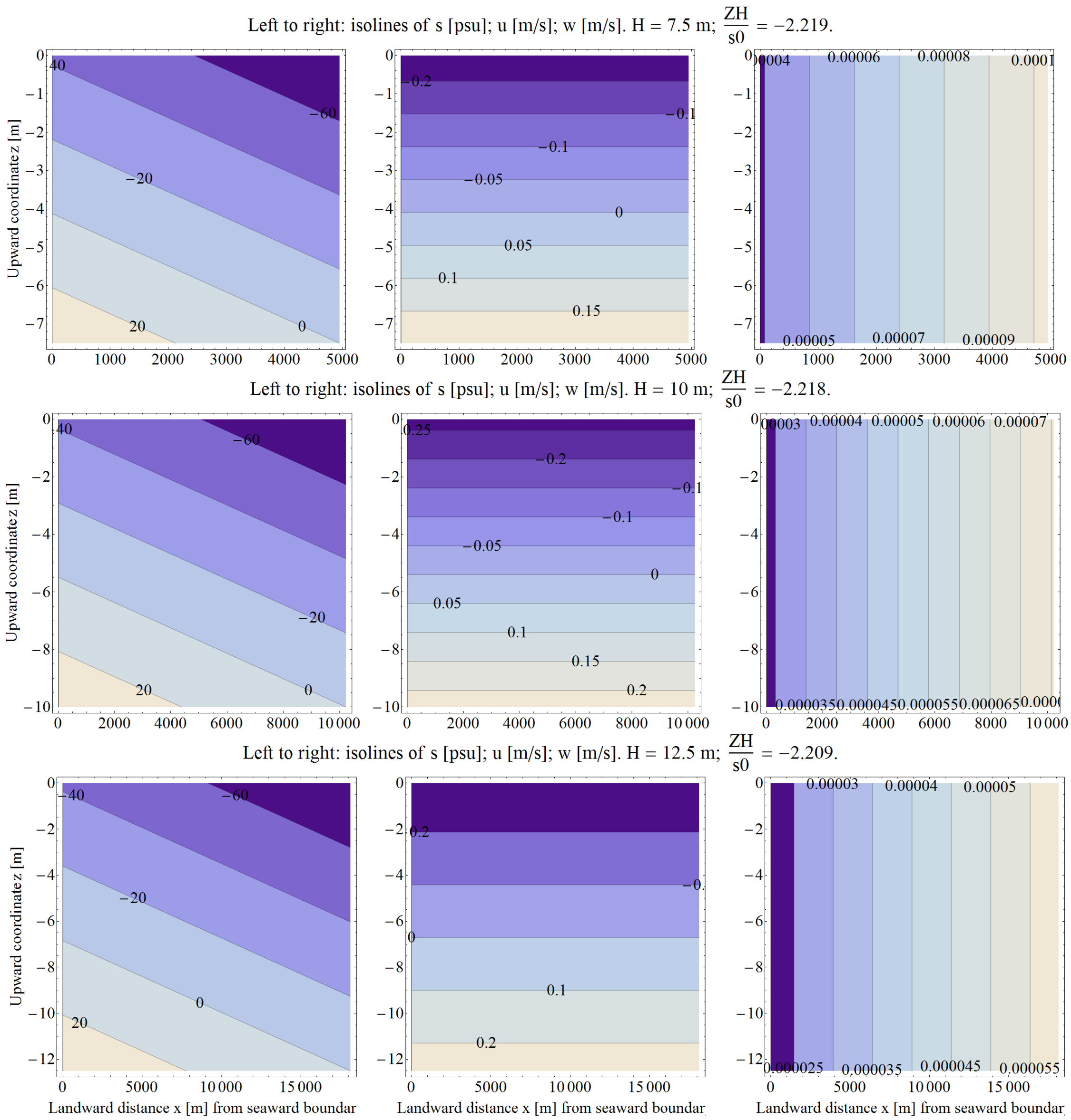

Figure 4.5: As in Figure 4.3, but for varying depth.

trance) in the FH76 results. Vertical velocities are typically a factor 10 larger than modelled by FH76. Despite this, J is only a factor 2 larger than the typical range estimated in §2.7.6. Most likely, the strong vertical velocities are compensated by a smaller intrusion length.

$(X, Z, J)_{est}$ as a function of H - description of results

Steady estuarine solutions are plotted versus water depth H in Figure 4.4. Horizontal density gradient X is infinitely steep for depth $H \downarrow 0$m and X

asymptotically weakens to zero, i.e. the domain length grows to infinity, as depth increases. For small depths, about $\leq$ 1m, dimensionless vertical straticifation ζ is approximately constantly -2. For depths about 1 to 6m, ζ becomes more negative, i.e. the weakening of Z with H is less strong in this regime. For H increasing from about 7m onwards, ζ asymptotically returns to -2, i.e. the weakening of Z with H slowly becomes stronger again. The top-to-bottom salinity difference is thus kept approximately constant for all depths, i.e. Z weakens as H increases. Contrary to expectations, ζ is always ≤ -2, as is illustrated in Figure 4.5.

Circulation J is always < 0, also for $H \uparrow 0.J$ intensifies with H; this

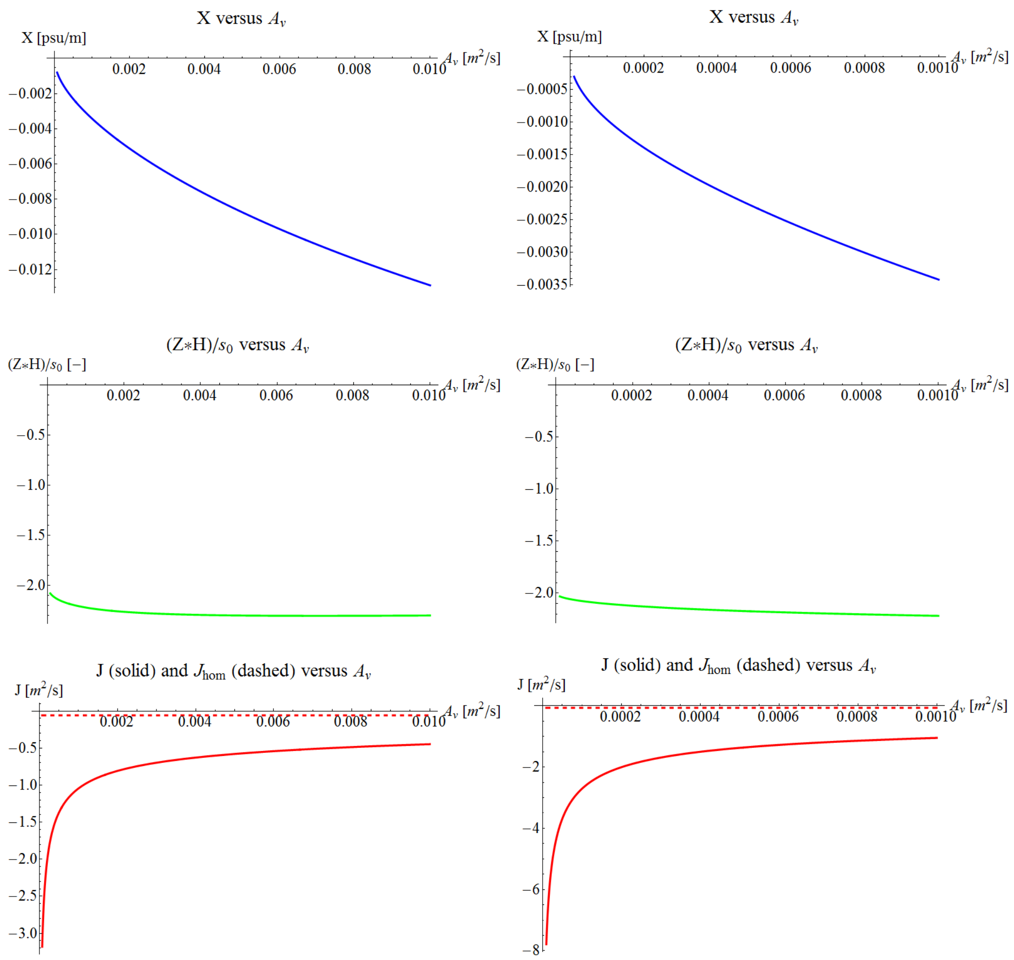

Figure 4.6: As in Figure 4.1, but for varying vertical eddy viscosity, A_v. Note that A_v varies along the horizontal axis.

intensification is stronger with growing H. J never approaches J_{hom}, because X and Z are nonzero.

For depths ranging from 7.5 to 12.5 m, the results are again translated back into salinity and baroclinic flow fields and compared to results by FH76. Intriusion length increases from 5 to 18 km as depth is increased. This is also modelled by FH76, but their intrusion lengths typically range from 20 to 100 km. Dimensionless stratification ζ slightly weakens as H increases, but much less than the weakening modelled by FH76. In agreement with FH76, the horizontal exchange flow becomes stronger with increased depth. Vertical velocity decreases, but is again a factor 10 larger than modelled by FH76.

$(X, Z, J)_{est}$ as a function of A_v - description of results

Estuarine steady solutions as a function of vertical exchange coefficient A_v are plotted in Figure 4.6. Here, $A_{v,int} = A_{v,bot} = A_v$ is assumed. For increasing vertical eddy viscosity, X becomes increasingly steep, or L increasingly short. $\zeta \leq -2$ for all A_v. ζ first becomes more negative as A_v increases, reaches a minimum around $A_v = 0.0025$ m^2 s^{-1} and then slowly approaches $\zeta \uparrow -2$ again for $A_v \to \infty$. Increasing A_v, i.e. vertical mixing of momentum, weakens exchange flow u_D and hence J. Since X and Z never vanish, J always remains stronger than J_{hom}. In the absence of vertical viscosity, $X < 0$, $\zeta \uparrow -2$ and $J << 0$.

4.2 Linear stability of steady state solutions

Physically, one expects that in the absence of river discharge, the estuary is homogenous and there is no circulation, i.e. $(X, Z, J, u_R) = (0, 0, 0, 0)$, which is part of the steady solution $(X, Z, J)_{hom}$. As soon as a river discharges into the estuary, one expects $(X, Z, J) < 0$, which is true for $(X, Z, J)_{est}$. **Hence to answer RO5, a linear stability analysis** will be applied on the solutions $(X, Z, J)_{hom}$ and $(X, Z, J)_{est}$.

4.2.1 Linear stability of $(X, Z, J)_{hom}$

When steady solution $(0, 0, J_{hom})$ is substituted in the eigenvalue-equation, this equation is of the form $(\lambda - a_1)(\lambda - a_2)\lambda = 0$, with solutions

$$\lambda_{hom,1} = 0, \tag{4.5}$$

$$\lambda_{hom,2} = -\frac{12K_{v,int}}{H^2}, \tag{4.6}$$

$$\lambda_{hom,3} = -\frac{3\left[A_{v,bot}(1-2\epsilon_b) + 4A_{v,int}\epsilon_b\right]}{2H^2\epsilon_b}. \tag{4.7}$$

Then, all three eigenvalues are always real-valued, and $\lambda_{hom,2}$ is always negative. For the current choice $A_{v,int} = A_{v,bot} = A_v$, also $\lambda_{hom,3} < 0$. Hence the maximum of $\Re\{\lambda_{hom,i}\}$ is zero, so the "homogeneous" steady solution is neutrally stable.

4.2.2 Linear stability of $(X, Z, J)_{est}$

The eigenvalue equation yields (complicated) algebraic expressions for $\lambda_{1,2,3}$. The numerical solutions $(X, Z, J)_{est}$ as a function of u_R, H and A_v are substituted in these expressions and the real parts of the eigenvalues are taken.

As a function of u_R, all three eigenvalues have negative real parts for all u_R (between 0 and -100 m/s). For strengthening river discharge these real parts become more negative, i.e. the "estuarine" steady solution becomes more stable. The estuarine solution is also stable for all depth H (varied between 0 and 10.000m). The real parts of the eigenvalues approach asymptotically to zero, i.e. stability decreases, for increasing depth. Also for all A_v (between 0 and 100 m^2/s), the estuarine solution is linearly stable; stability increases with A_v.

4.3 Time evolution of basin-averaged variables

It was shown that neither of the physically relevant solutions $(X, Z, J)_{hom}$ and $(X, ZJ)_{est}$ are linearly *unstable*. However, it is physically not expected that the estuary can remain in the neutrally stable state $(X, Z, J)_{hom}$ when there is nonzero river discharge. Hence it is expected that, if the estuary is initially homogeneous despite $u_R < 0$, it evolves into $(X, Z, J)_{est}$, once perturbed by *finite*-amplitude perturbations.

To test this expectation, choose a very small river discharge velocity, $u_R = -10^{-4}$ m/s and finite-amplitude perturbations

$$(dX, dZ, dJ) = (\pm\ 10^{-2}\ \text{psu/m},\ \pm\ 10^{-2}\ \text{psu/m},\ \pm\ 10^{-2}\ \text{m}^2/\text{s}).$$

For all eight combinations of initial conditions $(X, Z, J)_{t=0} = (X, Z, J)_{hom} + (dX, dZ, dJ)$, the system asymptotically returns to its initial state $(0, 0, J_{hom})$.

As a second experiment, keep dX and dJ the same, but instead choose

$$dZ = -\frac{s_0}{3H} \pm 10^{-2} \text{ psu/m}.$$

The value $Z = -\frac{s_0}{3H}$ is exactly the singular point of the new evolution equations derived in §3.2, i.e. the root of function $C(Z) = 1 + \frac{3HZ}{s_0}$, which occurs in almost all denominators. Therefore, since all evolution equations change sign when Z crosses $-\frac{s_0}{3H}$, it is expected that this new choice of dZ will drastically change the evolution of a finite-amplitude perturbation starting from $(X, Z, J)_{hom}$.

The results are as follows. Irrespective of the sign of small perturbations (dX, dJ), the perturbed system returns to $(X, Z, J)_{hom}$ for $dZ > -\frac{s_0}{3H}$, but evolves into another state for $dZ < -\frac{s_0}{3H}$.

For negative perturbations dX, the system ends up in $(X, Z, J)_{est}$, as expected. For positive dX, the system ends up in a different steady state. This state has $(X, J) \approx -(X, J)_{est}$, i.e. almost (but not exactly) the oppositie of the estuarine solution for X and J. The solution for Z is approximately (so not exactly) Z_{est} (but not its opposite value). The sign of small dJ has no influence on the end state in any of the cases.

To conclude, it appears that dZ should cross its threshold value $-\frac{s_0}{3H}$ before $(X, Z, J)_{hom}$ evolves into another state. It is here assumed that this "separation" in evolution holds for any $0 > dZ > -\frac{s_0}{3H}$ and any $dZ < -\frac{s_0}{3H}$. The sign of dX determines the sign of the end state for X. The sign of J seems to follow the sign of X. This is expected, beacuse the circulation-direction is related to the orientation of the channel. It is further assumed that this holds for any other (small) perturbations (dX, dJ). To conclude, the system indeed ends up in the physically expected steady state for $u_R < 0$, provided the vertical stratification perturbation is strong enough.

Chapter 5

Discussion

5.1 Discussion of model results

Steady solution $(X, Z, J)_{est}$ has been thouroughly analysed and interpreted as a function of river discharge, depth and vertical eddy viscosity. For this analysis, the magnitude of all individual terms from the steady versions of (2.56), (2.64) and (2.69) is considered as a function of u_R, H or A_v, after substitution of the corresponding solutions $(X, Z, J)_{est}$. For several specific parameter ranges, e.g. the limits of very weak or exceedingly strong river discharge, many of the terms in these balances can be neglected. The resulting reduced balance often has analytical solutions for X, Z and J separately. These analytical solutions prove to be good approximations to the numerical solution of the full steady balances. These analytical solutions can be interpreted in terms of all contributing physical processes; the analysis is shown in Appendix C. These analyses explain, amongst others, the remarkable weakening of angular momentum while river discharge increases, around $u_R = -0.4m/s$. Note that the results for variable depth H and eddy viscosity A_v use a larger default river discharge (10 cm/s) rather than the default value of 2 cm/s adopted throughout the rest of this study. These resuls are, however, not further discussed here. Although all contributing terms are individually understandable from a physical perspective, it is not obvious how to compare the results of this analysis directly to other modelling or observational studies. This is mostly because vertical stratification in the modelled results is unphysically strong (as is further discussed hereafter), and because the coupling of domain length to the horizontal density gradient makes the results not directly relatable to other studies. In addition, even though analytical solutions to several reduced balances are found, even these solutions are often to complex to grasp, mainly due to the complicated Z-dependency.

Both difficulties will be further addressed later onin this discussion.

5.1.1 Noticeable results

Unphysically strong vertical stratification for $(X, Z, J)_{est}$

Most remarkable in the steady results for $(X, Z, J)_{est}$is the unphysically strong vertical stratification of $\zeta \leq -2$ that is observed for all values of river discharge, depth and eddy viscosity. This is particularly unexpected for weak river discharge of about 2 cm/s, for which the estuary is expected to be partially or well mixed, with $\zeta \sim -0.4$ in the most stratified case (see §2.7.6). A possible explanation comes from Figure 5.1 (at the end of this section).

This figure shows the magnitude of all individual terms in the steady versions of (2.56), (2.64) and (2.69), as a function of u_R, after substitution of the corresponding solutions $(X, Z, J)_{est}$. Considering the steady X-balance, it can be seen that for very weak river discharge, the river induced horizontal salt fluxes ($2a$) and ($3a$) are indeed very small. The horizontal diffusive salt fluxes ($2c$) and ($3c$) are also very small, because the intrusion length is very large, so that the horizontal density gradient is negligibly small. The remaining terms are the horizontal exchange salt fluxes ($2b$) and ($3b$). This balance gives

$$0 = (2b) + (3b) = \frac{3A(Z)JX^2Z}{s_0^2 B(Z)} \left(2 + \frac{aHZ}{s_0}\right). \tag{5.1}$$

This yields

$$Z = -\frac{2s_0}{aH}, \tag{5.2}$$

i.e. when the domain-averaged exchange salt transport ($2b$) exactly balances the exchange salt transport at the seaward boundary ($3b$), since $u_D|_{x=0}$ is assumed to scale with $\frac{cHZ}{s_0}$. This solution for Z gives exactly $\zeta = -2$ under the current parameter choices. Moreover, for weak river discharge, the steady Z-balance is dominated by terms ($6b$), ($6d$) and ($7b$). This balance yields a complicated analytical solution for Z, which numerically yields $\zeta \approx -2.8$. Hence, for weak river discharge, it is likely that the system has $\zeta \leq -2$.

More generally, it is remarkable that the estuary is always $\zeta \leq -2$ and more often strongly attracted to $\zeta - 2$, namely also in the limit of exceedingly strong river discharge, very small and exceedingly large depth and very weak and exceedingly strong vertical viscosity. To interpret this, also the magnitude of the individual steady terms as a function of H and A_v shown in Figures 5.2 and 5.3 (at the end of this section). It can be seen that the steady X-balance is also dominated by exchange fluxes ($2b$) and ($3b$) in the case of very large H and very small A_v. In both cases, the intrusion length is very large, so that diffusive fluxes are negligible. The steady X-balance is dominated by the horizontal diffusive salt fluxes ($2c$) and ($3c$). These fluxes are dominant for very short estuaries, since $|X|$ is large in that case. Short estuaries are observed for very strong river discharge and for very small depths, which probably explains the limits $\zeta \to -2$ in these cases. The diffusive term ($3c$) imports salt at the seaward boundary and thus locally increases the horizontal salinity gradient and hence $|X|$. Diffusive term ($2c$) transports salt up the estuary, increasing the intrusion length, hence decreasing $|X|$. The balance reads

$$\begin{aligned} 0 &= (2c) + (3c) \\ &= -\frac{6X^3}{s_0^3}\left(2K_{h,int}s_0 + cHK_{h,sea}Z\right). \end{aligned} \tag{5.3}$$

The two fluxes balance when

$$Z = -\frac{2K_{h,int}s_0}{cHK_{h,sea}}, \tag{5.4}$$

i.e. when the domain-averaged diffusive salt transport ($2c$) exactly balances the diffusive salt transport at the seaward boundary ($3c$), which is assumed to scale with $\frac{cHZ}{s_0}$. This solution for Z gives exactly $\zeta = -2$ under the current parameter choices.

Apart from that, the steady Z-balance is often dominated by terms ($6b$), ($6d$), ($7b$) and sometimes also ($6a$). This balance yields a complicated relationship for Z, but numerically yields $\zeta < -2$.

Net salt transport in steady state

Because the modelled vertical stratification is unphysically strong, the question arises what the effect is on the net salt transport into the estuary. For steady states, there should be no net salt transport into the estuary. The net salt transport, $F_{S,net}$, into the domain takes place only through the seaward boundary, i.e.

$$F_{S,net} = \int_{-H}^{0} \left(us - K_{h,sea}\frac{\partial s}{\partial x}\right)|_{x=0}\, dz \tag{5.5}$$

$$= \underbrace{Hu_R\left(s_0 + \frac{HZ}{2}\right)}_{river} \underbrace{-\frac{aH^2A(Z)JZ^2}{2s_0B(Z)}}_{exchange} + \underbrace{\frac{cH^2K_{h,sea}XZ}{s_0}}_{diffusive}. \tag{5.6}$$

The diffusive and exchange salt fluxes are always positive, i.e. into the domain. The river-induced salt flux is always outward, as long as the depth-averaged salinity at the seaward boundary, $\bar{s}|_0 = s_0 + \frac{HZ}{2}$, is positive. This is the case for $|\zeta| < 2$, hence for the steady solution $(X, Z, J)_{est}$, the river flux is always positive as well! To conlude, there is always a net import of salt through the seaward boundary in the steady state $(X, Z, J)_{est}$. How can the system still be in steady state? This is due to the fact that the steady X-balance also contains the "domain-averaged" horizontal salt flux, i.e. proportional to terms $(2a + b + c)$. For $\zeta < -2$ these terms cause a net up-estuary transport of salt, which increases the domain length. This balances the positive net salt flux at the seaward boundary, which locally steepens the horizontal salt gradient and thus decreases the intrusion length.

5.2 Attempts to improve physical realism of steady solution $(X, Z, J)_{est}$

Several attempts were undertaken to better understand the large values for Z in $(X, Z, J)_{est}$ and to find more realistic values for this vertical stratification. These attempts are discussed hereafter.

Decreasing the Péclet number

The unphysically strong vertical stratification is not expected for partially to well mixed estuaries. In such estuaries, the salt tranport by vertical diffusion is typically much more effective than transport by horizontal diffusion. The ratio of advectional over diffusional importance can be expressed by the dimensionless Péclet number [*Cushman-Roisin & Beckers*, 2011],

$$Pe = \frac{|u_R|\ H^2}{K_v\ L}. \tag{5.7}$$

In partially to well mixed estuaries, Pe is typically much smaller than 1. Computing this ratio for default river discharge $u_R = 2$ cm/s, $K_v = K_{v,int} = 10^{-4}$ m^2/s and $H = 10$ m, the intrusion length is (according to $(X, Z, J)_{est}$ at this u_R) about 10 km, so that $Pe = 2$, hence the estuary actually is *not* diffusion-dominated, which possibly explains the strong vertical stratification.

Therefore, K_v is increased to see if the resulting $|Z|$ is smaller. An increase in K_v due to increased tidal forcing should logically be accompanied by an increase in A_v. Hence, the known steady solution $(X, Z, J)_{est}$ is computed again for default parameter settings ($u_R = -0.02$m/s), but variable $A_{v,int} = A_{v,bot} = A_v$ and $K_{v,int} = K_v$. Then A_v and K_v are slowly increased as

$$A_v = A_{v0}\ \mu, \tag{5.8}$$

$$A_v = K_{v0}\ \mu^2, \tag{5.9}$$

starting at default values $A_{v0} = 10^{-3}$ m^2/s and $K_{v0} = 10^{-4}$ m^2/s and dimensionless constant $\mu = 1$ and slowly increasing μ to 10, so that A_v and K_v are both maximal 10^{-2}m^2/s. The results are shown in Figure 5.4 (at the end of this section). Indeed, the Péclet number decreases, but even at $\mu = 10$, when $Pe \approx 0.5$, the estuary is not diffusion dominated. Correspondingly, $|\zeta|$ becomes smaller with increasing vertical mixing, but still $\zeta \leq -2$. Moreover, $|X|$ and $|J|$ become larger for increased vertical mixing. Possibly, the weaker vertical stratification allows the exchange flow to become stronger, because u_D is less suppressed by vertical stratification, as was also argued in §2.4.2. The fact that $|X|$ increases with enhanced mixing causes L to decrease, so that Pe does not become much smaller.

To conlude, for the current parameter settings, simultaneously increasing vertical eddy viscosity and diffusivity does not result in a significantly weaker vertical stratification.

Rescaling the steady equations

The unrealistic values for Z would be easier to solve if the origin of the Z-solution could be directly traced back from the model equations. This cannot be done, most importantly due to complicated Z-dependencies in most steady terms. Therefore, the typical magnitude of each individual term in the steady versions of (2.83), (2.84) and (2.85) is determined. To this end, the steady equations are first fully expanded, such that none of the individual terms contain a sum of multiple terms. All three equations have a prefactor proportional to $1/B(Z)$. This Z-dependent function in the denominator is kept unchanged and is not further expanded. After that, default parameters and the typical scales for X, Z and J found in §2.7.6 are substituted in these expanded equations. All terms whose magnitude is 10% or less than the largest-magnitude term is considered small. Each of these small terms is multiplied by dimensionless factor α. The remaining, large terms are kept unchanged.

For $\alpha = 1$, the equations are identical to the original steady equations. Then, the influence of the small terms is gradually decreased by decreasing α from 1 to 0 in small steps. Each previously computed result serves as a first guess value to compute steady solutions to (X, Z, J) for the new value of α. Unfortunately, no realistic values for X, Z and J could be obtained via this method. Most importantly, the vertical stratification becomes infinitely strong when α is reduced.

The fact that this method does not achieve the desired result is possibly due to the use of one common prefactor in front of all small terms. This method could be improved by using different prefactors, α_1, α_2, ..., for different kinds of small terms, e.g. dependent on their X- or J-dependency. Any way, making the evolution equations dimensionless and identifying typical magnitudes of each term is essential for future improvement and extension of the constructed model.

Sensitivity of results on seaward boundary conditions

Both dominant balances $0 = (2b)+(3b)$ and $0 = (2c)+(3c)$ yield a solution for Z that is dependent on the value of (a, b, c), i.e. the tuning parameters in the seaward boundary conditions. Since it was shown that these two balances are important in multiple ranges of u_R, H and A_v, and might explain the strong vertical stratification, it is expected that the solution for Z is very sensititve to the choice of these constants in the formulation of the seaward boundary conditions (2.52), (2.53) and (2.54). From the analytical solutions (5.2) and (5.4), vertical stratification is expected to become weaker with increasing values of (a, b, c). From Figure 5.5 can be seen that the weakest possible vertical stratification is $\zeta = -1$ for $(a, b, c) = 2$. For (a, b, c) larger than 2, $|\zeta| < 1$ for small u_R; the range $|\zeta| < 1$ becomes wider for increasing (a, b, c). One might thus expect that, for large enough (a, b, c), ζ can adopt realistic values for all realistic river discharges. Figures 5.6 and 5.7 show however, that when (a, b, c) becomes larger than ~ 2.7, $|X|$ starts to *decrease* for increasing $|u_R|$, contrary to the expectation. Hence more elaborate sensitivity studies should be performed to see if (a, b, c) can be tuned such that i) ζ reaches physically realistic values and ii) the dependency of steady X, Z and J on u_R, H and A_v is still physically understandable.

Further possible explanations for unphysical values of $(X, Z, J)_{est}$

Another possible explanation for the unphysically strong vertical stratification might be that the model has *another* steady solution that satisfies $(X, Z, J) < 0$, but with physically more realistic values. With the numerical solving procedures performed in this study, such alternative equilibria have not been found. The possibility can not be ruled out, however, that it does exist. For example, the *Mathematica*-command *NSolve* was used to find all steady states at the *default* parameter setting. It might be that different, realistic solutions can be found with *NSolve*, for slightly different default parameters, though. In that case, such another solution can be used as starting point for a numerical continuation method, as was done with *Mathematica*-command *FindRoot*.

Secondly, steady solutions were obtained from evolution equations (2.83), (2.84) and (2.85) by setting to zero all time-derivatives individually, even though their left-hand sides contain elaborate functions of time-derivatives. It is possible that *additional* steady states exist, however, to the steady equations which are first written in terms of dX/dt, dZ/dt or dJ/dt *only*, as explained in §3.2.

5.3 Outlook

One major limitation of the current model is the complexity of the equations, which complicates (analytical) study and interpretation of its solutions. There are several causes for this complexity.

A first cause is the complicated Z-dependency in the equations. This is mainly due to the functions $A(Z)$ and $B(Z)$, which result from relating streamfunction amplitude ψ_0 to angular momentum J. Hence it is key to find an alternative method to incorporate J (or another measure of estuarine circulation) into the model equations. Either should an alternative definition of the baroclinic flow field be pursued, which does not result in complicated Z-structures. Alternatively, the possibilities of *implicitly* closing terms $\propto J$ similarly to *Maas* [1994; 2004] could be reconsidered. If appropriate methods, i.e. physically realistic in the estuarine case, were found, this sidesteps the encountered difficulties of explicitly defining the linearised flow field.

Secondly, although the coupling of domain length L to the estuarine salt field is strictly necessary to accept a linear approximation of s, this coupling is another complicating factor in the model equations. Some terms in the evolution equations may for example contain X related to the horizontal salinity gradient, as well as one or multiple powers of X due to some factor $\frac{1}{L}$, $\frac{1}{L^2}$ or $\frac{1}{L^3}$, i.e. related to the size of the averaging-domain. Uncoupling the two effects is sometimes difficult. To overcome this complex coupling, domain length could be chosen fixed in time. Proper estimates of the intrusion length, dependent on river discharge strength and other physical parameters are given by *MacCready & Geyer* [2010].

Another possible way to reduce the complexity of the model is to restrict attention to the estuarine "inner domain". As argued in §2.5, the "outer layers", in which linearisation of salt and flow field is relaxed, are very thin compared to the inner domain. One might argue that the *essence* of estuarine dynamics lies within this inner domain. When restricting spatial integration also to this part of the estuary, linear salt and flow field expressions can in principle be *always* substituted in these integrals. No distinction has to be made between integrals that can be computed with the linearised salt and flow field, and integrals that can not, as was done in §2.5. This will significantly reduce the number of terms in the equations, as terms like

$$\iint z \frac{\partial}{\partial z} \left(K_v \frac{\partial s}{\partial z} \right) \, dxdz \tag{5.10}$$

simply vanish. However, the danger of this approach is that *all* contact between the inner and outer layers is lost, by which part of the essence of estuarine dynamics may be lost.

Apart from the issue of complexity, more physical processes can be included into the model. In the current approach, the effect of tides is only parametrically included through the diffusive and viscous coefficients. These coefficients are considered constant. The effect of e.g. stratification on the effectiveness of tidal mixing, i.e. the effect of tidal straining, is thereby ignored. This effect could be incorporated by parametrically relating mixing coefficients to e.g. the Richardson number.

Morevover, the current model assumes that the net inflow is always in balance with the net outflow. Hence the total free-surface elevation, averaged along the channel, is fixed. Allowing a net nonzero net in- or outflow from th estuarine domain, such a net flow is expected to be coupled to the dynamics of the average free-surface elevation; a net outflow of mass will result in a decrease of the total sea surface height. In addition, viscous and diffusive coefficients are also expected to vary with this net flow.

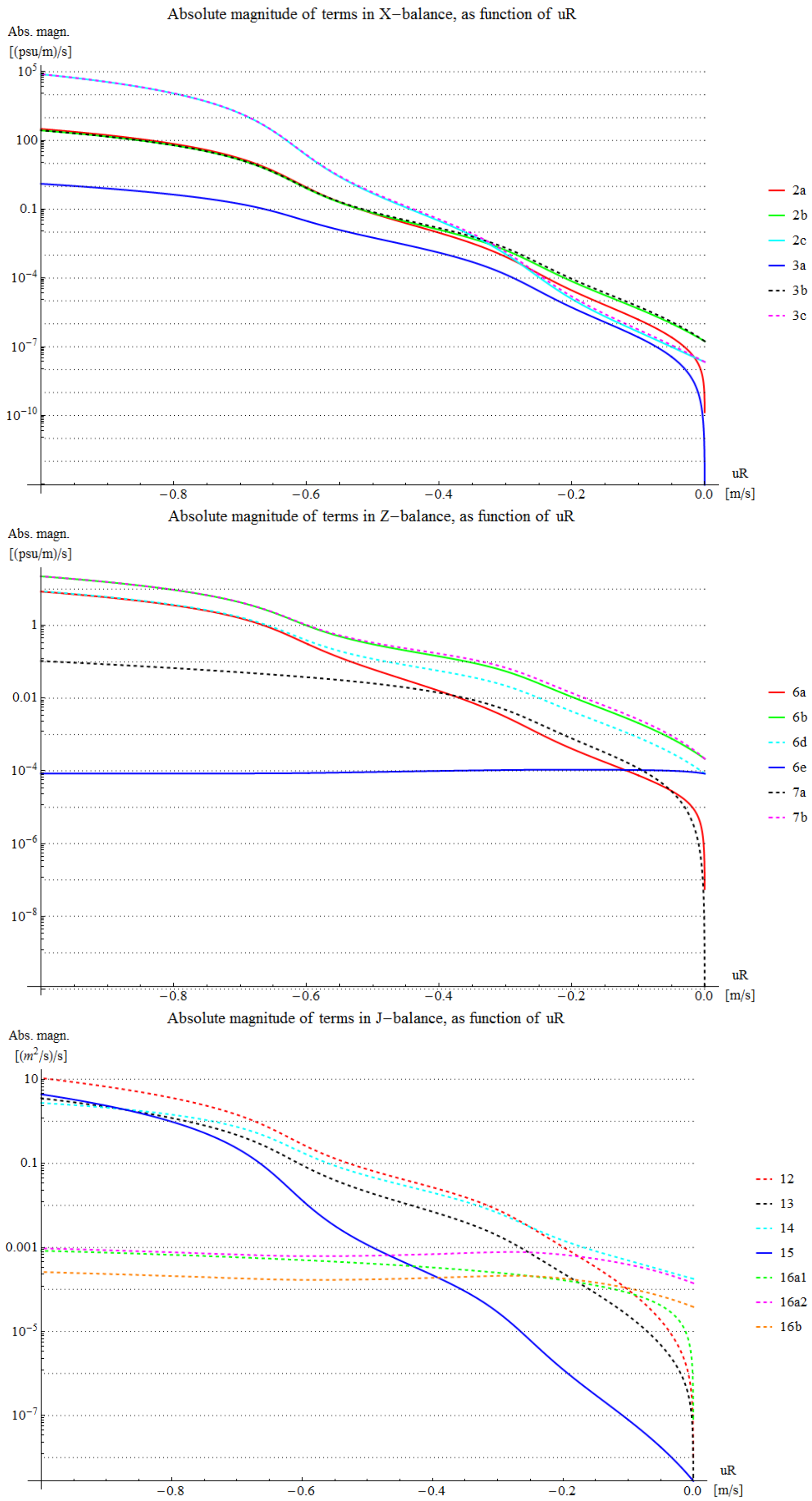

Figure 5.1: Absolute magnitude of steady terms in X-, Z- and J-balance (2.56), (2.64), (2.69), with "estuarine" steady solutions $(X, Z, J)_{est}$ substituted, as a function of river discharge u_R.

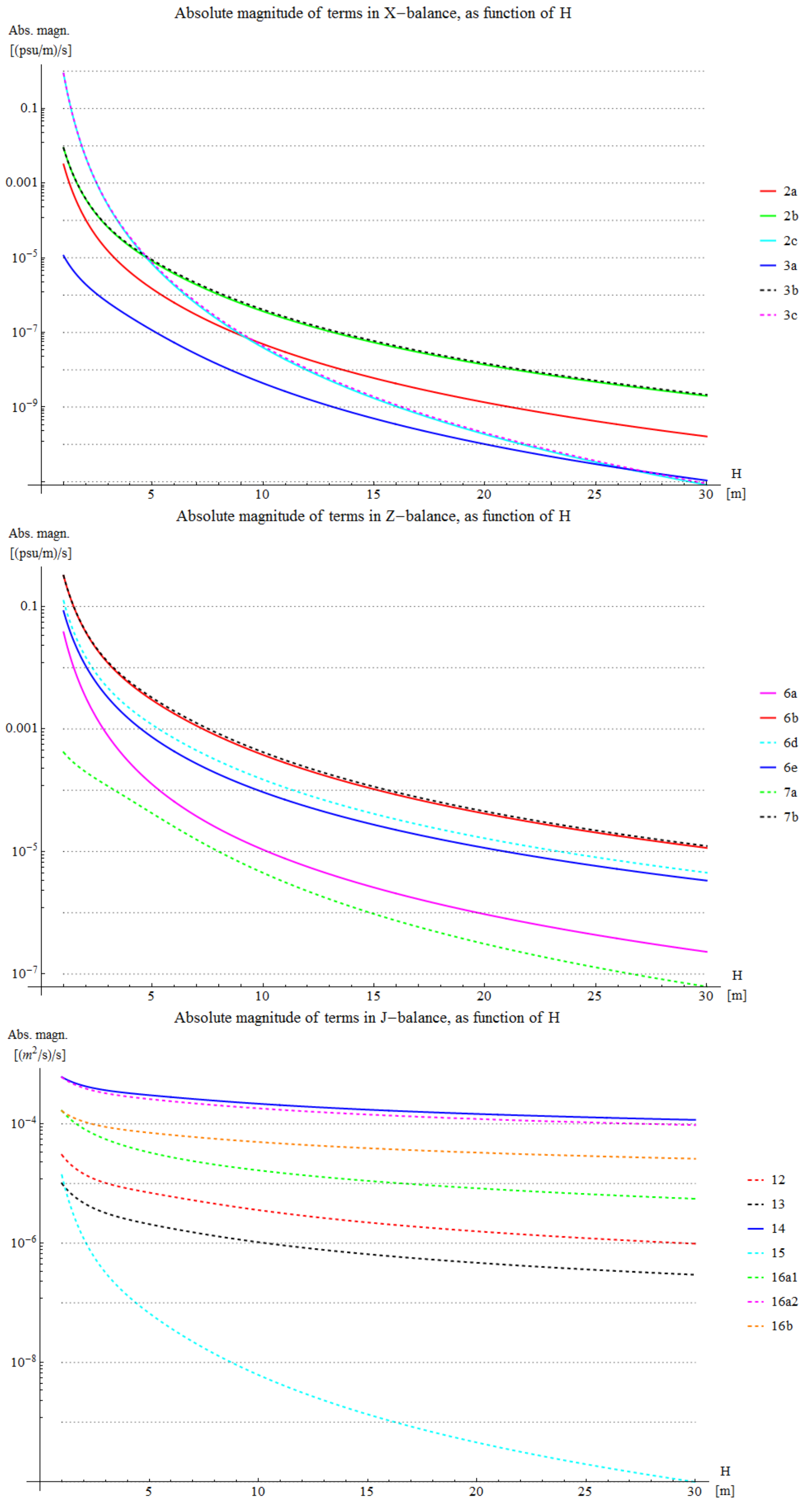

Figure 5.2: Absolute magnitude of steady terms in X-, Z- and J-balance (2.56), (2.64), (2.69), with "estuarine " steady solutions $(X, Z, J)_{est}$ substituted, as a function of depth H.

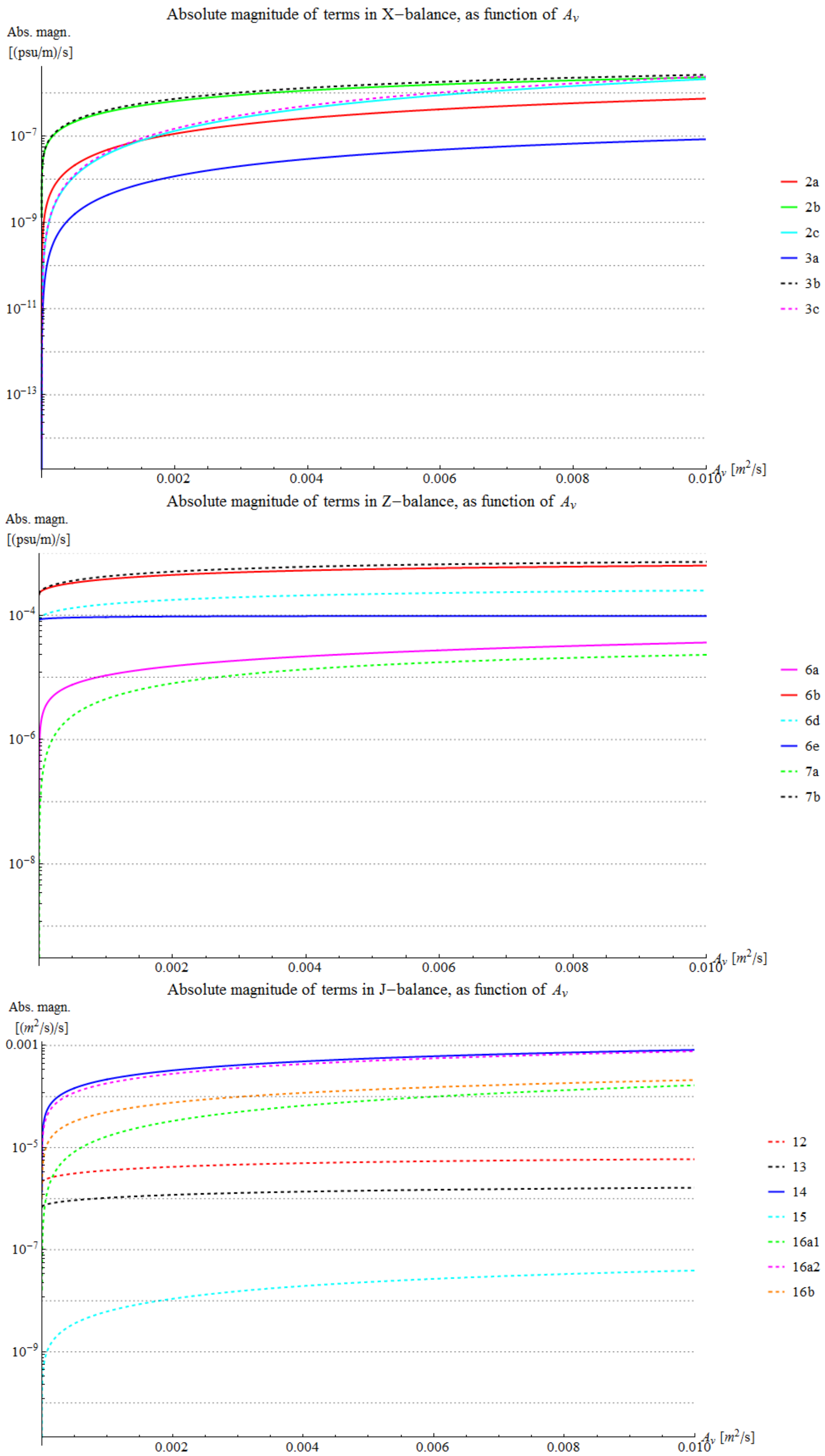

Figure 5.3: Absolute magnitude of steady terms in X-, Z- and J-balance (2.56), (2.64), (2.69), with "estuarine " steady solutions $(X, Z, J)_{est}$ substituted, as a function of vertical eddy viscosity A_v.

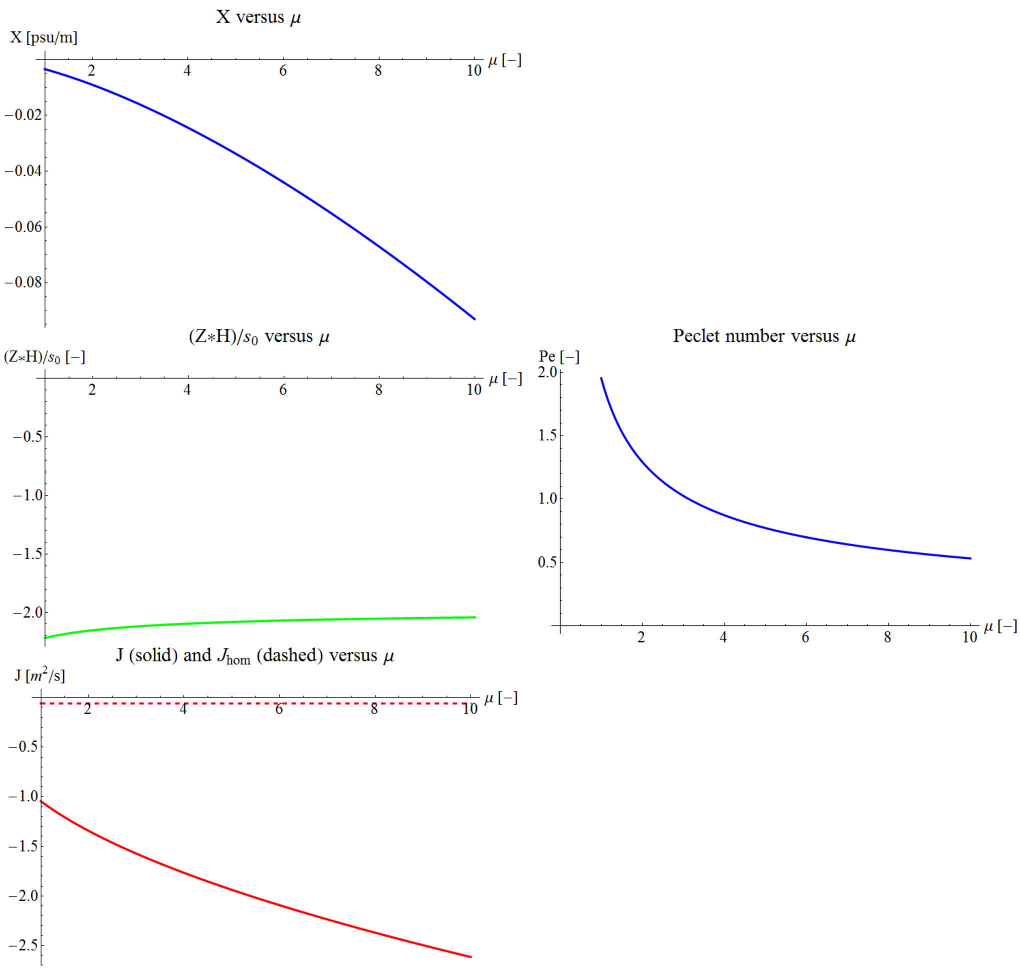

Figure 5.4: Left three figures: "estuarine" steady solution $(X, Z, J)_{est}$ as a function of factor μ, that scales the magnitude of A_v and K_v. Right figure: Peclet number Pe versus dimensionless factor μ.

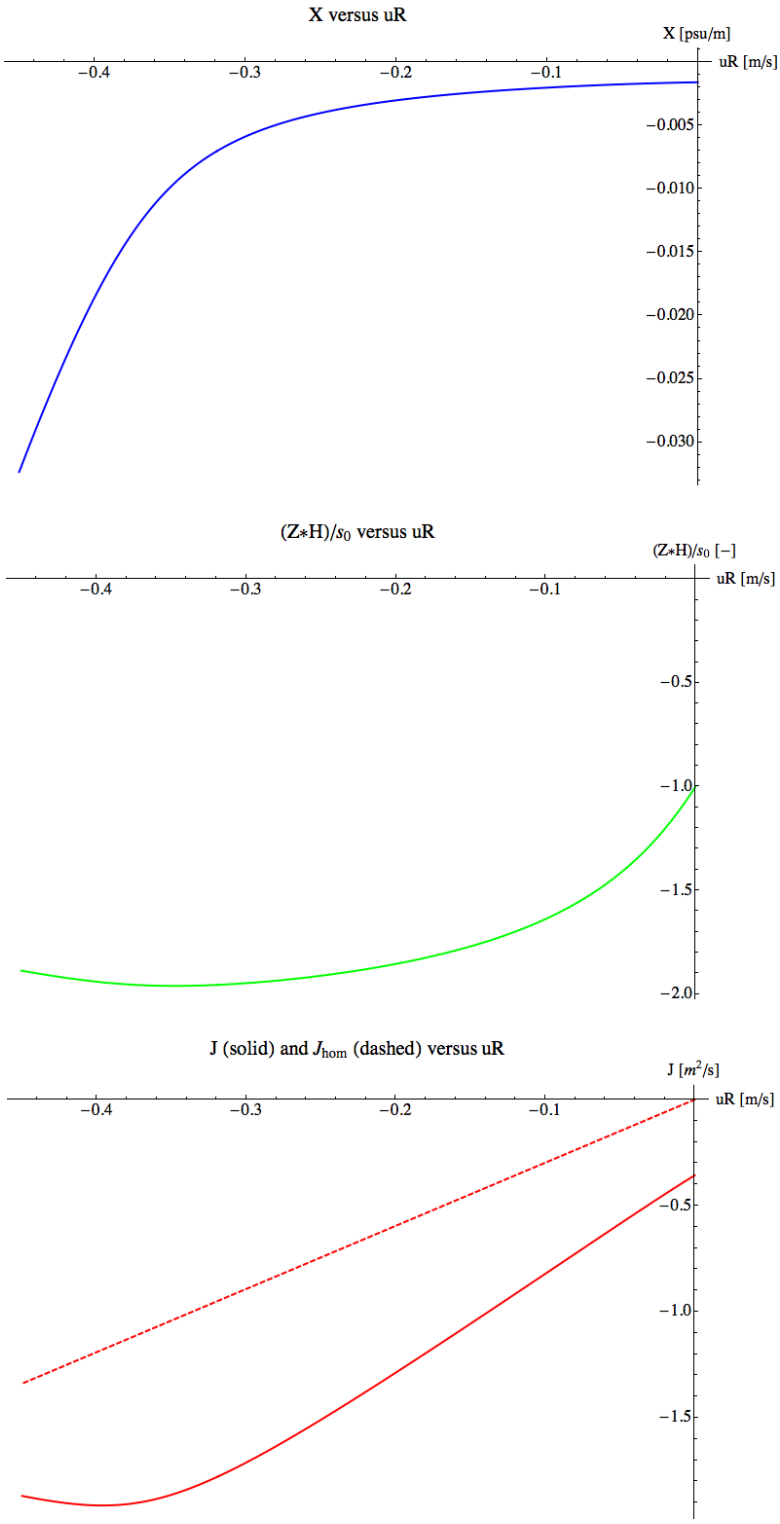

Figure 5.5: "Estuarine" steady solutions $(X,\ ZH/s_0,\ J)_{est}$, **for** $(a, b, c) = 2$, versus river discharge u_R. The remaining parameters are default, as defined in §3.1. **Note that** u_R varies along the **horizontal** axis.

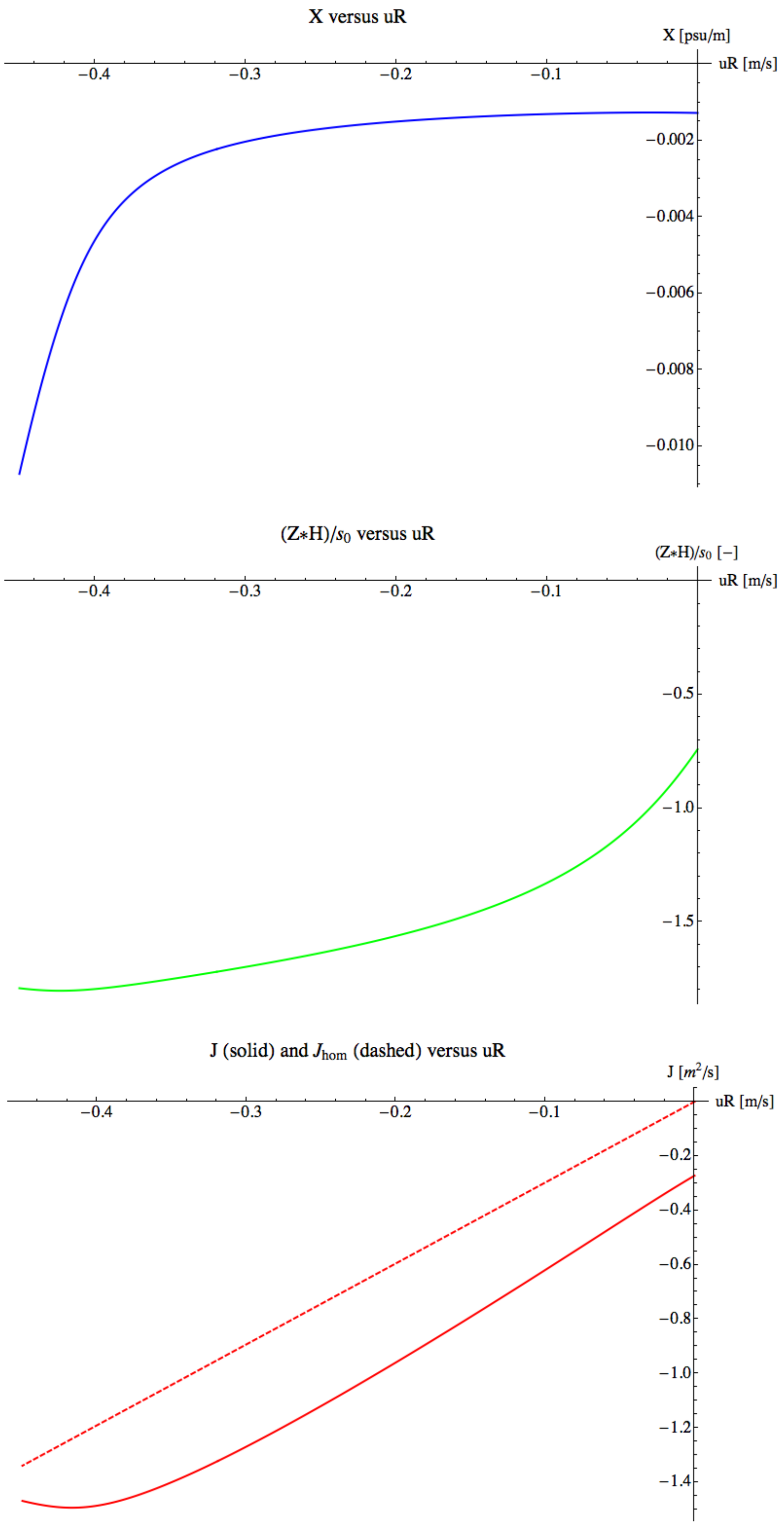

Figure 5.6: As Figure 5.5, but **for** $(a, b, c) = 2.7$. **Note that** u_R varies along the **horizontal** axis.

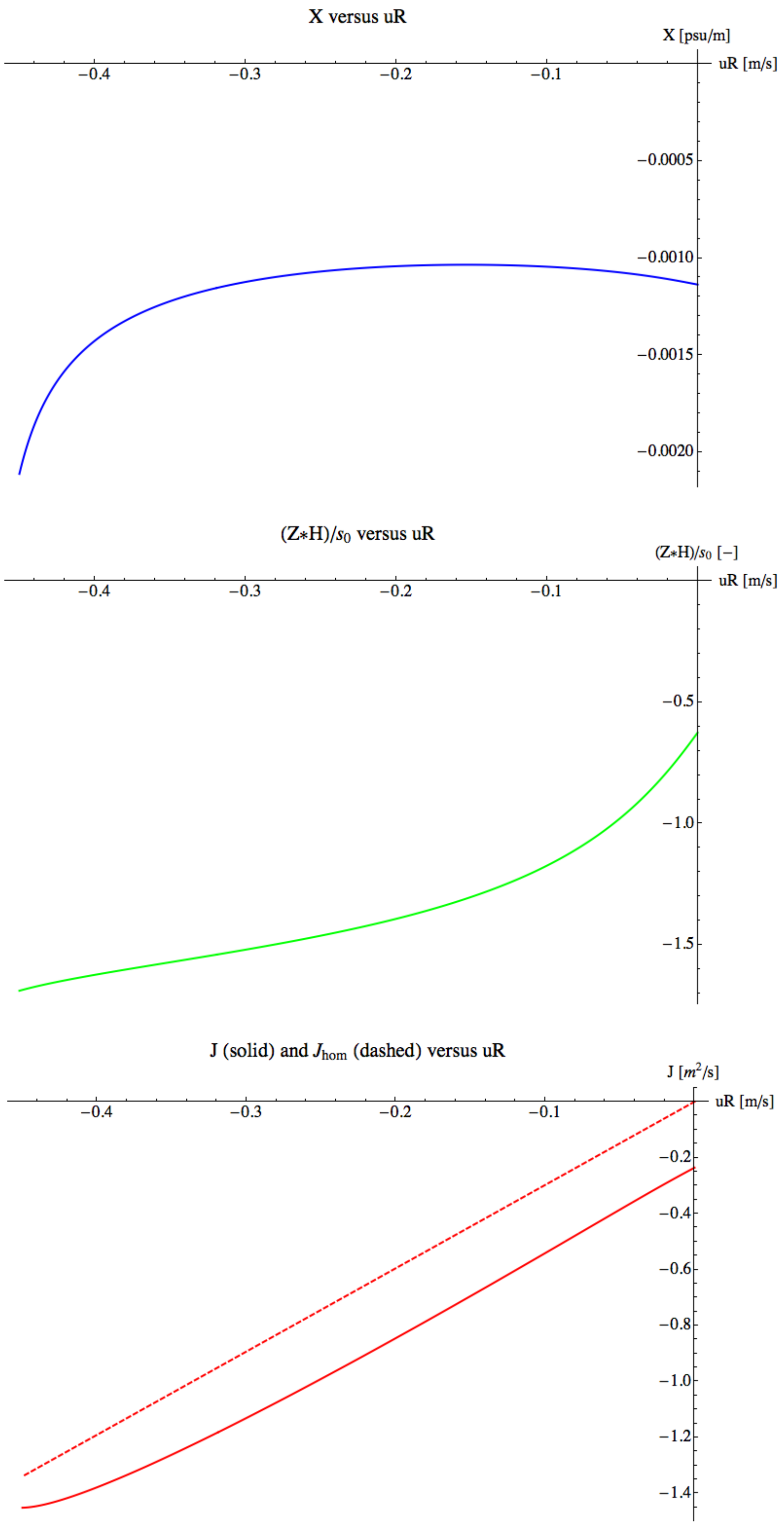

Figure 5.7: As Figure 5.5, but **for** $(a, b, c) = 3.2$. **Note that** u_R varies along the **horizontal** axis..

Chapter 6

Conclusions

Below, the research aims posed in §1.5 are recalled and considered.
Construct a model for estuarine subtidal hydrodynamics that

1 Is closed in terms of basin-averaged variables only.
A closed set of three evolution equations (ordinary differential equations) was derived. These describe domain-averaged horizontal and vertical salinity gradient, (X, Z), and domain-averaged (baroclinic) angular momentum, J. Domain-length L is defined as the furthest up-estuarine reach of salt and is directly related to internal dynamics, $L = -s_0/X$. All individual terms contributing to these equations have a clear physical meaning.

2 Has simple enough model equations so that analytic steady state solutions exist.
One physically explainable analytic solution has been found, i.e. $(X, Z, J) = (0, 0, J_{hom})$ has an analytical expression. This solution is for an infinitely long estuary, homogeneously filled with sea water. J_{hom} increases linearly due to bottom-layer shear induced by the river flow and thus is not related to the gravitational circulation. For several limiting parameter values for river discharge, depth and vertical eddy viscosity, analytical solutions were found that approximate the full steady balances. No further analytic solutions to the full steady evolution equations have been found so far. These must therefore be solved numerically. The diffulty of finding an analytical solution is especially due to complicated Z-dependencies. Several suggestions are done in §5 to decrease this complexity.

3 Allows detection of multiple equilibria, if existing.
For the default parameter settings, multiple steady states exist, at

least two of which are physically interesting, i.e. $(X, Z, J)_{est} < 0$ and $(0, 0, J_{hom})$.

4 **Has at least one steady state solution whose dependency on river and tidal influence is physically interpretable.** The dependency of $(0, 0, J_{hom})$ on its constituting terms could be fully explained. The dependency of $(X, Z, J)_{est}$ on river discharge velocity u_R, water depth H and vertical eddy viscosity A_v was considered. The solution $(X, Z, J)_{est}$ was compared to other model studies, for small variations in u_R and H around their default values. This behaviour quilitatively agrees with this reference study, although the values of X and especially Z are not of the right order of magnitude. Extremely strong vertical stratification was found, which is most likely due to the formulated seaward boundary conditions. For several specific parameter choices the full steady balances could be reduced, so that analytical solutions can be found. The terms contributing to these steady balances could almost all be explained physically. However, this interpretation is difficult to compare to other studies.

This model should describe time-evolution of the basin-averaged variables, so that

5 **Linear stability of the steady states can be computed.**
Linear stability can be computed for all (numerically) solved steady states. $(X, Z, J)_{est}$ is linearly stable for all $u_R \leq 0$, $H > 0$ and $A_v \geq 0$. Stability increases as a function of river discharge or vertical eddy viscosity, but decreases asymptotically for increasing depth. $(X, Z, J)_{hom}$ is neutrally stable.

6 **The variable's time evolution after perturbation from steady state can be computed.**
It is expected that $(X, Z, J) = (0, 0, 0)$, in the absence of river discharge, while $(X, Z, J) < 0$ for nonzero river discharge. Hence the system is expected to evolve from $(0, 0, J_{hom})$ at $u_R = 0$ to $(X, Z, J)_{est}$ at $u_R < 0$. It is indeed found that the system jumps from the former to the latter state, for very small and negative u_R. This was observed for small negative X-perturbation, small positive or negative J-perturbation and a relatively large negative Z-perturbation.

6.1 Added value of the constructed model

To conclude this study, all limitations and advantages of the constructed model are considered.

Although the numerical solution $(X, Z, J)_{est}$ could be fully interpreted in terms of various approximations to the full steady balances (see Appendix C), it proved difficult to connect these interpretations to physical reality. Several causes for this difficulty can be identified.

Firstly, the individual terms that contribute to the steady balances in §2.7 are all physically understandable, but can not be all directly compared to or tested with other theoretical, modelling or experimental studies. For example, the coupling of domain-averaged horizontal salinity gradient X to domain length L could be physically interpreted, but makes the results less comparable to other studies. Choosing a fixed domain length might hence be worth considering for future research.

Secondly, the complicated dependency on vertical stratification reduces the transparancy of model results. Even in some cases where analytical approximations to the full steady balances exist, the complex Z-structure hinders the interpretation of these solutions. The Z-dependency is mainly due to the explicitly formulated baroclinic flow field. Exploring alternative ways to incorporate a measure of overturning, or angular momentum J into the model is therefore worthwile.

Thirdly, the model results investigated have unrealisticly strong vertical stratification. Due to this stratification, some individual terms that are physically undertandable, e.g. the river-induced outflow of domain-averaged salinity, loose their connection with physical reality in case of such strong stratification. Formulating more appropriate boundary conditions at the seaward boundary might solve this problem and should therefore have priority.

To conclude, *at this stage* in its development, the constructed model cannot be used yet to gain more insight into global estuarine subtidal dynamics. However, it was shown that the attempted description of global variables has the potential to gain more insight. After all, it has proven possible to identify and interpret all physical processes *individually* contributing to the evolution of global variables. Furthermore, methods have been explored to sidestep the complexity of the model and to elucidate even very complicated, numerically obtained steady solutions. This method comprises identification of the dominantly contributing terms and solving steady balances in reduced form. Finally, the model has the capability of predicting the *evolution* of global variables, contrary to other analytical models. The existence of bifurcations between multiple equilibria can hence be investigated. With some further simplifications to the model constructed in this study, also the appearance of multiple equilibria and time-dependence will be physically interpretable.

Acknowledgements

Concluding this study, I would like to thank my supervisors, Leo Maas and Huib de Swart, for their continuous support and for their inspiring comments. Moreover, I owe many thanks to Aart, Ellen and Annemarie for their everlasting support during all phases of the project. Working at the IMAU wouldn't have been as enjoyable without all my fellow master students, sharing the IMAU student's room, our thesis experiences and our walk during lunch time. Finally, I would like to thank Elisha for her support in the concluding phase of this study.

Bibliography

[1] Burchard, H., Bolding, K., & Villarreal, M. R. (2004). Three-dimensional modelling of estuarine turbidity maxima in a tidal estuary. *Ocean Dynamics, 54*(2), 250-265.

[2] Cushman-Roisin, B., & Beckers, J. M. (2011). *Introduction to geophysical fluid dynamics: physical and numerical aspects* (Vol. 101). Academic Press.

[3] De Swart, H.E. (2012). Physics of Coastal Systems: lecture notes 2012-2013. Utrecht University, The Netherlands.

[4] Dijkstra, H. A. (2013). *Nonlinear climate dynamics.* Cambridge University Press.

[5] Dyer, K. R. (1997). Estuaries: a physical introduction. 2nd edition. John Wiley & Sons.

[6] Festa, J. F., & Hansen, D. V. (1976). A two-dimensional numerical model of estuarine circulation: The effects of altering depth and river discharge. *Estuarine and coastal marine science, 4*(3), 309-323.

[7] Hansen, D. V., & Rattray, M. (1965). Gravitational circulation in straits and estuaries.

[8] Hansen, D. V., & Rattray, M. (1966). New dimensions in estuary classification. *Limnology and Oceanography, 11*(3), 319-326.

[9] Maas, L. R. (1994). A simple model for the three-dimensional, thermally and wind-driven ocean circulation. *Tellus A, 46*(5), 671-680.

[10] Maas, L. R. (2004). Theory of basin scale dynamics of a stratified rotating fluid. *Surveys in geophysics, 25*(3-4), 249-279.

[11] MacCready, P. (1999). Estuarine adjustment to changes in river flow and tidal mixing. *Journal of Physical Oceanography, 29*(4), 708-726.

[12] MacCready, P. (2004). Toward a unified theory of tidally-averaged estuarine salinity structure. *Estuaries, 27*(4), 561-570.

[13] MacCready, P., & Geyer, W. R. (2010). Advances in estuarine physics. *Annual Review of Marine Science, 2*, 35-58.

[14] Marshall, S., & Elliott, M. (1998). Environmental influences on the fish assemblage of the Humber estuary, UK. *Estuarine, Coastal and Shelf Science, 46*(2), 175-184.

[15] Schramkowski, G. P., De Swart, H. E., & Schuttelaars, H. M. (2010). Effect of bottom stress formulation on modelled flow and turbidity maxima in cross-sections of tide-dominated estuaries. *Ocean dynamics, 60*(2), 205-218.

[16] Stienstra, J. (2009). Wiskundige Technieken 3 (lecture notes). Mathematisch Instituut. Universiteit Utrecht.

[17] Talke, S. A., de Swart, H. E., & Schuttelaars, H. M. (2009-a). Feedback between residual circulations and sediment distribution in highly turbid estuaries: an analytical model. *Continental Shelf Research, 29*(1), 119-135.

[18] Talke, S. A., de Swart, H. E., & De Jonge, V. N. (2009-b). An idealized model and systematic process study of oxygen depletion in highly turbid estuaries. *Estuaries and coasts, 32*(4), 602-620.

[19] Valle-Levinson, A. (Ed.). (2010). Contemporary issues in estuarine physics. Cambridge University Press.

[20] Winterwerp, J. C., & Wang, Z. B. (2013). Man-induced regime shifts in small estuaries - I: theory. *Ocean Dynamics, 63*(11-12), 1279-1292.

Appendix A

Derivation of linear approximation of the flow-field

A.1 Linearly approximated salt field

Modelling results by *Festa & Hansen* [1976], Figures 5 and 10, indicate that the width- and depth-averaged salt profile can be roughly divided into two alongchannel regions. In the first part, between the seaward boundary and some point $x = \mathcal{L}$ up-estuary, depth-averaged salinity steeply decreases up-estuary to some small value, about $0.05 \cdot s_0$, as indicated by the end of the green area in Figure 1.2. In the second region, from $x = \mathcal{L}$ up to some point far up-river, the horizontal salinity gradient is much weaker and salinity decreases almost asymptotically to zero. *Festa & Hansen* let their domain length vary with the up-estuary reach of the $0.0015 \cdot s_0$ isopycnal. Hence their model length dynamically changes with forcing conditions, parameter settings and internal dynamics. A similar "dynamic" basin length is pursued here. Yet linearising the salinity profile is only acceptable in the first, seaward region and not in the second, riverward region. However, since the salinity at the end $x = \mathcal{L}$ of the first region is also relatively small, it is safe to define the salt intrusion length alternatively, namely up to $x = \mathcal{L}$. To conclude, basin length L is here defined as the salt intrusion length, $x = L_i$, such that linearising s is acceptable along the entire estuarine domain.

Linearising the vertical salinity structure is assumed always acceptable, as motivated by e.g. Figures 4b and 9b in *Festa & Hansen* [1976].

A.2 Derivation of linear velocity profiles

A.2.1 Linearisation of u and w

The simplified momentum balances used by e.g. *MacCready* [2004] yield quadratic river profile u_Q and cubic baroclinic profile u_c,

$$u_c = -|u_E| \left(1 - 9\left[\frac{z}{H}\right]^2 - 8\left[\frac{z}{H}\right]^3\right) \quad \text{and} \quad u_Q \propto -\frac{3}{2}|u_R| \left(1 - \left[\frac{z}{H}\right]^2\right)., \tag{A.1}$$

with exchange flow strength u_E (constant in depth) and depth-averaged horizontal velocity $u_R (< 0)$. u_c can be roughly divided into a relatively thin surface and bottom layer and a large middle layer. $\frac{\partial u_c}{\partial z}$ is small in the surface layer, in the absence of along-channel wind stress; u_c changes steadily with depth in the middle layer and changes sign at $z = z_j$, about halfway the middle depth layer; in the bottom layer u_c decreases to zero at the bottom.

To first approximation, u_c can be linearised, say $\widehat{u_c}$, within the middle depth layer. u_c is different and not strictly linear in the surface and bottom layers, satisfying $\frac{\partial u_c}{\partial z}|_{z=0} = 0$ and $u_c|_{z=-H} = 0$. River flow profile u_Q is quadratic due to bottom friction, but here it is assumed that bottom friction only affects u_Q within the bottom layer, decreasing it to zero at the bottom. It is then convenient to approximate u_Q as a constant, $\widehat{u_Q}$, within surface *and* middle layer.

Motivated by several model studies, e.g. *Talke et al.* [2009-a], *Festa & Hansen* [1976], *Hansen & Rattray* [1965], the depth of the top and bottom layers are relatively small compared to total column depth. The top- and bottom-layer deviations of u_c and u_Q from the linear resp. constant middle-layer profiles is thus assumed here to be of minor importance, when considering *domain-averaged* properties. In practice, when integrating u_c or u_Q over the entire domain, one can replace them by their linear resp. constant approximations for the entire column-depth. Boundary conditions at top and bottom are assumed to be satisfied within very thin "outer layers".

To ensure that this full-depth simplification still obeys the discharge condition and the condition for zero net baroclinic transport, i.e

$$\frac{1}{H}\int_{-H}^{0} u_Q \, dz = u_R \quad \text{and} \quad \int_{-H}^{0} u_c \, dz = 0, \tag{A.2}$$

assume that $u_Q = u_R$ and $u_c \propto -\left(z + \frac{H}{2}\right)$, i.e. $z_j \to -\frac{H}{2}$. Rename u_c as u_D, the depth-dependent velocity part, to indicate that it is used for all depths.

The exact expression for u_D is found when considering the streamfunction profiles in e.g Figures 5 and 10 of *Festa & Hansen* [1976]. Between $x = 0$ and the intrusion length L_i (taken at $x = \mathcal{L}$ in Appendix A.1), this streamfunction is almost perfectly elliptic around some rotation axis position (x_j, z_j), with $w > 0$ ($w < 0$) riverward (seaward) of x_j. It is assumed here that also w can be linearised. The expression for baroclinic streamfunction profile ψ_D, and hence $w = \frac{\partial \psi_D}{\partial x}$ and $u_D = -\frac{\partial \psi_D}{\partial z}$, will be explained in the next section.

A.2.2 Expression for elliptic baroclinic streamfunction

So far, the vertical "outer layers" for u have been specified. However, the linear approximation of the flow field doesn't hold for the entire *length* of the domain either. On the riverward and seaward edges of the domain, "outer layers" have to be specified as well, such that boundary conditions can be satisfied. Physically, salinity is restricted to $0 \leq s \leq s_0$ within the estuary. Linear salt field (2.29) prescribes that $s > s_0$ seaward of the $(s = s_0)$-isopcynal, which intersects the bottom at $x = 0$ and the surface at

$$x_{0,top} = -\frac{HZ}{X}. \tag{A.3}$$

Likewise does it prescribe that $s < 0$ riverward of the $(s = 0)$-isopcynal, which intersects the bottom at $x = L_i$ and the surface at

$$L_{i,top} = -\frac{s_0 + HZ}{X}. \tag{A.4}$$

The latter position is indicated by the vertical blue dashed line close to $x = L_i$ in Figure 2.1. Now one could imagine that the salt field is linear within this parallelogram-shaped region, and that linearity is quickly relaxed within infinitely thin "outer layers" around the $(s = s_0)$- and $(s = 0)$-isopycnals. However, using such a non-rectangular domain would significantly complicate domain-integration. Moreover, linearly approximating the flow field as explained hereafter would then be impossible. Instead, the riverward integration boundary was chosen vertically downward at $x = L_i$ and the seaward integration boundary vertically downward at $x = 0$.

It will thus be *accepted* here that the linear salinity expansion gives values $s < 0$ within the integration domain, between $L_{i,top}$ and L_i. However, *physically* arguing that s remains zero riverward of the $(s = 0)$-isopycnal, one could imagine that depth-averaged salinity smoothly decreases from its inner-domain value X at $L_{i,top}$ to zero at $x = L_i$. See Figure A.1 for an illustration. Physically arguing that no salt penetrates further up-river than L_i *at all depths*, the imposed boundary conditions are

$$s|_{x=L} = 0 \quad \text{and} \quad \frac{\partial s}{\partial x}|_{x=L} = 0 \text{ for all } z.$$

The latter condition implies that baroclinic driving force and hence baroclinic flow (u_D, w) vanishes at $x = L_i$, which agrees with streamfunction figures in *Festa & Hansen* [1976] at position $x = \mathcal{L}$. These same figures indicate the elliptic circulation cell is closed at some point seaward of $x = 0$, i.e. outside the adopted integration domain. Using similar arguments as above, one could physically argue that s remains s_0 everywhere seaward of the $(s = s_0)$-isopycnal, *without* explicitly imposing this. Then, the depth-averaged salinity gradient can be thought of as smoothly decreasing from its inner-domain value X at $x = 0$ to zero at $x = x_{0,top}$. See Figure A.1. Then salinity has reached its maximum value *for all depths* at $x_{0,top}$, so that $\frac{\partial s}{\partial x}|_{x=x_{0,top}} = 0$ for all z. Similarly, the baroclinic driving force thus vanishes here. To conclude, the elliptic circulation cell is assumed to be confined between $x = x_{0,top}$, $z = -H$, $x = L_i$ and $z = 0$. For linear (u_D, w), this yields expression (2.42).

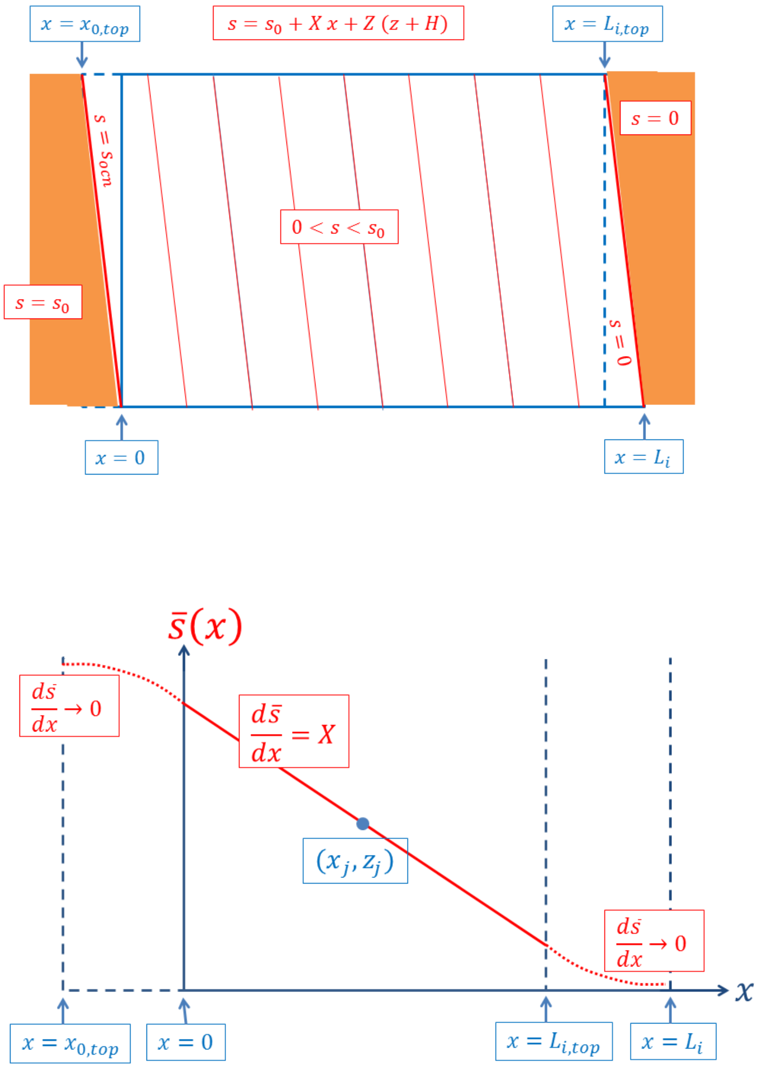

Figure A.1: Top figure: Linear salinity-field expansion, following (2.29), but "keeping in mind" (although not imposing this as a boundary condition) that $s = 0$ landward of the $(s = 0)$-isopycnal and $s = s_0$ seaward of the $(s = s_0)$-isopycnal. Bottom figure: depth-average $(1/H \int s\; dz = \bar{s}(x))$ of the salinity profile from the top figure. It can be seen that, when "keeping in mind" that $0 \leq s \leq s_0$, the depth-averaged salinity gradient weakens of to zero at $x_{0,top}$ and L_i.

Appendix B

Derivation of evolution equations

B.1 Derivation of evolution equations in general form

Throughout this study and unless specified otherwise, integrals imply integration over full basin length or depth, i.e. $\int dx = \int_0^L dx$ and $\int dz = \int_{-H}^0 dz$.

Following the explanations in §2.5, all viscous and diffusive exchange coefficients are assumed constant within any domain-integral. Although $A_{h,v}, K_{h,v}$ are assumed different and spatially dependent in the "outer layers", these differences are assumed not to affect domain integrals. However, whenever a domain-integral has to be rewritten in terms of domain-integrals, these different outer-layer values are assumed to play a role. Note that boundary condition (2.17) has been replaced by (2.48).

Derivation of $\frac{dX}{dt}$

To derive $\frac{dX}{dt}$, take the time-derivative of definition

$$X(t) = \frac{\iint \left(x - \frac{L}{2}\right) s \; dxdz}{\iint \left(x - \frac{L}{2}\right)^2 \; dxdz} = \frac{f}{g}, \tag{B.1}$$

with $f = \iint \left(x - \frac{L}{2}\right) s \; dxdz$ and $g = \iint \left(x - \frac{L}{2}\right)^2 \; dxdz = \frac{1}{12}L^3 H$. Write $\frac{dX}{dt} = \frac{g\frac{df}{dt} - f\frac{dg}{dt}}{g^2}$ and substitute $f = gX$ therein to obtain

$$\frac{dX}{dt} = \frac{\frac{df}{dt} - X\frac{dg}{dt}}{g}. \tag{B.2}$$

Then $\frac{df}{dt}$ and $\frac{dg}{dt}$ are obtained by employing Leibniz' differentiation rule for the time-dependent boundaries $x = L(t)$ and adopting a Eulerian viewpoint, such that $\frac{dx}{dt} = \frac{dz}{dt} = 0$. Then the evolution equation reads

$$\frac{dX}{dt} = \underbrace{-\frac{6}{L^3 H}\frac{dL}{dt}\iint s\ dxdz}_{(1)} + \underbrace{\frac{12}{L^3 H}\iint x\frac{\partial s}{\partial t}\ dxdz}_{(2)} \qquad \text{(B.3)}$$

$$\underbrace{-\frac{6}{L^2 H}\iint \frac{\partial s}{\partial t}\ dxdz}_{(3)} + \underbrace{\frac{6}{L^2 H}\frac{dL}{dt}\int s|_{x=L}\ dz}_{(4)} \underbrace{-\frac{3}{L}\frac{dL}{dt}X}_{(5)},$$

Salt balance (2.3) is substituted in the integrands of terms (2) and (3). As explained in §2.5, the linearised expressions (2.29), (2.43) and (2.44) for s, u and w cannot be substituted in the resulting domain-integrals. Instead, integrating by parts, they yield

$$(2) = \frac{12}{L^3 H}\left[-L\int f_S|_{x=L}\ dz\ +\ \iint f_S\ dxdz\ -\ \int x\ g_S|_{z=-H}^{z=0}\ dx\right], \qquad \text{(B.4)}$$

$$(3) = \frac{6}{L^2 H}\left[\int f_S|_{x=0}^{x=L}\ dz\ +\ \int g_S|_{z=-H}^{z=0}\ dx\right]. \qquad \text{(B.5)}$$

Derivation of $\frac{dZ}{dt}$

Similarly, take the time-derivative of definition

$$Z(t) = \frac{\iint \left(z + \frac{H}{2}\right) s\ dxdz}{\iint \left(z + \frac{H}{2}\right)^2\ dxdz} = \frac{j}{k}, \qquad \text{(B.6)}$$

with $j = \iint \left(z + \frac{H}{2}\right) s\ dxdz$ and $k = \iint \left(z + \frac{H}{2}\right)^2\ dxdz = \frac{1}{12}LH^3$. Again, writing $j = kZ$, one finds

$$\frac{dZ}{dt} = \frac{\frac{dj}{dt} - Z\frac{dk}{dt}}{k}. \qquad \text{(B.7)}$$

Computing $\frac{dj}{dt}$ and $\frac{dk}{dt}$ likewise as for X, one finds

$$\frac{dZ}{dt} = \underbrace{\frac{12}{LH^3}\iint z\ \frac{\partial s}{\partial t}\ dxdz}_{(6)} + \underbrace{\frac{6}{LH^2}\iint \frac{\partial s}{\partial t}\ dxdz}_{(7)} \qquad \text{(B.8)}$$

$$+\underbrace{\frac{12}{LH^3}\frac{dL}{dt}\int z\ s|_{x=L}\ dz}_{(8)} + \underbrace{\frac{6}{LH^2}\frac{dL}{dt}\int s|_{x=L}\ dz}_{(9)} \underbrace{-\frac{1}{L}\frac{dL}{dt}Z}_{(10)}.$$

Again, substituting the salt balance in terms (6) and (7) and integrating by parts, as explained in §2.5,

$$(6) = \frac{12}{LH^3}\left[-\int z\ f_S|_{x=0}^{x=L}\ dz\ -\ \int (z\ g_S)|_{z=-H}^{z=0}\ dx\ +\ \iint g_S\ dxdz\right] \tag{B.9}$$

$$(7) = \frac{6}{LH^2}\left[-\int f_S|_{x=0}^{x=L}\ dz\ -\ \int g_S|_{z=-H}^{z=0}\ dx\right] \tag{B.10}$$

Derivation of $\frac{dJ}{dt}$

Take the time derivative of definition

$$J(t) = \frac{1}{LH}\iint \left[(z-z_j)\,(u-u_R) - (x-x_j)\,w\right]\ dx\ dz, \tag{B.11}$$

employ Leibniz'rule and a Eulerian perspective. Then, treating u_R as a constant in time,

$$\begin{aligned}\frac{dJ}{dt} =& \underbrace{-\frac{1}{L}\frac{dL}{dt}J}_{(11)} + \underbrace{\frac{1}{LH}\iint\left[(z-z_j)\frac{\partial u}{\partial t}\ -\ (x-x_j)\frac{\partial w}{\partial t}\right]\ dxdz}_{(12-16)} \\ &+ \underbrace{\frac{dx_j}{dt}\frac{1}{LH}\iint w\ dxdz}_{(17)}\underbrace{-\frac{dz_j}{dt}\frac{1}{LH}\iint (u-u_R)\ dxdz}_{(18)} \\ &+ \underbrace{\frac{1}{LH}\frac{dL}{dt}\left[\int (z-z_j)\ u|_{x=L}\ dz\ -\ u_R\int (z-z_j)\ dz\ -\ (L-x_j)\int w|_{x=L}\ dz\right]}_{(19)}.\end{aligned} \tag{B.12}$$

Several of these terms can be specified further, as is explained hereafter. For the remaining terms, either the linearised salt- and flow field expressions or boundary conditions are required.

Substitute horizontal momentum balance $x-$momentum balance (2.5). Rewrite the advective terms, using continuity relation (2.8) as $\frac{\partial(uu)}{\partial x} + \frac{\partial(uw)}{\partial z}$. Substitute "0" for the term $\frac{\partial w}{\partial t}$. Then, after integration by parts,

$$(12) = -\frac{1}{LH}\iint (z-z_j)\frac{\partial(uu)}{\partial x}\ dxdz = -\frac{1}{LH}\int (z-z_j)u^2|_{x=0}^{x=L}\ dz, \tag{B.13}$$

$$\begin{aligned}(13) &= -\frac{1}{LH}\iint (z-z_j)\frac{\partial(uw)}{\partial z}\ dxdz \\ &= -\frac{1}{LH}\int (z-z_j)uw|_{z=-H}^{z=0}\ dx\ +\ \frac{1}{LH}\iint uw\ dxdz.\end{aligned} \tag{B.14}$$

The pressure-gradient term reads

$$(14) = -\frac{1}{LH}\iint (z - z_j)\frac{1}{\rho_0}\frac{\partial p'}{\partial x}\ dxdz \tag{B.15}$$

and will be solved later. Using partial integration, the next term becomes

$$(15) = \frac{1}{LH}\iint (z - z_j)\frac{\partial}{\partial x}\left(A_h\frac{\partial u}{\partial x}\right)\ dxdz = \frac{1}{LH}\int \left[(z - z_j)A_h\frac{\partial u}{\partial x}\right]\Big|_{x=0}^{x=L}\ dz,$$

which can be further simplified using continuity and integrating by parts,

$$(15) = -\frac{1}{LH}\left[\{(z - z_j)\ A_h\ w\}\,|_{x=0}^{x=L}\right]\Big|_{z=-H}^{z=0}\ +\ \frac{1}{LH}\int (A_h\ w)\,|_{x=0}^{x=L}\ dz. \tag{B.16}$$

Also term (16) must be integrated by parts, to yield

$$\begin{aligned}(16) &= \frac{1}{LH}\iint (z - z_j)\frac{\partial}{\partial z}\left(A_v\frac{\partial u}{\partial z}\right)\ dxdz \qquad (B.17)\\ &= \frac{1}{LH}\int \left((z - z_j)A_v\frac{\partial u}{\partial z}\right)\Big|_{z=-H}^{z=0}\ dx\ -\ \frac{1}{LH}\iint A_v\frac{\partial u}{\partial z}\ dxdz.\end{aligned}$$

Term (18) vanishes by definition of $u - u_R = u_D$ and vanishing net baroclinic transport, i.e. $\int u_D\ dz = 0$.

B.2 Further reduction of the evolution equations in general form

Several of the boundary conditions posed in §2.2.3 are applied here. The boundary conditions used are

$$s|_{x=L} = 0, \tag{B.18}$$
$$f_S|_{x=L} = 0, \tag{B.19}$$
$$w|_{z=-H} = w|_{z=0} = 0, \tag{B.20}$$
$$g_S|_{z=-H} = g_S|_{z=0} = 0, \tag{B.21}$$
$$u|_{x=L} = u_R, \tag{B.22}$$
$$w|_{x=L} = 0 \text{ and} \tag{B.23}$$
$$\frac{\partial u}{\partial z}|_{z=0} = 0. \tag{B.24}$$

Then, the following terms can be reduced.

$$(2) = \frac{12}{L^3 H} \iint f_S \; dxdz \tag{B.25}$$

$$(3) = -\frac{6}{L^2 H} \int f_S|_{x=0} \; dz \tag{B.26}$$

$$(4) = 0 \tag{B.27}$$

$$(6) = \frac{12}{LH^3} \left[\int z \; f_S|_{x=0} \; dz \; + \; \iint g_S \; dxdz \right] \tag{B.28}$$

$$(7) = \frac{6}{LH^2} \int f_S|_{x=0} \; dz \tag{B.29}$$

$$(8) = 0 \tag{B.30}$$

$$(9) = 0 \tag{B.31}$$

$$(13) = \frac{1}{LH} \iint u \; w \; dxdz \tag{B.32}$$

$$(15) = -\frac{1}{LH} \int A_{h,sea} \; w|_{x=0} \; dz \tag{B.33}$$

$$(16) = -\frac{1}{LH} \int \left((z - z_j) A_{v,bot} \frac{\partial u}{\partial z} \right) |_{z=-H} \; dx \; - \; \frac{1}{LH} \iint A_{v,int} \; \frac{\partial u}{\partial z} \; dxdz \tag{B.34}$$

$$(18) = 0 \tag{B.35}$$

$$(19) = 0. \tag{B.36}$$

With these simplified terms, the general form evolution equations (B.3), (B.8) and (B.12) reduce to the "final form" evolution equations (2.56), (2.64) and (2.69) in §2.7.

Furthermore, term (12) can be further simplified using the fact that $u|_{x=L} = u_R$ is a constant. Then $(12) = \frac{1}{LH} \int (z - z_j) u^2|_{x=0} \; dz$. The integrand contains products of several odd and even terms. Only the part $\propto (z - z_j) \; u_R \; u_D$ hence remains.

Appendix C

Reduced steady balances: algebraic relations and plots

C.1 Analysis of reduded steady balances

Finally, some limiting parameter settings will be studied, such as $u_R \uparrow 0$ and $u_R \to -\infty$. It turns out that for many of these limits, several terms in the steady versions of (2.56), (2.64) and (2.69) can be neglected. For these reduced steady balances, analytical solutions for (X, Z, J) can often be found that are reasonable approximations to the full numerical solution $(X, Z, J)_{est}$. In Figure C.1, C.2 and C.3 at the end of this section, the absolute magnitude of each of the (non-time-dependent) terms in the evolution equations is plotted as a function of the varying parameter, i.e. u_R, H or A_v. This is done by substituting the steady solutions (X, Z, J) and corresponding u_R, H or A_v in each of the seperate terms. Any term is neglected whose absolute magnitude is approximately 10% or less of the *largest-magnitude* term at that particular u_R, H or A_v.
Note that the analyses for varying H and A_v below have been performed with *different* default river discharge value, namely $u_R = -0.10$m/s instead of the default $u_R = -0.02$m/s that is used throughout this study.

$(X, Z, J)_{est}$ as a function of u_R - reduced balances

For several ranges of u_R, the full steady balances (2.56), (2.64), (2.69) can be significantly reduced. This is shown in Figure C.1 Four such ranges are treated here.

Physically, one does not directly expect $(X, Z, J) < 0$ in the absence of river flow. To explain this, **consider the reduced balance for $u_R \uparrow 0$.** All terms proportional to u_R are negligible. The reduced X-balance is between domain-averaged exchange salt flux (2b), which elongates L_i, and exchange salt flux (3*b*) through the seaward boundary, which steepens the along-channel density gradient. The magnitude of the latter flux scales with Z, and balances the former when

$$Z|_{u_R \uparrow 0} = -\frac{2s_0}{aH}. \tag{C.1}$$

Now substitute $Z|_{u_R \uparrow 0}$ into the reduced Z-balance, which is between (6*b*), (6*d*), (6*e*) and (7*b*). Then horizontal exchange flux, depth-weighted over the seaward bound, term (6*b*) $\propto -JX$, enhancing vertical stratification. Also term (6*d*) $\propto -JX$. This implies that, although the flow is predominantly upward in the integration-domain, salinity is predominantly negative, leading to a *negative* vertical advective salt flux, which enhances Z. Term (6*e*) becomes a positive constant, representing diffusional damping of Z. The exchange salt flux depth-averaged over the seaward bound, (7*b*) $\propto +JX$, increases salinity at all depths above the bed, while $s|_{x=0,z=-H}$ is fixed to s_0. Hence, this term weakens domain-averaged vertical stratification, contrary to the exchange-flow in term (6b). To conclude, for $u_R \uparrow 0$, the net effect of the three exchange fluxes is an enhancement $\propto -JX$ of the vertical stratification. This is balanced by diffusional damping, so that $J|_{u_R \uparrow 0} \propto +1/X$, or $L \propto -J$, i.e. the combined exchange fluxes transport salt up-estuary, increasing the salt intrusion L_i or weakening X.

Finally, substitute $Z|_{u_R \uparrow 0}$ into the J-balance. In balance, J is driven by baroclinic pressure gradient force (14) $\propto X$ and damped by friction on u_D in the bottom layer resp. inner domain, (16*a*2) resp. (16*b*), both $\propto -J$. The resulting expressions for X, Z and J are, numerically

$$X|_{u_R \uparrow 0} = -0.002811 \text{ psu/m}, \;\; \zeta|_{u_R \uparrow 0} = -2, \;\; J|_{u_R \uparrow 0} = -0.7825 \text{ m}^2/\text{s},$$

which corresponds well to the (non-approximated) numerical value obtained at $u_R = 0$.

Hereafter, the notation c_i will be used for the absolute magnitude (hence $c_i \geq 0$) of term number (i), only excluding X, J and u_R. Note that c_i hence may contain the absolute value of the Z-dependent part of term (i) at the specified u_R-value and all parameter-magnitudes other than u_R. **At default value $u_R = -0.10$ m/s, the Z-balance is between** (6*b*), i.e. depth-weighted horizontal exchange flux through the seaward bound, vertical exchange flux (6*d*) and horizontal exchange flux through the seaward bound, (7*b*). If the numerical solution to Z is substituted, all three terms are $\propto \pm JX$, and their balance yields a complicated algebraic expression for $Z|_{u_R=-0.1}$. Numerically,

$$Z|_{u_R=-0.1} - 9.791 \leftrightarrow \zeta|_{u_R=-0.1} = -2.797, \tag{C.2}$$

hence *constant* in u_R and more negative than the exact result. Nevertheless, it is the best analytical approximation that can be found for small u_R.

The X-balance is dominated by terms $(2a)$, $(2b)$ and $(3b)$. $Z|_{u_R=-0.1}$ is substituted. Domain length is shortened, i.e. X steepened, due to exchange flux at the seaward bound, $(3b) \propto +JX^2$. This shortening is partly compensated by the elongation due to domain-averaged exchange flux $(2b) \propto -JX^2$. The resulting net, exchange-flow induced domain shortening is balanced by river salt flux $(2a) \propto -u_R X^2$, which elongates L because $M < 0$ for $Z|_{u_R=-0.1}$. The terms balance as long as

$$J|_{u_R=-0.1} \propto +u_R. \tag{C.3}$$

Finally, the J-balance is between (12), (14), $(16a1)$, $(16a2)$ and $(16b)$. Substitute again $Z|_{u_R=-0.1}$. Then J is driven by baroclinicity, $(14) \propto X$, and river-induced bottom-shear, $(16a1) \propto u_R$, and slowed down by river-induced advection of u_D-momentum, $(12) \propto -u_R JX$ and friction on u_D in bottom layer and inner domain, $(16a2)$ and $(16b) \propto -J$. This yields an expression for X in terms of J and u_R, which is easier interpretable in terms of $L = -s_0/X$,

$$L|_{u_R=-0.1} = s_0 \frac{c_{14} \;-\; c_{12}\, u_R J}{c_{16a1}\, u_R \;-\; c_{16a2+16b}\, J}. \tag{C.4}$$

If c_{14} becomes larger, X must be smaller, i.e. L is stretched, to generate the same baroclinic pressure gradient force. Weakening of J, either due to an increase in c_{12} or $c_{16a2+16b}$, reduces the up-estuary exchange flux and hence the intrusion length. An increase in c_{16a1} enhances bottom layer shear and hence J, so that L increases. In other words, for larger c_{16a1}, weaker u_R is required to generate the same term $(16a1)$, hence reduced river discharge increases L_i.

In the region $u_R \in [-0.6, -0.2]$ m/s, J weakens with strenghening u_R, remarkably opposite to its behaviour for larger or smaller river discharge. **To explain this, consider the dominant balance at $u_R = -0.4$ m/s.** Substitute the numerical Z-value at this u_R. Then the X-balance contains $(2a) \propto -u_R X^2$, $(2b) \propto -JX^2$, $(2c) \propto -X^3$, $(3b) \propto +JX^2$ and $(3c) \propto +X^3$. Dividing out the common factor X^2 yields

$$X = \frac{c_{2a}\, u_R - (c_{3b} \;-\; c_{2b})J}{c_{3c} \;-\; c_{2c}}, \tag{C.5}$$

with $(c_{3b} - c_{2b}) > 0$ and $(c_{3c} - c_{2c}) > 0$. Then X is steepened, or L_i reduced, if u_R is stronger. The net effect of (2b) and (3b) is an elongation of L with intensified J. Hence X is weakened (L_i longer) for increased exchange flow.

The Z-balance is between (6a), (6b), (6d), (7a) and (7b), but the relations are too complex to further interpret. The J-balance is between (12), (13) and (14). Substitute the numerical solution $Z|_{u_R=-0.4}$. The combined effect of (12) and (13) is $\propto -u_R JX$, i.e. slowing down the circulation, balancing baroclinic driving force (14) $\propto X$, to yield

$$J|_{u_R=-0.4} = \frac{c_{14}}{c_{12} - c_{13}} \frac{1}{u_R}, \tag{C.6}$$

with $(c_{12} - c_{13}) > 0$. Hence, for $u_R = -0.4$ m/s, u_R and J *act together* to dampen J. This explains that a strengthening of u_R is compensated by a weakening of J, for $u_R \in [-0.6, -0.2]$ m/s.

As observed in Figure 4.1, Z approaches a constant and X and J become linear in u_R, as $u_R \to -\infty$. **To see why, compute the dominant balances at $u_R = -10$ m/s.**

The X-balance is then dominated by terms (2c) and (3c), hence the domain-averaged horizontal diffusive salt flux (2c) extends domain length L, while horizontal diffusive salt flux (3c), depth-averaged over the seaward bound steepens the alongchannel salt gradient. The latter flux is proportional to Z and the two fluxes balance for

$$Z|_{u_R\to-\infty} = -\frac{2K_{h,int}s_0}{cHK_{h,sea}}. \tag{C.7}$$

The Z-balance is between (6a), (6b), (6d) and (7b). Substitute $Z|_{u_R\to-\infty}$ in these terms. Then the river salt flux, depth-weighted over the seaward boundary, (6a) $\propto u_R X$, weakens vertical stratification, because u_R pushes negative salinity outward, i.e. *increases* the total seaside-salinity. This can only be achieved by reduction of the vertical salt gradient at $x = 0$, since $s|_{x=0,z=-H}$ is fixed. Vertical stratification is enhanced by depth-weighted horizontal exchange salt flux at the seaside, (6b) $\propto -JX$, and by vertical exchange salt flux (6d) $\propto -JX$. The latter is idem to the case $u_R \uparrow 0$. Finally, the horizontal exchange flux, depth-averaged over the seaward boundary, (7b) $\propto +JX$, reduces vertical stratification. This is because u_D increases total seaside salinity, and since s is fixed at the bottom, this requires a reduction of $\frac{\partial s}{\partial z}|_{x=0}$. The proportionality $\propto X$ can be cancelled out in all terms. The remaining balance is between river discharge in term (6a) and J in the other three. J has a net strenghtening influence on Z, which can balance the weakening by u_R; a balance arises when $J|_{u_R\to-\infty} \propto +u_R$.

The J-balance is between (12), (13) and (15). First substute $Z|_{u_R\to-\infty}$ in these terms. J is driven by river-induced advection of w-momentum, (13) $\propto +u_R JX$ and "Rayleigh-damping" of w at the seaside, (15) $\propto JX^2$. The latter "damping" *enhances* J because, for the current $Z < -\frac{s_0}{H}$, the rotation axis x_j is seaward of $x = 0$. J is damped by river-induced advection of u_D-momentum at the seaward bound, (12) $\propto -u_R JX$. The proportionality $\propto JX$ can be cancelled out in all three terms. Only term (15) has an "extra" power of X, hence it can balance with the "extra" u_R-dependence of the other two terms. Hence $X|_{u_R\to-\infty} \propto +u_R$, i.e. the intrusion length is reduced as u_R gets stronger. Numerically, the final result is

$$X|_{u_R\to-\infty} = 70u_R;\ Z|_{u_R\to-\infty} = -7 \leftrightarrow \zeta|_{u_R\to-\infty} = -2;\ J|_{u_R\to-\infty} = 5.238u_R, \tag{C.8}$$

which agrees well with the observed linear and constant asymptotes as $u_R \to -100$ m/s.

$(X, Z, J)_{est}$ as a function of H - reduced balances

For specific depth-ranges, the steady balances can be significantly reduced, as shown by Figures C.2 (for different default river discharge, $u_R = -0.10$m/s). Three of these ranges are treated here. Hereafter, the notation c_i will be used for the absolute magnitude (hence $c_i \geq 0$) of term number (i), only excluding X, J and H. Note that c_i hence may contain the absolute value of the Z-dependent part at the specified H-value and all parameter-magnitudes other than H.

For exceedingly small depths, i.e. $H \downarrow 0$, the X-balance is dominated by diffusive salt fluxes (2c) and (3c), which yields

$$Z|_{H\downarrow 0} = -\frac{2K_{h,int}s_0}{cHK_{h,sea}}. \tag{C.9}$$

$Z|_{H\downarrow 0}$ is then substituted into the Z-balance, which has reduced to (6b), (6d), (6e) and (7b). Vertical diffusive salt flux then is (6e) $\propto 1/H^3$. The other three terms are horizontal and vertical exchange fluxes $\propto \frac{JX}{H^2}$, where the combination of J and X is because u_D and w depend on J and are divided by L. The $\frac{1}{H^2}$-depedence of u_D and w is due to the definition of ψ_D. The Z-balance yields $X|_{H\downarrow 0} \propto \frac{1}{HJ}$ or $L|_{H\downarrow 0} \propto -HJ$, i.e. the salt intrusion increases when either the exchange flux ($\propto J$) or water depth increases.

J-balance is between (15), (16a1), (16a2) and (16b). Friction acting on u_D at the bottom and in the interior, (16a2) and (16b) $\propto -\frac{J}{H^2}$. The "Rayleigh-damping" in the seaward boundary, term (15) $\propto JX^2$, *enhances* J because the currents are upward at the seaward boundary. Finally, (16a1) $\propto -1/H$, i.e. the effect of river-induced shear is diluted if the domain is deeper. This balance gives

$$J|_{H\downarrow 0} = -\frac{c_{16a1}H}{c_{16a2+16b} - c_{15}H^2X^2},$$

with c_i positive constants. The resulting analytic expressions for X and J are very complicated, but are reasonable approximations to $(X, Z, J)_{est.}$.

At small depths, say $H = 1.5$m, the X-balance is between $(2c)$ and $(3c)$, and hence yields $Z|_{H=1.5} = -\frac{2K_{h,int}s_0}{cHK_{h,sea}}$, idem to $H \downarrow 0$m.

The Z-balance is between depth-weighted exchange flux at the seaward bound, $(6b)$, depth-averaged seaside exchange flux $(7b)$, domain-averaged vertical exchange flux $(6d)$ and depth-weighted river-induced seaside flux $(6a)$. Substituting $Z|_{H=1.5}$, the first three fluxes, related to u_D and w, are all $\propto \pm\frac{JX}{H^2}$, i.e. proportional to circulation strength J and strongly dependent on water depth. Their combined effect is $\propto -\frac{JX}{H^2}$, i.e. enhancing vertical stratification. This is balanced by a weakening of Z due to $(6a) \propto -\frac{X}{H}$. Since river discharge velocity u_R is a constant, flux $(6a)$ is less dependent on H than the other three terms. All four terms scale with X, i.e. their effect is more diluted for longer L. Since all three exchange fluxes are stronger when either J is stronger or H is smaller, channel-deepening should be compensated by a weakening of J in order to retain balance, i.e. $J|_{H=1.5} \propto -H$.

The J-balance is between (12), (13), (14), $(16a1)$, $(16a2)$ and $(16b)$. This yields an expression for X, which is more easily interpreted in terms of L,

$$L|_{H=1.5} = s_0H\frac{c_{14}\ H^2 + (c_{12}\ -\ c_{13})J}{c_{16a2+16b}\ \left(-\frac{J}{H}\right)\ -\ c_{16a1}}, \tag{C.10}$$

with all c_i positive-valued constants or functions of Z. Also $(c_{12} - c_{13}) > 0$, implying that the *net* effect of (12) $\propto +JX$ and (13) $\propto -JX$ is a damping of J. Hence if $(c_{12} - c_{13})$ is larger, J can be smaller to yield the same amount of damping. Smaller J implies smaller up-estuary salt flux, so L_i shorter, as can be seen in (C.10). If c_{14} is larger, density gradient X can be weaker, i.e. L longer, to generate the same baroclinic pressure gradient force (14) $\propto +X$. If c_{16a1} becomes larger, the river-induced bottom shear $(16a1) \propto -\frac{1}{H}$ intensifies, enhancing angular momentum J. Hence J and thus the up-estuarine exchange flux increase, extending L_i. If $(c_{16a2+16b})$ is larger, J can be smaller to have the same amount of frictional damping $(16a2), (16b) \propto -\frac{J}{H^2}$; smaller J results in shorter intrusion length.

The balances can also be reduced for e.g. default depth $H = 10$m and large depth $H = 25$m, but the resulting algebraic expressions are too complex to interpret further.

For exceedingly large H however, the algebraic expressions *can* be interpreted. The X-balance is then dominated by domain-averaged resp. seaside horizontal exchange flux ($2b$) resp. ($3b$), balancing when $Z|_{H\to\infty} = -\frac{2s_0}{aH}$.

The reduced Z-balance is exactly equal to the Z-balance for $H \downarrow 0$, and similarly gives $X|_{H\to\infty} \propto \frac{1}{HJ}$ after substitution of $Z|_{H\to\infty}$.

The J-balance is between (14), ($16a2$) and ($16b$). Baroclinic pressure gradient (14) $\propto +H^2X$ grows with water depth. Substituting $Z|_{H\to\infty}$, u_D is decreased by friction at the bottom and in the inner domain, $(16a2), (16b) \propto -\frac{J}{H^2}$. u_D and hence frictional damping increase when J increases. Gradient $\frac{\partial u_D}{\partial z}$ and thus internal friction become stronger as H becomes smaller. Concludingly, J is driven by baroclinic pressure gradient force $\propto X$ and very strongly dependent on H, because larger depth causes stronger baroclinic forcing as well as weaker friction, resulting in $J|_{H\to\infty} \propto XH^4$. This strong H-dependence is tempered by $X|_{H\to\infty}$, but J still intensifies with increasing H, $J|_{H\to\infty} \propto -H^{3/2}$. The intrusion length is hence strongly increased by channel-deepening, $L|_{H\to\infty} \propto H^{5/2}$.

$(X, Z, J)_{est}$ as a function of A_v - reduced balances

Reduced balances for three different viscosities A_v were deduced, based on Figure C.3 (for different default river discharge, $u_R = -0.10$ m/s. Hereafter, the notation c_i will be used for the absolute magnitude (hence $c_i \geq 0$) of term number (i), only excluding X, J and A_v. Note that c_i hence may contain the absolute value of the Z-dependent part at the specified A_v-value and all parameter-magnitudes other than A_v.

For very weak vertical mixing, $A_v = 10^{-5}$ **m^2/s**, the X-balance is between exchange fluxes ($2b$) and ($3b$), again yielding $Z|_{A_v=10^{-5}} = -\frac{2s_0}{aH}$.

Substitute $Z|_{A_v=10^{-5}}$ in the Z- and J-balances. The Z-balance is identical to that at $u_R \uparrow 0$, yielding $X|_{A_v=10^{-5}} \propto +1/J$. The J-balance yields

$$J|_{A_v=10^{-5}} = \frac{c_{14}X}{(c_{16a2+16b})A_v - (c_{12} - c_{13})X}. \tag{C.11}$$

J is driven by baroclinicity (14) $\propto +X$. $(c_{12} - c_{13}) > 0$, since the combination of w-induced "rotation" (13) $\propto -JX$ and river-induced advection of u_D-momentum, (12) $\propto +JX$, causes a net damping of J. Friction $(16a2), (16b) \propto -A_vJ$ damps J. This damping is stronger if exchange coefficient A_v is larger.

For default vertical viscosity, $A_v = 10^{-3}$ $\mathbf{m^2/s}$, all reduced balances are equal to those at $u_R = -0.1$m/s. The expression for Z is obtained from the Z-balance, and yields numerically $Z|_{A_v=10^{-3}} = -9.791$ psu/m.

Substitute $Z|_{A_v=10^{-3}}$ into the X-balance. Then, idem to $u_R = -0.1$, exchange fluxes $(2b)$ and $(3b)$ cause a *net* steepening of X, i.e. $\propto +JX^2$. This is balanced by the domain-stretching effect of $(2a) \propto +X^2$, i.e. river-induced ouflow of negative domain-averaged salinity. The balance arises for $J|_{A_v=10^{-3}} = -\frac{c_{2a}}{c_{3b}-c_{2b}} \approx -2.173$ m^2/s.

The J-balance yields an expression for X, or for L. This reads

$$L|_{A_v=10^{-3}} = s_0 \frac{c_{14} \ + \ c_{12}J}{A_v \left[c_{16a2+16b} \ (-J) - c_{16a1}\right]}. \tag{C.12}$$

If c_{14} is larger, X can be weaker, or L longer, to have the same baroclinic driving force $(14) \propto +X$. If c_{12} is larger, weaker J is needed to have the same damping $(12) \propto +JX$; weaker J results in less up-estuary salt transport, i.e. shorter L_i. If either $c_{16a2+16b}$ or A_v is larger, J can be weaker as well to induce equal friction $(16a2), (16b) \propto -A_vJ$. However, larger c_{16a1} induces more bottom-layer shear $(16a1) \propto -A_v$, hence enhances J. The up-estuarine salt intrusion thus becomes larger. For increased A_v, however, J can be *smaller* to generate the same shear $(16a1)$.

Finally, for very strong vertical momentum exchange, say $A_v = 0.15$ $\mathbf{m^2/s}$, the X-balance is again between horizontal diffusive fluxes $(2c)$ and $(3c)$, yielding $Z|_{A_v=0.15} = -\frac{2K_{h,int}s_0}{cHK_{h,sea}}$. Substitute $Z|_{A_v=0.15}$ in Z- and J-balance. The Z-balance is then equal to that for $H = 1.5$m, but the combined effect of vertical/horizontal exchange fluxes $(6b), (7b)$ and $(6d)$ is now $\propto -JX$, enhancing Z. This is balanced by $(6a) \propto -X$. The balance yields a constant $J|_{A_v=0.15}$. If river discharge is stronger, so is $(6a)$ and hence J has to be stronger to balance this.

The J-balance yields an expression for X or for L

$$L|_{A_v=0.15} = \frac{s_0 \ c_{14}}{A_v \left(c_{16a2+16b} \ (-J) \ - \ c_{16a1}\right)}. \tag{C.13}$$

If c_{14} is larger, X can be weaker to generate the same baroclinicity $(14) \propto +X$. If $c_{16a2+16b}$ or A_v is larger, J can be weaker to induce the same amount of friction $(16a2), (16b) \propto -A_vJ$. Weaker J reduces the up-estuary salt intrusion. Yet if c_{16a1} or A_v is stronger, river-induced bottom shear $(16a1) \propto -A_v$ generates angular momentum, J, so that L_i increases again. Finally, substitution of the constant $J|_{A_v=-0.15}$ in (C.13) yields $L|_{A_v=0.15} \propto -A_v$.

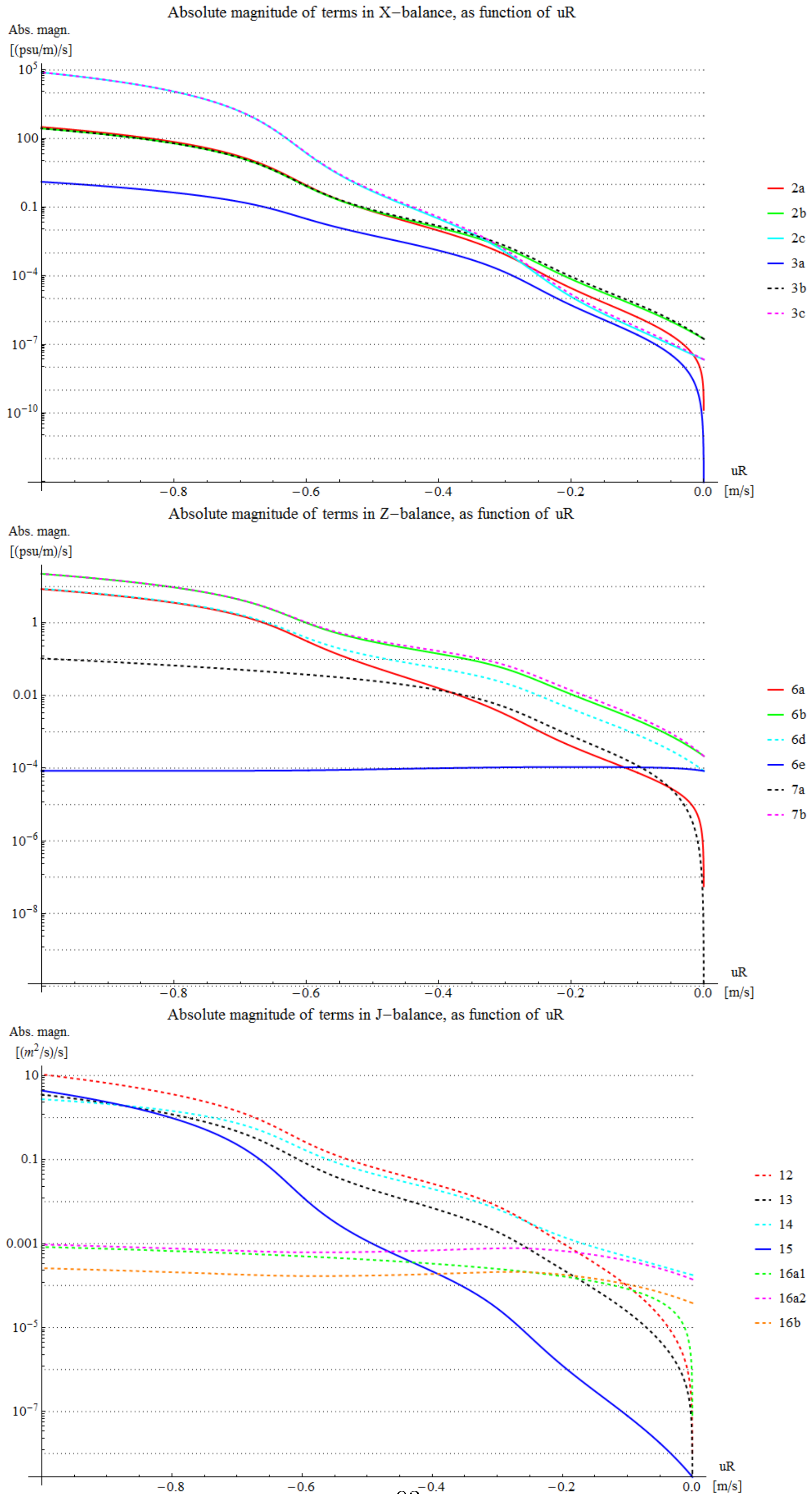

Figure C.1: Absolute magnitude of steady terms in X-, Z- and J-balance (2.56), (2.64), (2.69), with "estuarine " steady solutions $(X, Z, J)_{est}$ substituted, as a function of river discharge u_R.

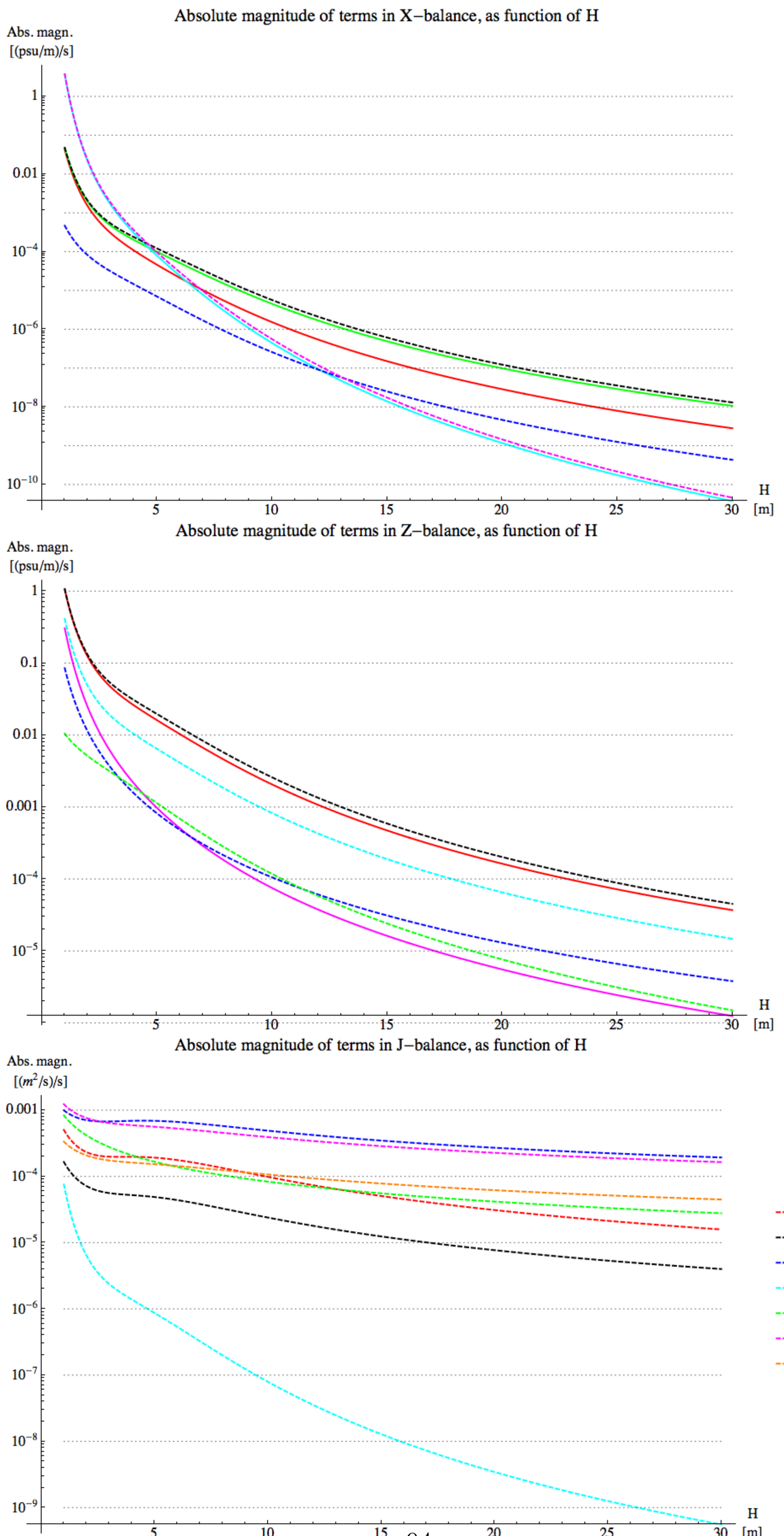

Figure C.2: Absolute magnitude of steady terms in X-, Z- and J-balance (2.56), (2.64), (2.69), with "estuarine " steady solutions $(X, Z, J)_{est}$ substituted, as a function of depth H. Note that the different default value for $u_R = -0.10$m/s is used here.

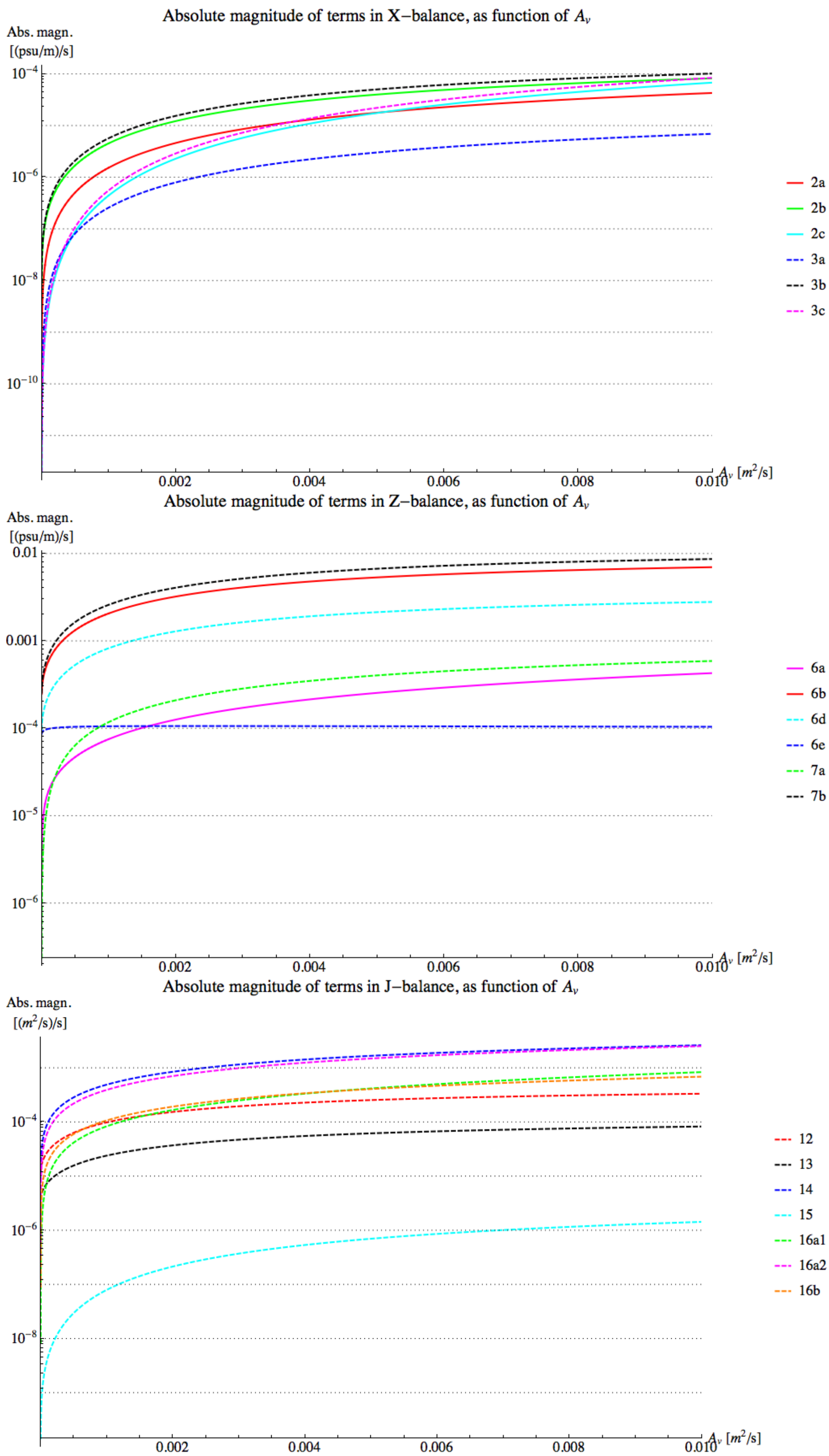

Figure C.3: Absolute magnitude of steady terms in X-, Z- and J-balance (2.56), (2.64), (2.69), with "estuarine" steady solutions $(X, Z, J)_{est}$ substituted, as a function of vertical eddy viscosity A_v. Note that the different default value for $u_R = -0.10$m/s is used here.